2018

FUNCTIONAL CHARACTERIZATION OF SCAFFOLD PROTEIN SHOC2

Hyeln Jang
University of Kentucky, hyein.jang.hj@gmail.com
Author ORCID Identifier:
https://orcid.org/0000-0002-4947-9943
Digital Object Identifier: https://doi.org/10.13023/etd.2018.514

Right click to open a feedback form in a new tab to let us know how this document benefits you.

Recommended Citation

Jang, Hyeln, "FUNCTIONAL CHARACTERIZATION OF SCAFFOLD PROTEIN SHOC2" (2018). *Theses and Dissertations--Molecular and Cellular Biochemistry*. 39.
https://uknowledge.uky.edu/biochem_etds/39

STUDENT AGREEMENT:

I represent that my thesis or dissertation and abstract are my original work. Proper attribution has been given to all outside sources. I understand that I am solely responsible for obtaining any needed copyright permissions. I have obtained needed written permission statement(s) from the owner(s) of each third-party copyrighted matter to be included in my work, allowing electronic distribution (if such use is not permitted by the fair use doctrine) which will be submitted to UKnowledge as Additional File.

I hereby grant to The University of Kentucky and its agents the irrevocable, non-exclusive, and royalty-free license to archive and make accessible my work in whole or in part in all forms of media, now or hereafter known. I agree that the document mentioned above may be made available immediately for worldwide access unless an embargo applies.

I retain all other ownership rights to the copyright of my work. I also retain the right to use in future works (such as articles or books) all or part of my work. I understand that I am free to register the copyright to my work.

REVIEW, APPROVAL AND ACCEPTANCE

The document mentioned above has been reviewed and accepted by the student's advisor, on behalf of the advisory committee, and by the Director of Graduate Studies (DGS), on behalf of the program; we verify that this is the final, approved version of the student's thesis including all changes required by the advisory committee. The undersigned agree to abide by the statements above.

<div align="right">

Hyeln Jang, Student

Dr. Emilia Galperin, Major Professor

Dr. Trevor Creamer, Director of Graduate Studies

</div>

FUNCTIONAL CHARACTERIZATION OF SCAFFOLD PROTEIN SHOC2

DISSERTATION

A dissertation submitted in partial fulfillment of the
Requirements for the degree of Doctor of Philosophy in the
College of Medicine
at the University of Kentucky

By
HyeIn Jang

Lexington, Kentucky

Director: Dr. Emilia Galperin

Associate Professor of Molecular and Cellular Biochemistry

Lexington, Kentucky

2018

ABSTRACT OF DISSERTATION

FUNCTIONAL CHARACTERIZATION OF SCAFFOLD PROTEIN SHOC2

Signaling scaffolds are critical for the correct spatial organization of enzymes within the ERK1/2 signaling pathway and proper transmission of intracellular information. However, mechanisms that control molecular dynamics within scaffolding complexes, as well as biological activities regulated by the specific assemblies, remain unclear.

The scaffold protein Shoc2 is critical for transmission of the ERK1/2 pathway signals. Shoc2 accelerates ERK1/2 signaling by integrating Ras and RAF-1 enzymes into a multi-protein complex. Germ-line mutations in *shoc2* cause Noonan-like RASopathy, a disorder with a wide spectrum of developmental deficiencies. However, the physiological role of Shoc2, the nature of ERK1/2 signals transduced through this complex or mechanisms regulating the function of Shoc2 remain largely unknown. My dissertation addresses the mechanisms by which Shoc2 accelerates ERK1/2 signal transmission and the biological outputs of the Shoc2-guided signals.

To delineate Shoc2-mediated ERK1/2 signals, I have utilized a vertebrate zebrafish model. I demonstrated that loss of Shoc2 protein expression leads to early embryonic lethality resulting from a significant reduction in the number of circulating erythropoietic and myelopoietic blood cells, underdeveloped neurocranial and pharyngeal cartilages, and a profound delay in calcification of bone structures. Together, this data demonstrates that the Shoc2 scaffolding module transmits ERK1/2 signals in neural crest development and blood cell differentiation.

This dissertation also addresses the mechanistic basis of how allosteric ubiquitination of Shoc2 and RAF-1 is controlled. I have characterized a molecular interaction of Shoc2 with its previously unknown binding partner Valosin-Containing Protein (VCP/p97). These studies demonstrated that hexametric ATPase VCP modulates ubiquitination of Shoc2 and RAF-1 through the remodeling of the scaffolding complex in a spatial-restricted manner. Experiments utilizing fluorescence microscopy and biochemical methods show that VCP/p97 sequesters the E3 ligase HUWE1 from the

Shoc2 module, thereby altering the ubiquitination of Shoc2 and RAF-1 as well as the amplitude of ERK1/2 signals. These studies also show that the levels of Shoc2 ubiquitination and ERK1/2 phosphorylation are imbalanced in fibroblasts isolated from Inclusion Body Myopathy with Paget's disease of bone and Frontotemporal Dementia (IBMPFD) patients harboring VCP germline mutations. This data also suggests that ERK1/2 pathway deregulation is part of IBMPFD pathogenesis.

In summary, these studies make a significant advance in our understanding of the mechanisms by which the Shoc2 scaffold regulates specificity and the dynamics of the ERK1/2 signaling networks. They also make important insights into our understanding of biological activities and targets of Shoc2-mediated ERK1/2 signals at the early stages of embryonic development and disease.

KEYWORDS: ERK1/2 signaling, Shoc2, RASopathy, Zebrafish, VCP

_____ HyeIn Jang _____

_____ Oct. 24th, 2018 _____

FUNCTIONAL CHARACTERIZATION OF SCAFFOLD PROTEIN SHOC2

By

HyeIn Jang

Emilia Galperin, Ph.D.
Director of Dissertation

Trevor Creamer, Ph.D.
Director of Graduate Studies

Oct. 24th, 2018

To my family

ACKNOWLEDGEMENTS

<div align="center">**TABLE OF CONTENTS**</div>

CHAPTER 3. HEMATOPOIETIC AND NEURAL CREST DEFECTS IN ZEBRAFISH *SHOC2* MUTANTS: A NOVEL VERTEBRATE MODEL FOR NOONAN-LIKE SYNDROME

CHAPTER 4. SHOC2 COUPLES THE E3 LIGASE HUWE1 WITH VCP/P97 TO CONTROL ERK1/2 SIGNALING

LIST OF TABLES

LIST OF FIGURES

CHAPTER 1

Introduction

1. The Extracellular-Signal-Regulated Kinases 1/2 (ERK1/2) signaling cascade

The ERK1/2 (or mitogen-activated protein kinase, MAPK) signaling cascade is a canonical signaling pathway that converts extracellular cues into an intracellular signals that regulate a wide range of cellular processes [1, 2]. The molecular events linking cell surface receptors to ERK1/2 activation are well studied. Receptor tyrosine kinases (RTKs) such as epidermal growth factor receptor (EGFR) activate the ERK1/2 pathway upon ligand binding [3]. The binding of the ligand to the receptor induces dimerization and auto-phosphorylation of the receptor, which is followed by the recruitment of the cytosolic adaptor proteins such as growth-factor-receptor-bound protein 2 (Grb2) to the plasma membrane [4]. Grb2 is bound constitutively to the GTP activating protein (GAP) Son of Sevenless (Sos) [5]. The binding of the Grb2-Sos complex to EGFR results in the activation of the small Ras GTPases (K-, H-, N- and M-Ras), recruitment of serine/threonine-specific protein kinase RAF (RAF-1, B-RAF or A-RAF) to the plasma membrane that leads to phosphorylation of MEK (MEK1 and MEK2), and further transmission of the signal via the ERK1/2 cascade (**Figure 1.1**) [6]. The ERK1/2 kinases are the main effectors of the cascade. ERK1/2 phosphorylate a plethora of substrates in various locations including the nucleus, cytosol, and the plasma membrane [7]. Currently, about 200 distinct ERK1/2 substrates that are involved in cell proliferation, differentiation, survival, and apoptosis have been reported [7].
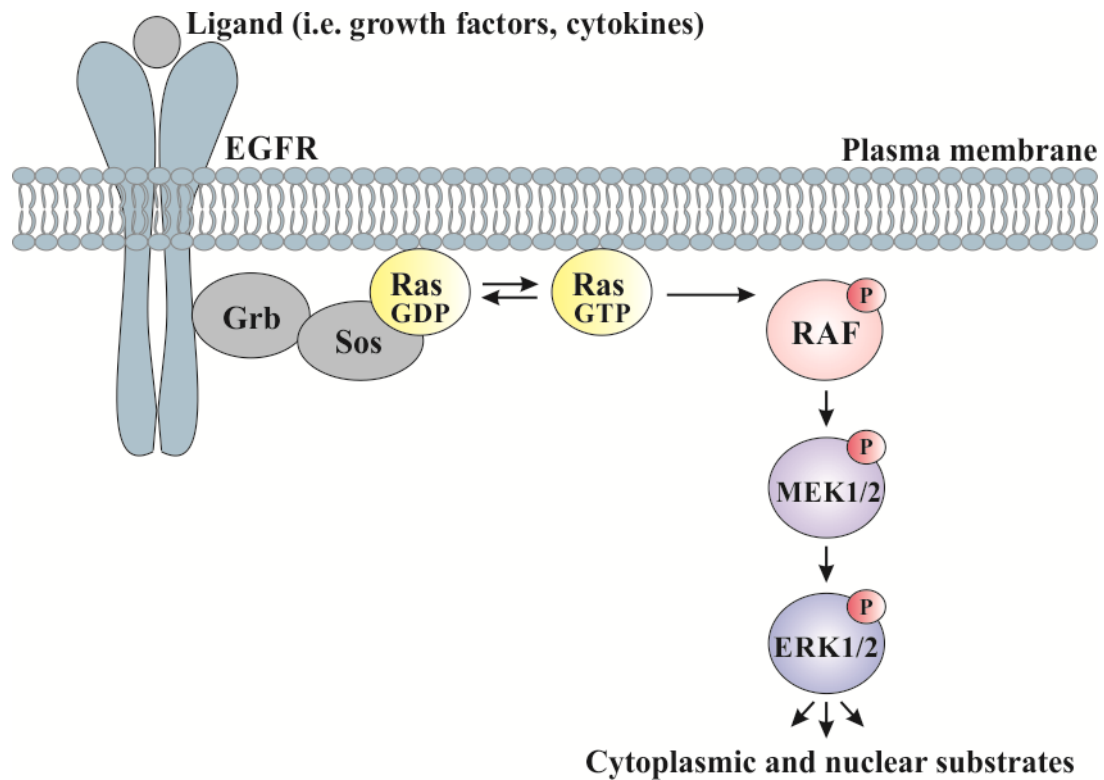
Figure 1.1 Mechanism of ERK1/2 activation.

The RAF-MEK-ERK cascade is a three-tiered core signaling component. In brief, signaling is initiated when extracellular ligands (growth factors and cytokines) bind to growth factor receptors (e.g. EGFR) at the plasma membrane. The activated receptor transmits the signal by recruiting the adaptor protein Grb2 and guanine nucleotide exchange factor Sos that, in turn, induces the activation of Ras at the plasma membranes. The activated GTP-bound Ras then transmits the signal by activating the protein kinase RAF (RAF-1, B-RAF, and A-RAF). This activation occurs by recruiting RAFs to the plasma membrane, where they are then phosphorylated and activated. The activated RAF phosphorylates MEK1/2, which in turn phosphorylates ERK1/2. Phosphorylated ERK1/2 then activates multiple downstream targets, including nuclear, cytosolic, membrane-associated, and cytoskeletal substrates.

2. ERK1/2 signal specificity determination

The ability of the ERK1/2 cascade to regulate a large number of distinct, and sometime opposing cellular processes requires mechanisms that control specificity of signals transmitted via the cascade. Factors that determine signal specificity include; **(1)** duration and strength of the signals; **(2)** subcellular compartmentalization; **(3)** extensive cross-talk and interplay between the ERK cascade and other intracellular signaling pathways [8-16].

2.1 Duration and strength of the signals

The duration and amplitude of ERK1/2 activity is a key factor in cell fate decisions [9]. The activation of the ERK1/2 cascade upon extracellular stimulation may last between 15 minutes (transient activation) and 2 to 3 hours (sustained activation). For instance, both EGF and nerve growth factor (NGF) induce strong activation of the ERK1/2 cascade in PC12 cells but the outcomes are distinct [17]. EGF stimulation provokes a rapid and transient activation of ERK1/2 that reaches the maximum at 15 min and then returns down to basal levels after 40 min, leading to cell proliferation. In contrast, NGF induces a swift monophasic ERK1/2 response that is followed by a sustained second phase leading to cell differentiation [18, 19]. Murphy et al. demonstrated that this difference in cell response could be interpreted as an activation of immediate early genes (i.e. c-Fos, c-Jun, c-Myc and Egr1) that induce distinct cellular processes dependent on the signal length [20, 21]. Studies also have shown that duration and strength of ERK1/2 signals are influenced by specialized interacting proteins, action of protein phosphatases, and chromatin remodeling affects [2, 7, 9, 10, 16, 21].

2.2 Subcellular compartmentalization

Spatial segregation of ERK1/2 signals can also define the specificity of the ERK1/2 signals [22]. In resting cells, the components of the ERK1/2 cascade are localized to the cytosol owing to their interaction with specialized anchors or scaffold proteins (these proteins are discussed separately in this chapter). Upon activation of the pathway, a portion of the activated ERK1/2 residing in the cytosol phosphorylate targets such as ribosomal S6 kinase (RSK) family proteins and cytoskeletal proteins (i.e. neurofilaments and paxillin) [7]. The other portion of ERK1/2 are released from the cytoplasmic anchors and translocate into the nucleus or to other subcellular organelles (i.e. mitochondria, endosomes, Golgi apparatus, endoplasmic reticulum) [23-26]. The nucleus-localized ERK1/2 phosphorylate transcription factors that regulate the expression of immediate early genes [1]. Several studies reported that nuclear ERK1/2 phosphorylate substrates mainly responsible for cell proliferation, differentiation, and survival [7]. Shortly after stimulation, MEK1/2 are exported from the nucleus by the exportin system, while active ERKs stay in the nucleus longer, possibly due to interaction with newly synthesized nuclear anchors [23, 27-29]. Nucleocytoplasmic shuttling of MEK1/2 also induces an export of ERK1/2 from the nucleus, bringing the signaling back to the basal level [30]. Overall, differential subcellular distribution of activated ERK1/2 enhances the complexity of the ERK1/2 cascade and constitutes an essential mechanism to provide variability to its signals, thereby enabling their participation in the regulation of a broad variety of functions [31].

2.3 Crosstalk with other signaling cascades

Additionally, the specificity of ERK1/2 signals is also achieved via interplay of ERK1/2 with other signaling cascades. Although the Ras-RAF-MEK-ERK signaling pathway is often presented as a simple linear unidirectional cascade, signals actually propagate through an interwoven network of interconnected events rather than through independent linear routes [32-34]. Thus, other signaling pathways such as JNK and p38 regulate the activity of components in several tiers of the ERK1/2 cascade and modify activation of these components upon distinct physiological conditions [1]. Signaling components of different signaling cascades can either positively or negatively regulate each other, and thereby significantly influence the specificity of the signals [33]. This connectivity is generally referred to as "signaling crosstalk".

3. The ERK1/2 pathway in human diseases

Somatic mutations in the genes of the ERK1/2 pathway or deregulation of ERK1/2 activity leads to a number of human pathologies, including developmental and neurodegenerative diseases, diabetes or cancer [35-38]. The involvement of the ERK1/2 pathway in cancer pathogenesis is well-documented and has been studied extensively [35, 36]. The "activating" mutations in genes of the ERK1/2 pathway are responsible for over half of all diagnosed cancers [35, 36, 39-48]. Mutations in the B-RAF gene drive about 60% of malignant melanomas, colorectal, thyroid, and non-small lung cancers, and are often found in patients with hairy cell leukemia [39, 40, 43, 44, 47-51]. Similarly, K-Ras mutations are common in leukemias, colorectal, peritoneal, bladder, pancreatic and lung

cancers [41]. Aberrations in genes of other Ras and RAF isoforms (A-RAF, RAF-1, H-Ras, and N-Ras) are also found in cancers but are less prevalent [52].

A different group of inherited mutations in the genes of the ERK1/2 pathway cause a number of congenital diseases cumulatively called RASopathies. RASopathies are estimated to affect about 1/1000 human births [53]. Individuals with these conditions are characterized by pleiotropic phenotypes including craniofacial dysmorphisms, heart defects, poor growth with skeletal abnormalities, variable degrees of intellectual disability, neurocognitive impairment, relative macrocephaly, and increased risk for certain malignancies [37, 54, 55]. Each of the RASopathy syndromes has a set of unique characteristics, but individuals with distinct mutations share morphological and behavior phenotypes [37, 38, 53, 55]. To date, hundreds of mutations have been described by molecular and genetic studies and more continue to be added. The germline RASopathies identified so far are shown in **Figure 1.2**.
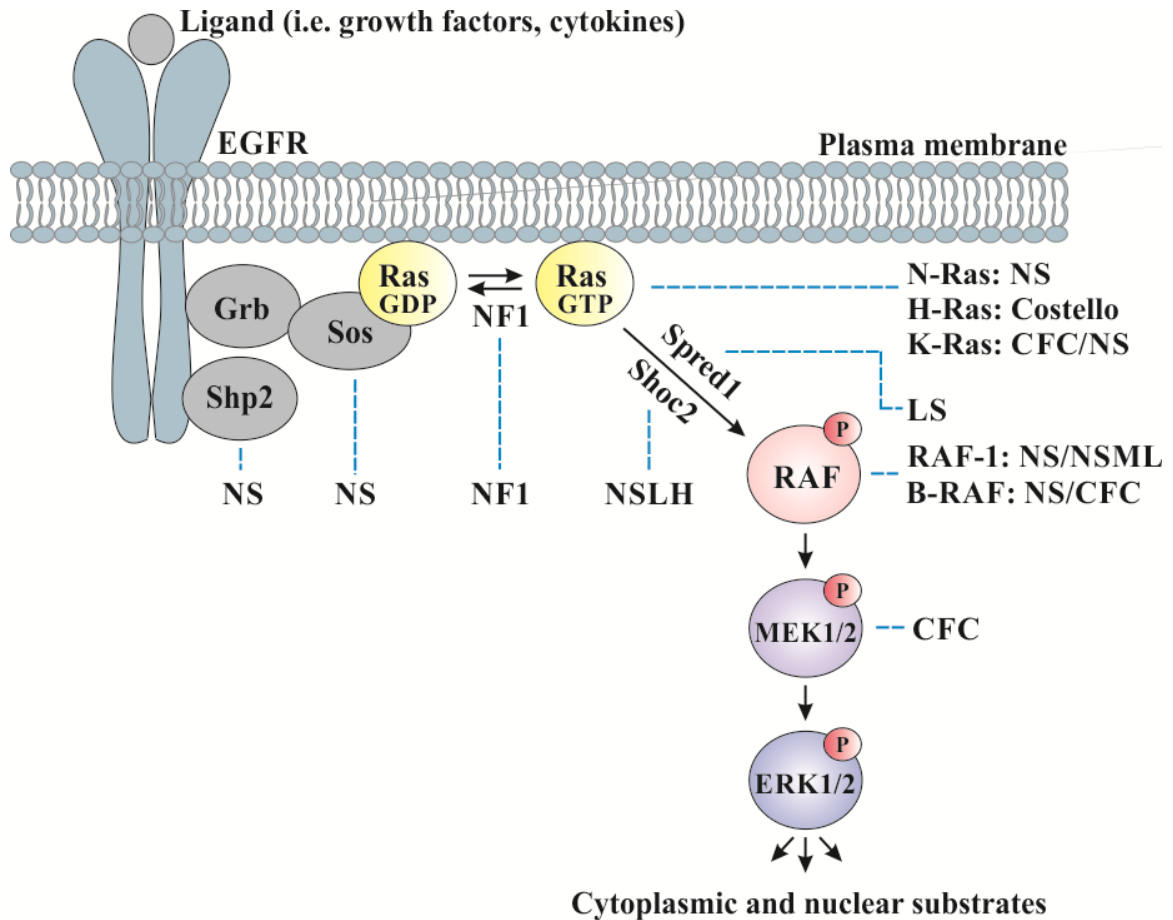
Figure 1.2 The Ras/ERK1/2 signaling pathway and associated RASopathies.

Proteins commonly mutated in RASopathies are indicated by the dashed lines. The Ras/ERK1/2 pathway proteins with germline mutations in their respective genes are associated with Noonan syndrome (NS), Noonan syndrome with multiple lentigines (NSML), Noonan syndrome with loose anagen hair (NSLH), Neurofibromatosis type 1 (NF1), Costello syndrome (CS), Legius syndrome (LS), and Cardio-facio-cutaneous syndrome (CFC). EGFR- Epidermal growth factor receptor.

4. The regulatory mechanism in ERK1/2 signaling cascade

As mentioned previously (section 2.2), the ERK1/2 cascade is regulated by several distinct scaffold proteins [1, 2, 15, 22, 29, 56]. Scaffolds tether signaling proteins into a close proximity, target complexes to a particular cellular location, and coordinate positive/negative feedback mechanisms (**Figure 1.3**). In this manner, scaffold proteins modulate kinetics of signaling cascade activation, modify duration and intensity of transmitted signals, secure interactions between distinct signaling components, regulate the localization of the components of the cascade, or modify crosstalk with other signaling pathways [10, 15, 22, 56-59]. In summary, scaffolds support several mechanisms that can independently determine signaling specificity, and therefore, are key components in the signaling cascades [1, 2, 15, 16, 22, 29, 56, 58, 59].

The importance of the scaffold proteins in ERK1/2 signaling was demonstrated when prototypic scaffold Ste5 was shown to bind to multiple components of the *Saccharomyces cerevisiae* mating pheromone response pathway, thereby conducting the mating signal to the Fus3 kinase [58, 60-65]. Ste5 integrates the three-tiered core ERK1/2 signaling components Fus3, Ste7, and Ste11 and increases their local concentration at the tips of mating projections in response to mating pheromones [58, 60, 61, 63-67]. The signals transmitted through the Ste5 complex initiate cellular processes necessary for mating, including transcriptional activation of mating-specific genes, cell-cycle arrest in G1 phase, polarized growth, and cell fusion [58, 61, 63].

Over the past decade, several studies have demonstrated that scaffold proteins are critical for regulating of the ERK1/2 cascade in mammals. The mechanisms by which the

key scaffolds modulate duration, strength, activity, or cellular distribution of signals within the ERK1/2 pathway are briefly reviewed below (**Figure 1.3**).

(A) **(B)**

(C) **(D)**
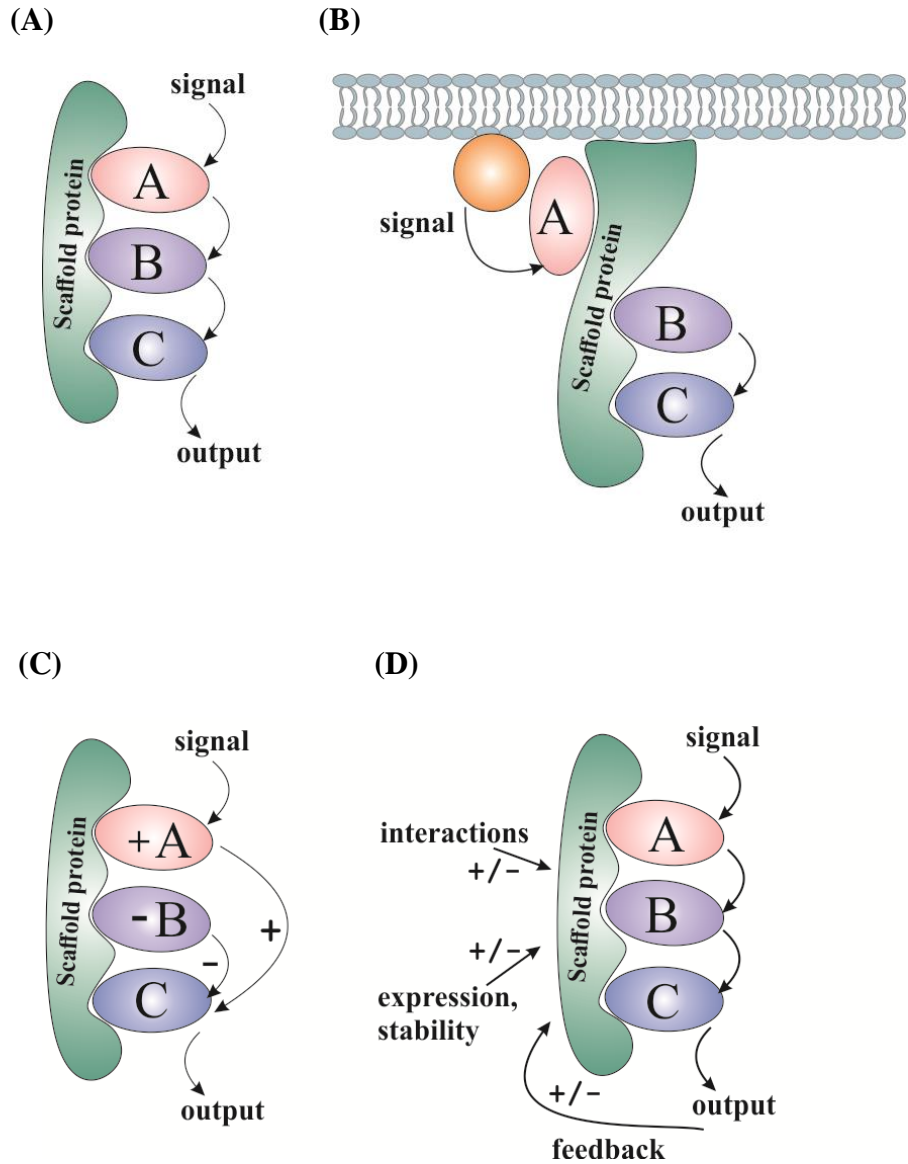
Figure 1.3 Properties of scaffold proteins. Scaffold proteins can hold more than two molecules and allow an efficient signal transduction **(A)**, focus the signaling activity at a particular site of action **(B)**, integrate both positive and negative signaling components **(C)**, mediate feedback mechanisms, coordinate allosteric modification of signaling molecules, and regulate stability of the signaling components **(D)**.

4.1 Kinase Suppressor of Ras (KSR)

One of the best-studied scaffolds of the ERK1/2 pathway is Kinase Suppressor of Ras 1 and 2 (KSR1 and 2) [68, 69]. Identified in genetic screens performed in *Drosophila melanogaster* (D. *melanogaster*) and *Caenorhabditis elegans* (C. *elegans*), KSR1 is a positive regulator of Ras pathway signaling [68-70]. KSR1 facilitates MEK phosphorylation by RAF-1, leading to increased ERK1/2 activation [69, 71-75]. In quiescent cells, KSR1 is associated with MEK1/2 and 14-3-3. In response to EGFR activation, dephosphorylated KSR1 releases 14-3-3 and translocates to the plasma membrane. At the plasma membrane, KSR1 facilitates MEK1/2 activation via assembly of Ras and RAF-1 complexes [71]. Loss or overexpression of KSR1 in cells alters the degree to which ERK1/2 are activated [1, 69, 72-74, 76-79].

Genetic studies in mammalian systems demonstrated that KSR1 knockout mice are fertile and phenotypically and developmentally normal [75]. *Ksr1*$^{-/-}$ mice presented with attenuated ERK1/2 activation and marginally impaired immunological response (particularly in regards to T-cell activation). Interestingly, KSR1 knockouts were found to be resistant to Ras-driven tumors with subsequent studies showing that KSR1 is required for the complete oncogenic potential of Ras-driven cancer cells [75, 80].

Even though KSR1 and KSR2 are structurally similar, KSR2 has a distinct physiological role in regulating energy balance [78, 81]. *Ksr2*$^{-/-}$ knockout mice have reduced fertility and become spontaneously obese [82, 83]. Importantly, Pearce et. al., have identified multiple rare variants in the *Ksr2* gene that disrupt signaling through the ERK1/2 pathway, causing severe early-onset obesity in patients [84]. Carriers of K*sr2* mutations present with childhood hyperphagia, low heart rate, reduced basal metabolic

rate, and severe insulin resistance [84]. Overall, both KSRs are physiologically important for the ERK1/2 signal transmission [1, 69, 73, 75, 77].

4.2 MAPK/ERK kinase 1 partner (MP1)/p14/p18 complex

An additional scaffold module that was shown to regulate ERK1/2 activity is the MP1/p14/p18 protein complex [85, 86]. A small 14 kDa protein, MP1, was identified as a MEK scaffold in a yeast two hybrid screen. MP1 forms stable heterodimers with an adaptor protein p14, which is responsible for the localization of MEK1 to the late endosomal compartment. On endosomes, the MP1-p14 complex promotes the assembly and interaction with signaling molecules MEK1 and ERK1 [87, 88]. *In vitro* studies by Schaeffer et al. demonstrated that MP1 stimulates phosphorylation of MEK1 by RAF and the interaction of MEK1-ERK1 [1, 85, 86].

The endosomal localization of the MP1-p14 complex is crucial for the complete ERK1 activation in response to EGF stimulation [85, 86, 88]. Depletion of p14 results in mislocalization of MP1 from late endosomes to the cytoplasm and decreased phosphorylation of ERK1 [85, 89]. The MP1-p14 scaffolding complex is anchored on the endosomal membrane by the small polypeptide p18 [90]. p18 is recruited to late endosomal lipid rafts by N-terminal myristoylation and palmitoylation and anchors the scaffold MP1-p14 heterodimer to the cytoplasmic surface of late endosomes [90]. The MP1/p14/p18 scaffold complex is also known as the LAMTOR1-2-3 complex for its function in the mTORC1 mediated sensing of amino acids [91-93].

Properties of the MP1-p14-p18 complex support the notion that scaffold proteins provide means for the spatial organization of signaling cascades and that endosomes serve as a meeting ground for signaling components [94, 95].

4.3 IQ motif-containing GTPase activating protein 1 (IQGAP1)

Another notable scaffold protein, IQGAP1, is the best-characterized member of the IQGAP family that includes three paralogs in humans, IQGAP1, IQGAP2, and IQGAP3. [96]. IQGAP1 is a large (190 kDa) ubiquitously expressed protein that regulates many signaling pathways, including ERK1/2 [1, 97].

As a scaffolding protein, IQGAP1 mediates numerous protein-protein interactions via its multiple domains. Its IQ domain is similar to the catalytic domain of Ras-GTPase-activating proteins (GAPs). IQGAP's domain, including calponin-homology domain (CHD), WW domain, a GTPase-activating protein-related (GRD) domain, and a RasGAP C-terminal domain, mediate binding of partners such as Cdc42 and Rac1, actin, calmodulin, E-cadherin, β-catenin, S100B, nectin, CLIP-170, mTOR and Akt, and form multiprotein complexes [97-106].

IQGAP1 interacts with B-RAF, MEK1/2, and ERK1/2, recruits them to the actin filaments, and positively regulates ERK1/2 signals [107]. Alterations in the levels of IQGAP1 expressed in cells abrogated EGF-dependent activation of MEK1/2 and ERK2, indicating its crucial role for efficient ERK1/2 signaling propagation [59].

4.4 Suppressor of Ras-8 (Sur-8 or Shoc2)

Sur-8/Soc2, *suppressor of clear* were isolated in *C. elegans* genetic screens [108]. Several following studies suggested that Sur-8/Shoc2 enhances ERK1/2 activity by forming a ternary complex with Ras and RAF-1 kinase in response to growth factors stimuli [109-111] and showed that Shoc2 can interact with several Ras isoforms [109, 110, 112, 113]. Mammalian Shoc2 is a remarkably evolutionarily well-conserved protein [111]. All known Shoc2 orthologues are comprised of two major domains: the short, unstructured N-terminal domain followed by the long stretch of leucine-rich repeats (LRRs) [111]. Similar to other proteins that contain tandem arrays of multiple LRRs, Shoc2 likely forms a horseshoe-shaped solenoid structure which generates a platform holding several binding partners with only a few being identified. The involvement of each known interacting partner (i.e. PP1c, SCRIB, Erbin, HUWE1, PSMC5) in the regulation of the Shoc2 function, assembly of the scaffolding complex, and/or subsequent control over the ERK1/2 signaling is discussed separately.

The biological significance of Shoc2 was explored in several studies [114-120]. The total knockout of Shoc2 in mice led to an early embryonic lethality [121]. This study made a surprising conclusion: Shoc2 is able to regulate atrioventricular canal development in an ERK-independent manner [121]. Yet a number of other groups demonstrated that this non-enzymatic protein enhances ERK1/2 activation in response to EGFR and fibroblast growth factor receptor (FGFR) activation [108, 117, 122, 123]. Although our current understanding of biological processes and targets regulated via signals transmitted through the complex is incomplete, several attempts have been made to delineate the physiological role of Shoc2. Along with the potential role of Shoc2 in

13

differentiation and proliferation of neuronal progenitor cells, Shoc2's role was examined in tumorigenesis of cells such as pancreatic, colon, breast, and non-small cell lung carcinomas, melanoma and hepatoma cells [112, 114, 115, 119, 124]. Activity of ERK1/2 transduced by Shoc2 was shown to contribute to the malignant properties of various tumor cells via regulating contact inhibition, anchorage-independent proliferation and orientation of the microtubule-organizing center of these cells. The Galperin lab showed that Shoc2 modulates ERK1/2 signals for cell motility and attachment, in part, through regulating expression of the protein of extracellular matrix lectin galactoside-binding soluble 3-binding protein (LGALS3BP) [118].

Efforts to understand the mechanisms by which Shoc2 controls ERK1/2 activity revealed the intricate machinery that governs the ability of Shoc2-transduced Ras-RAF signals. **Catalytic subunit of protein phosphatase 1c (PP1c)** is one of the three catalytic subunits of serine/threonine specific protein phosphatase 1 (PP1) [125, 126]. PP1c, known for its capacity to cooperate with various regulatory subunits, forms a holoenzyme with Shoc2 [110]. The Shoc2-PP1 holoenzyme is targeted to stimulate RAF-1 kinase activity by dephosphorylating the S259 inhibitory site. It was hypothesized that M-Ras/Shoc2/PP1c complexes then activate RAF-1 recruited by other Ras proteins or Ras family GTPases [110].

Scribbled homolog (SCRIB) is a member of the evolutionarily conserved LAP (LRR and PDZ) protein family and a known regulator of the ERK1/2 pathway [127]. SCRIB is involved in regulating cell polarity and has properties of a tumor suppressor

[127-130]. In *Drosophila*, loss of SCRIB results in neoplastic outgrowth, and SCRIB cooperates with activated Ras to promote invasion and metastasis [131]. Young et al. showed that SCRIB antagonizes Shoc2-mediated RAF-1 (S259) dephosphorylation through a mechanism involving competition for PP1c molecules within the same scaffolding complex [119]. Competition of Shoc2 and SCRIB for PP1c is part of the intricate mechanisms that controls the frequency and amplitude of Shoc2-transduced ERK1/2 activity and affects cell polarity and tumorigenic growth [119].

Erbb2 Interacting Protein (Erbin), also known as ERBB2IP, is another member of the LAP protein family [132]. Erbin interacts, via its PDZ domain, specifically with Erbb2, but not with Erbb3, Erbb4, or EGFR [133, 134]. Similar to SCRIB, Erbin is a negative regulator of the Ras-RAF-ERK1/2 signaling pathway [135]. In keratinocytes and cardiomyocytes, Erbin dampens ERK1/2 activity by disrupting the interaction of Ras-RAF-1 that is mediated by Shoc2 [136-139]. The depletion of Erbin increases the interaction of Shoc2 with Ras and RAF, and ERK1/2 activation. Both SCRIB and Erbin appear to provide an essential mechanism to control signaling strength of Shoc2-ERK1/2 activation in a spatio-temporal manner [109, 119, 139].

Proteins of ubiquitin machinery

Shoc2-ERK1/2 signals are fine-tuned through Shoc2 partnering with proteins of the ubiquitin machinery: the HECT-domain E3 ubiquitin ligase HUWE1 and the AAA+ ATPase PSMC5 [116, 120].

HECT, UBS and WWE domain containing 1 (HUWE1)

The HECT-domain E3 ubiquitin ligase HUWE1 (also called ARF-BP or MULE) is an interacting partner in the Shoc2-Ras-RAF-1 scaffold complex [120]. HUWE1 has been implicated in the regulation of cell proliferation, apoptosis, neural differentiation, and the DNA damage response [140-142]. It is mainly expressed in heart, placenta, and brain. Increased HUWE1 levels have been found in cancers (i.e. lung, breast, and colorectal carcinomas) and HUWE1-mediated ubiquitination has been linked to cancer via its ability to target substrates such as p53 and c-Myc for degradation [143-148]. In the Shoc2 scaffolding module, HUWE1 ubiquitinates Shoc2 which is a prerequisite for the subsequent ubiquitination of the RAF-1 kinase by HUWE1. HUWE1-mediated ubiquitination regulates the stability of both Shoc2 and RAF-1. Importantly, abrogated Shoc2 ubiquitination leads to impaired RAF-1 ubiquitination, increased ERK1/2 phosphorylation, and higher rates of cell proliferation [120]. HUWE1 acts as the ERK1/2 signal-tuning component in the scaffold complex, thereby controlling the intensity of ERK1/2 signaling flow through Ras and RAF-1. Hence, HUWE1 provides a negative feedback mechanism that modifies the amplitude of Shoc2-mediated ERK1/2 signaling through allosteric post-translational modifications [120].

ATPase associated with diverse cellular activities (AAA+) ATPase 5, (PSMC5)

An additional protein of the ubiquitin machinery regulating Shoc2-mediated ERK1/2 signaling is the AAA+ ATPase PSMC5 [149]. PSMC5 (rpt6 or Sug1), widely known for its essential role in the 19S proteasome [150], also functions as an unfoldase/remodeler of AAA+ Proteins Independent of 20S (APIS) complexes [116, 151]. In the Shoc2 assembly, PSMC5 has a unique role that does not involve a control over stability of Shoc2 or its known partners. Experiments using ATPase activity deficient mutants of PSMC5 demonstrated that PSMC5 is required for the remodeling of the Shoc2 complex in a spatially defined manner. PSMC5 targets Shoc2 complexes to endosomes for the Shoc2 complex remodeling. While HUWE1-mediated ubiquitination of Shoc2 and RAF-1 allows for the dynamic range of RAF-1 activity to be fine-tuned, PSMC5 controls the ability of HUWE1 to modify the non-catalytic scaffold Shoc2, thereby actively modulating the assembly of molecules in the complex [116, 120].

5. Shoc2 mutations in RASopathy patients

Importantly, Shoc2 is the only scaffold protein for which mutations have been identified in RASopathy patients. In 2009, Cordeddu and coworkers reported that the c.4A>G (p.S2G) missense mutation in the Shoc2 gene causes a Noonan-like syndrome with loose anagen hair (NSLH)(OMIM 607721) [152]. The c.4A>G (p.S2G) substitution subsequently leads to a protein with the abnormally added myristate fatty acids that is aberrantly targeted to the plasma membrane. The first group of patients carrying the c.4A>G mutation were reported to have an unusual combination of features where

17

reduced growth associated with growth hormone deficiency, cognitive deficits, distinctive hyperactive behavior, and a unique hair anomaly [152]. These findings were then expanded from distinctive craniofacial dysmorphisms and a wide spectrum of congenital heart defects to variable neurocognitive impairments, brain anomalies, epilepsy, severe hydrops fetalis, and even Moyamoya syndrome [152-157]. A different substitution (c.519G>A; p.M173I) in *shoc2* was later recently reported by Hannig et al. in patients with the mild NSLH [158]. Molecular studies by the Galperin lab revealed that an impaired ability of the Shoc2 M173I mutant to interact with protein phosphatase 1c (PP1c) which activates Shoc2 bound RAF-1 kinase [110, 158]. These clinical and molecular studies further emphasized the importance of the cellular localization of Shoc2 and the proper assembly of the Shoc2 scaffold complex. Interestingly, patients with *de novo* missense mutations in PP1c were reported to closely resemble Noonan syndrome with loose anagen hair [159]. Patients had relative or absolute macrocephaly, low-set and posteriorly positioned ears, developmental delay, slow growing and/or sparse hair and/or an unruly hair texture, which are all overlapping phenotypes in Shoc2 patients. Therefore, in order to understand the pathology of NSLH it is necessary to decipher the mechanism by which the Shoc2 scaffold regulates ERK1/2 pathway activity as well as the functions of each Shoc2-interacting partners in the module.

6. Scope of the dissertation study

The studies presented in this dissertation are focused on understanding specific biological signals transmitted through the scaffold module Shoc2 as well as deciphering the molecular mechanisms regulating the Shoc2 signaling module. Chapter 3 summarizes

studies that examine the physiological role of Shoc2-transmitted ERK1/2 signals using a heritable zebrafish vertebrate model. I found that Shoc2 is essential for early development and its loss is detrimental to a normal hematopoiesis and development of the neural crest in zebrafish. Chapter 4 characterizes the novel molecular interaction of Shoc2 with its previously unknown binding protein Valosin-containing protein (VCP). I found that VCP is critical for the proper remodeling of the Shoc2 signaling complex and a fine-tuning of the ERK1/2 signals transmitted via the Shoc2-Ras-RAF-1 complex. I also found that alterations in the ubiquitination of Shoc2 and ERK1/2 activity are novel aspects in the pathology of Inclusion Body Myopathy with Paget's disease of bone and Frontotemporal Dementia (IBMPFD).

CHAPTER 2

Material and Methods

A. Materials and Methods used in CHAPTER 3

1. Zebrafish strains and maintenance

All zebrafish (*Danio rerio*) strains (*AB* and *Sanger AB Tubingen*) were bred, raised, and maintained in accordance with established animal care protocols for zebrafish husbandry [160]. Adult fish, embryos, and larvae were housed at 28 °C, on a 14 h light: 10 h dark cycle. Embryos were staged as previously described [161]. All animal procedures were carried out in accordance with guidelines established by the University of Kentucky Institutional Animal Care and Use Committee.

2. Cloning of zebrafish Shoc2 cDNA

Total RNA of 120 hours post fertilization (hpf) zebrafish was extracted with RNAzol reagent (Bio-Rad) and reverse-transcribed using iScript RT Supermix according to the manufacturer's recommendations (Bio-Rad). Primers used to amplify Shoc2 are:

Forward primer: 5-ATGTGCCATTGGACTGCGG-3'

Reverse primer: 5'-GTCCAAGGTAAAGGCCACCG-3'

Primers used to amplify Shoc2 insensitive to ATG morpholino are:

Forward primer: 5'- ATGTCATCGACTCTGGGCAAAGATAAAGAC-3'

Reverse primer: 5'-TCAGACCATGGCGCGGTA-3'

PCR products were cloned into TA vector and validated by Sanger sequencing.

3. Whole-mount in situ hybridization

Sense and antisense *shoc2* RNA probes were prepared by *in vitro* transcription of linearized plasmids containing a portion of the coding sequence of Shoc2, using T7 polymerase and digoxigenin (DIG) labeling mix (Roche).

A standard protocol used to perform whole-mount in situ hybridization is as follows:

1. Embryos were fixed overnight at 4 °C in freshly prepared 4% paraformaldehyde in PBS (pH 7.0). Samples were dehydrated with 4 changes of 100 % methanol and stored at -20 °C for a minimum of 24 h.

2. Tissues were gradually rehydrated from methanol into PBST (PBS, 0.1% Tween-20) and permeabilized in proteinase K (20 µg/ml in PBST). Frequent observations were made under the microscope for signs of digestion. Enzyme reaction was stopped by washing samples with PBST, followed by replacement with hybridization buffer (50% Formamide, 5X Saline Sodium Citrate buffer (SSC), 5 mg/ml yeast RNA, 50 µg/ml heparin sulfate, 0.1% Tween-20) for a minimum of 2 h at 60 °C.

3. Riboprobes (*shoc2* sense and anti-sense) were hybridized to the tissue overnight at 60 °C at a final concentration of 2 ng/µl in hybridization buffer.

4. Samples were washed with a gradual series of SSC at 60 °C and 70 °C, and a graded PMST series at room temperature, before blocking for a minimum of 2 h at 4 °C in PBST containing 2% BSA and 2% sheep serum.

5. Samples were incubated overnight at 4 °C with an anti-DIG-AP antibody (Roche) diluted 1:1500 in blocking buffer, and equilibrated in NTMT buffer (0.1 M Tris pH 9.5, 0.05 M MgCl$_2$, 0.1 M NaCl, 0.1% Tween-20) before coloration with 4-Nitro blue tetrazolium (NBT; Roche) and 5-bromo-4-chloro-3-indolyl-phosphate, 4-toluidine salt (BCIP; Roche)

in NTMT. Frequent observation was made under the microscope and the coloration reaction was stopped by stop solution (PBS pH 5.5, 1 mM EDTA).

4. Morpholino (MO) and mRNA injection

All MOs were obtained from Gene Tools, LLC. MO (5.2 ng) were injected into 1-2 cell stage zebrafish embryos. A standard control MO and two non-overlapping *shoc2*-specific MO used is the experiments are as following:

standard control MO: 5'- CCTCTTACCTCAGTTACAATTTATA-3'

shoc2 MO1: 5'- TACTGCTCATGGCGAAAGCCCCGCA-3'

shoc2 MO2: 5'- TCCAATGGCACATGGGACCCTCAGT-3'.

Both *shoc2* MO1 and MO2 generated similar phenotypes. All data presented in this study were from embryos injected with *shoc2* MO1.

The human *shoc2* cDNA was amplified using primers introducing silent mutations rendering RNA insensitive to *shoc2*-MO and then cloned into the pGEM-T-easy vector (Promega). Primer sequences used to generate human shoc2 cDNA are as following:

Forward primer: 5'-ATGAGTAGTAGTTTAGGAAAAG-3'

Reverse primer: 5'-TCAGACCATGGCACGATATGG-3'

The capped mRNAs were synthesized with the mMessage mMACHINE transcription kit (Life Technologies) according to the manufacturer's recommendations. For mRNA rescue experiments, 100 pg/embryo of WT *shoc2* mRNA was co-injected with 5.2 ng of *shoc2* MO1 into 1-2 cell stage zebrafish embryos.

5. *shoc2* **CRISPR sgRNA target design**

      Shoc2 CRISPR target sites were identified and the corresponding sgRNA oligos were designed using the ZiFiT online software package (www.zifit.partners.org/ZiFiT). To note, it is helpful to choose multiple sites and co-target them by co-injecting more than one gRNA.

      How to use ZiFiT software:

1. Navigate to the ZiFiT website and follow links to the "CRISPR/Cas9 nucleases" site.

2. Copy and paste the target region from the target gene's genomic sequence file into the text box.

3. Select "T7 promoter" which will ensure that the CRISPR target begins with "GG", the preferred starting bases for T7 RNA polymerase.

4. Specify the length of target site as 20 bp.

5. Select "Zebrafish" for species.

6. Click "Identify target sites".

7. Click "Identify potential off target sites". Eliminate candidate targets that have off-target sites containing only 1 bp or 2 bp mismatches compared to the target.

8. Choose a few non-overlapping targets with low predicted off-targeting on the mRNA sequence file.

9. Eliminate candidate CRISPR target sites with an obvious stretches of self-complementary sequence that might cause hairpin formation.

10. Prioritize candidate CRISPR targets containing restriction enzyme (RE) sites as RE analysis provides an alternative method to screen for genotypes.

11. Choose the most preferred target site(s), and annotate onto genomic sequences.

12. Generate high resolution melting analysis (HRMA) primers using genomic sequence and check that the amplicon sequence predicts a smooth melting curve using uMelt online software.

6. Plasmid-based CRISPR sgRNA and Cas9 mRNA synthesis and injection

Oligonucleotides corresponding to the *shoc2*-specific sgRNA CRISPR/Cas9 target site were purchased (standard primers with salt-free clean up). If using a different design software, the insert-oligos can be designed using the target site. To generate "insert-oligo 1 (forward)", simply add "TA" 5' to the target sequence. To generate "insert-oligo 2 (reverse)", delete the GG at the beginning of the target sequence, then reverse complement the target sequence, and finally add "AAAC" to 5' of this sequence. When mixed together, the insert-oligos will create a double-stranded targeting sequence flanked by 4 bp single-stranded overhangs, compatible with the overhangs generated by Bsa1 digestion of pDR274. The sequences for targeting *shoc2* exon 2 and exon 3 were as follow:

Target site (exon 2) sequence: GGTGGGATGCCTGTCAGGAT

Oligo 1: <u>TA</u>GGTGGGATGCCTGTCAGGAT

Oligo 2: <u>AAAC</u>ATCCTGACAGGCATCCCA

Target site (exon 3) sequence: GGATGTAGCCCACAACCAGT

Oligo 1: TAGGATGTAGCCCACAACCAGT

Oligo 2: AAACACTGGTTGTGGGCTACAT

1. pDR274 (AddGene; plasmid #42250) was linearized with Bsa1-HF (NEB #R3535S) at 37 °C for at least 3 h.

300~1000 ng of pDR274

1 µl Bsa1-HF

1 µl CutSmart Buffer

Up to 10 µl Sterile water

2. Linearized vector was purified using PCR clean up kit and ran on a 1% agarose gel.

Single band at 2.1 kb was observed.

3. Oligonucleotide annealing:

    a. Mixed an equal amount of oligonucleotides of forward and reverse strands;

        10 µl of NEB buffer #4

        10 µl of 100 µM forward

        10 µl of 100 µM reverse

        70 µl of water

    b. Used PCR machine for annealing

        5 min 97 °C

        2 min 50 °C

        2 min room temperature

        5 min 4 °C

4. Ligation:

    a. Mixed 3 µl of annealed oligos

        digested vector   300-1000 ng

        ligation buffer   5 µl

        sterile water   30 µl

        Total   48 µl

b. Incubated at 50 °C for 2 min

c. Incubated at room temperature for 5 min

d. Incubated on ice for 5 min

e. Added 2 µl of T4 DNA ligase and incubated overnight at 16 °C

5. Transformation was performed using 5 µl of the ligation product.

6. 5 bacterial colonies were chosen and cultured in 5 ml of LB media (+ Kanamycin) overnight. Plasmid DNA was purified using Plasmid Miniprep™ –Classic kit (Zymo Research) and validated by Sanger sequencing using M13F primer (5'-TGTAAAACGACGGCCAGT-3').

7. Plasmids were digested using DraI (NEB #R0129S) at 37 °C for at least 3 h.

Plasmid	5 µg
DraI	4 µl
CutSmart NEB buffer	5 µl
Sterile water up to	50 µl

8. Digested plasmids were analyzed on a 1% agarose gel. The 286 bp DNA band was gel extracted and used for *shoc2* sgRNA synthesis.

9. To generate Cas9 mRNA:

1) Purified high quality pCS-nCas9n (Addgene) plasmid DNA (Midiprep).

2) Linearized pCS-nCas9n using NotI-HF (NEB, #R3189S) at 37 ºC for at least 3 h.

Plasmid	20 µg
NotI-HF	10 µl
CutSmart buffer	10 µl

Sterile water to 100 µl

3) Purified linearized plasmid using PCR cleanup kit (Qiagen) and resolve the digested on a 1% agarose gel for diagnosis.

4) sgRNA and Cas9 mRNA were synthesized using the mMESSAGE mMACHINE SP6 Transcription Kit (Life Technologies). To confirm the quality of sgRNA and Cas9 mRNA, each RNA was mixed with formamide, heated at 72 °C for 5 min and resolved on a 1% (w/v) agarose gel.

7. Microinjection of *shoc2* sgRNA and Cas9 mRNA

The following injection mixture was prepared and 0.2 mm-diameter droplet was injected into each 1-2 cell stage wild-type embryos:

200 pg/embryo of *shoc2* sgRNA	x µl
300 pg/embryo of Cas9 mRNA	x µl
Danieu's buffer (20x)	1 µl
DesRed (10x)	2 µl
Sterile water (DNAase/RNAse free) to	20 µl

8. High Resolution Melting Analysis (HRMA)

When designing sgRNA, it is important to ensure that the target sites have good primers flanking the CRISPR target site for HRMA and sequencing. The Following primer design was recommended in the manual of "LightCycler 480 Real-Time PCR System" that was utilized in our experiments.

To choose the best HRMA primers:

1. Choose primer pair that produces amplicons no longer than 150 bp (75 bp < product length < 150 bp works the best). Short amplicons are more likely to show the effects of small sequence variations.

2. Design PCR primers that have annealing temperatures around 60 ⁰C.

3. Avoid primers that are likely to form primer dimers or nonspecific products.

4. BLAST the primer sequences to ensure they are specific for the target species and gene.

5. Order the primers at 10 nM scale with salt-free clean up.

6. Check the specificity of the PCR product on agarose gel. Check if the reaction contains primer dimers or nonspecific products as these are not suitable for HRMA.

7. Reorder the primers at 200 nM in HPLC purification grade.

To isolate genomic DNA from un-injected or sgRNA/Cas9 injected individual embryos, 24 hpf de-chorionated embryos were placed into individual wells of a 96-well plate containing 20 µl of 1X ThermoPol Buffer (New England Biolabs). The plate was placed in a PCR cycler at 95 °C for 10 min, after which 5 µl of 10 mg/ml Proteinase K (Sigma) was added to each well and the plate was incubated at 55 °C for 1 h and 95 °C for 10 min. HRMA was performed using a LightCycler 96 RealTime PCR System (Roche) and LightCycler 480 High Resolution Melting Master (Roche) according to the manufacturer's instructions. At least 3 un-injected embryos were included as a control along with 3 no-template control.

2x Master mix	10 µl
Forward primer (10 µM)	0.2 µl
Reverse primer (10 µM)	0.2 µl

MgCl$_2$ stock solution (25 mM)   1.2 µl

Water (PCR grade)   6.4 µl

Genomic DNA   2 µl

Primer sequences (HPLC grade):

shoc2^{Δ22} 5'-CCATCAAGGAGCTGACCCAG-3'

5'-TCTGACCAGCCTACCTGACT-3',

shoc2^{Δ14} 5'-AGCGACTCTGTTGTCTTGTGTTA-3'

5'- AGGTTGGTGATCTGAGTGCAA-3'

9. DNA extraction and genotyping

Genomic DNAs were extracted from individual embryos or adult tail clips.

Briefly, 20 µl of the ThermoPol Buffer (New England Biolabs) was added to the samples

and boiled for 5 min and digested with Proteinase K (10 mg/ml) for 2 h at 55 °C.

Proteinase K (10 mg/ml) was then inactivated by boiling for 10 min after digestion. PCR

was carried out in a 25 µl reaction solution containing: 1 µl of 10 mM dNTP, 1 µl of 10

mM forward and reverse primer, 2.5 µl of 1x ThermoPol buffer (New England Biolabs),

and 0.5 units of TaqPolymerase (New England Biolabs).

Primers (salt-free grade):

shoc2^{Δ22} 5'-CCATCAAGGAGCTGACCCAG-3'

5'-TCTGACCAGCCTACCTGACT-3',

shoc2^{Δ14} 5'-AGCGACTCTGTTGTCTTGTGTTA-3'

5'- AGGTTGGTGATCTGAGTGCAA-3'

10. Real-time quantitative RT-PCR

Total RNA was isolated from the pool of five embryos at 6 dpf using PureZOL/Aurum Total RNA Isolation Kit (Bio-Rad) according to the manufacturer's recommendations. Aliquots containing equal amounts of RNA were subjected to RT-PCR analysis. qPCR was performed using SoAdvanced SYBR green Supermix and a Bio-Rad CFX detection system (Bio-Rad). Relative amounts of RNAs were calculated using the comparative C_T method [162]. Sequence-specific primer sets are presented in Table. 1. The values for the samples were normalized against those for the reference gene, and the results are presented as the fold change in the amount of mRNA recovered from WT and mutant embryo. The data represent the means ± SEM from three independent experiments.

11. Western Blot Analysis using zebrafish embryos

Protein lysates were extracted from pools of 30-60 de-chorionated and de-yolked embryos at 12, 24, 48, and 72 hpf. Protein concentrations were measured using the Bio-Rad protein assay dye reagent (Bio-Rad). 35 µg of total protein per lysate was diluted with Laemmli buffer and 2.5% β-mercaptoethanol, boiled for 5 min, and then separated by SDS-PAGE on 10% polyacrylamide gels. Proteins were transferred to nitrocellulose membranes and visualized using ChemiDoc analysis system (Bio-Rad). Several exposures were analyzed to determine the linear range of the chemiluminescence signals. Quantification was performed using the densitometry analysis mode of Image Lab software (Bio-Rad). Antibodies against the following proteins were used: Shoc2 (Genetex), total ERK1/2 (tERK1/2), phosphorylated ERK1/2 and β-actin (pERK1/2, Santa Cruz Biotechnology).

12. Staining methods for zebrafish embryos

Whole embryo staining for erythropoietic cells was performed using o-dianisidine histochemistry according to previously described methods [163]. PTU (1-phenyl-2-thioure) treated de-chorionated embryos were stained for 30 min in the dark in o-dianisidine (0.6 mg/ml), 0.01 M sodium acetate, 0.65% H_2O_2, and 40% (vol/vol) ethanol. After staining, embryos were washed with PBS-T (Phosphate buffer saline with 0.1% Tween-20) and then post-fixed in 4% paraformaldehyde (PFA) overnight in 4 °C. Sudan Black B staining was performed to detect neutrophils and macrophages. Whole embryos were fixed with 4% PFA for 2 h at room temperature, rinsed in PBS, and incubated with Sudan Black B solution (2 mg/ml Sudan Black B dissolved in 70% ethanol) in the dark for 30 min. Stained embryos were then washed with 70% ethanol and stored in 90% glycerol for imaging. Histochemical staining for the myeloperoxidase activity of whole zebrafish embryos was performed according to the manufacturer's instructions (Sigma-Aldrich).

For Alcian blue staining, zebrafish larvae were washed with sterile water and fixed in 4% paraformaldehyde for 2 h at room temperature and stained according to Kimmel et al., 1998 [164]. Calcified structures were examined by acid-free Alizarin Red S staining. Embryos were fixed in 4% PFA for 2 h and stained in a 0.05% Alizarin Red S solution in water for 30 min in the dark on low agitation, rinsed in a 50% glycerol, 0.1% KOH solution to remove excessive staining, and kept at 4 °C in the same solution for imaging.

13. Isolation of hematopoietic cells from zebrafish embryos

Embryos of homozygous *gata1-DsRed* transgenic fish were collected and treated with PTU after 24 hpf.

1. Embryos were collected at 72 hpf and sedated using tricaine.

2. Embryos were incubated with 0.05% Trypsin-EDTA solution and dissociated the tissue using 20 G syringe.

3. Cells were filtered through 40 µm cell strainer (DNAse/RNAse free) to obtain a single cell suspension and spun down at 4 °C for 10 min at 3500 rpm.

4. Cell pellet was re-suspended in PBS (+ 2mM EDTA) and processed with a flow cytometer.

14. Cytology of peripheral blood

For cytological analyses, blood cells collected from zebrafish larvae were transferred onto glass slides by cytospin (2500 rpm, 3 min) and stained with May-Grünwald Giemsa stain (Sigma-Aldrich) following the manufacturer's instructions.

1. Diluted Giemsa Stain (Cat# GS500) 1:20 with deionized water.

2. Placed slides in May-Grünwald Stain (Cat# MG500) for 5 minutes.

3. Placed slides in working phosphate buffer (0.1 M, pH 7.2) for 1.5 minutes.

4. Placed slides in diluted Giemsa solution from step 1 for 15-20 minutes.

5. Rinsed slides briefly in deionized water.

6. Air dried and imaged.

15. Statistical analyses

Results are expressed as means ± SEM. The statistical significance of the differences between groups was determined using either Student's t-test or one-way ANOVA (followed by the Tukey's test). $P < 0.05$ was considered statistically significant. All statistical analyses were carried out using SigmaStat 13.0 (Systat Software Inc).

16. Photography and image analysis

Images of the phenotypes of embryos or larvae and images of whole-mount *in situ* hybridization were captured with a Nikon DS-Ri2 digital camera mounted on a dissecting microscope (Nikon SMZ18) or an inverted microscope (Nikon Eclipse Ti-U; Nikon Instruments). NIS-Elements software (Nikon) was used to calculate the body lengths, eye size and areas of Alcian blue and Alizarin Red S -positive signals. Images of mpx staining were photographed with a Leica DFC450 digital camera and May-Grünwald Giemsa staining were imaged with Leica DFC 7000 T mounted on a dissecting microscope (Leica S9D). All images were compiled in Adobe Photoshop CS6 Portable (Adobe Systems Incorporated) and resized.

B. Materials and methods used in CHAPTER 4

1. Antibodies and other reagents

EGF was obtained from BD Biosciences. Antibodies against the following proteins were used: RAF-1, glutathione S-transferase (GST), GFP, HA, phosphorylated ERK1/2 (pERK1/2), M-Ras, and GAPDH (Santa Cruz Biotechnology); Shoc2 (Proteintech); EEA1 and phosphorylated RAF-1 (pRAF-1, Cell signaling); Rab5 (BD Bioscience); RFP and Na+/K+-ATPase (Thermo Scientific), VCP (BioLegend), HUWE1 (Bethyl); ubiquitin (Covance); and CB-5083 was kindly provided by Cleave Bioscience.

2. Yeast two-hybrid screening assays

Full-length human Shoc2 was cloned into the lexA vector pB27 as an N-LexA-Shoc2-C fusion and screened against a human embryo ventricle and heart prey cDNA library. Yeast two-hybrid screens were performed by Hybrigenics SA.

3. DNA constructs and cell cultures

VCP-GFP constructs (WT, R155H, E305Q/E578Q) were purchased from Addgene (plasmid #23971, 23972, 23974). Shoc2-GST, Shoc2(LRR12-14)-GST, Shoc2-tRFP truncated mutants, Shoc2(Δ21-C)-tRFP, Shoc2-YFP, Shoc2(7KR)-YFP, PSMC5-GST, MRas-YFP, MRas-HA, YFP-RAF-1, HA-HECT and HA-Ub constructs were described previously [120]. Shoc2(Δ12-14)-GST construct was generated as described previously [120]. All constructs were verified by dideoxynucleotide sequencing. HEK 293FT cells (Invitrogen), Cos1 (ATCC), and stable cell lines (SR, SY, S2G, Δ21-C) (derivative of Cos1

cells) were cultured in Dublecco Modified Eagle's Medium (DMEM, Sigma) containing 10% fetal bovine serum (FBS, Biowest) and Penicillin-Streptomycin solution (Hyclone). Primary fibroblasts (GM22757, GM23284, GM22600, GM22085) were obtained from Coriell Institute and were maintained in FibroLife S2 Cell Culture Medium containing FibroLife S2 LifeFactors (Lifeline Cell Technology).

4. Transfection

DNA transfections were performed using PEI (Neo Transduction Laboratories) reagent. Briefly, 200 µl of DMEM, 2 µg of DNA construct, and 7 µl of PEI reagent were mixed together in a 1.5 ml Eppendorf tube and incubated at room temperature for 20 min. The ratio of DNA:PEI was always kept as 1:3.5.

5. siRNA transfections

To silence protein expression, small interfering RNA (siRNA) transfections were performed at 24 to 36 h intervals according to the manufacturer's recommendations, using DharmaFECT reagent 2 (Thermo Fisher Scientific/Dharmacon). The siRNA sequence used to target the HUWE1 and Shoc2 transcripts were described previously [120]. The following protocol was implemented:

1. Plate cells a day before transfection to ensure that the cells are actively dividing and reach 70% confluence cell density at the time of transfection.

2. Prepare a 20 µM siRNA stock solution using siRNA buffer.

3. In separate tubes, prepare the following:

Tube 1 – Add 2.5 µl of siRNA stock to 100 µl of serum-free medium.

Tube 2 – Add 7 µl of DharmaFECT reagent 2 to 100 µl of serum-free

medium.

4. Mix the contents of each tube gently by pipetting carefully up and down and incubate for 5 min at room temperature.

5. Add contents of Tube 1 to Tube 2. Mix by pipetting carefully up and down and incubate for 20 min at room temperature.

6. Add the mixture onto the cells and incubate for 24-48 h.

6. Sucrose gradient subcellular fractionation

Sucrose gradient subcellular fractionation was performed as described previously [116, 165]. Briefly, cells were cultured on 15-cm^2 dishes, washed, and collected using a rubber policeman into cold PBS. The cells were then pelleted, resuspended in homogenization buffer (250 mM sucrose, 3 mM imidazole (pH 7.4), EDTA 1 mM, protease and phosphatase inhibitors, and 0.03 mM cycloheximide), and homogenized using 22G needle. Homogenization was carried out until ~90% of cells were broken without major breakage of the nucleus, as carefully monitored under the microscope. Samples were then centrifuged for 10 min at 2000 g at 4°C and the resulting supernatant was designated as the post nuclear supernatant (PNS). The PNS was adjusted to 40.6% sucrose concentration using 62% sucrose (2.351 M sucrose, 3 mM imidazole (pH 7.4), 1 mM EDTA, sterile water) and then overlaid with 1.5 volumes of 35% sucrose (1.177 M sucrose, 3 mM imidazole (pH 7.4), 1 mM EDTA, sterile water) and the rest of the tube was filled with 8.6% sucrose. Sucrose gradients were centrifuged for 6 h at 100,000 g at 4°C and the crude endosomal fraction and Golgi/ER membrane fraction were collected. The percentage of each sucrose

solution (HB buffer, 35% and 62%) used in these experiments were accurately adjusted using a refractometer.

7. Immunoprecipitation and Western blot analysis

Cells were placed on ice and washed with Ca^{2+}- and Mg^{2+}-free phosphate-buffered saline (PBS), and the proteins were solubilized in 20 mM HEPES (Sigma, pH 7.6), containing 10 mM NaCl, 1.5 mM $MgCl_2$, 1 mM EDTA (Sigma), 1 mM EGTA (Sigma), 0.5 mM phenylmethylsulfonyl fluoride (Sigma), 10 μg/ml of leupeptin (Roche), 10 μg/ml of aprotinin (Roche), 5 μg/ml of pepstatin A (Sigma), and 50 mM β-glycerophosphate (Sigma) for 15 min at 4 °C. Lysates were then centrifuged at $2,500 \times g$ for 15 min to remove insoluble material. Cleared lysates were incubated with appropriate antibodies for 2 h, and precipitated using protein A- or G-Sepharose. Immunoprecipitates were denatured in the sample buffer at 95 °C, resolved by electrophoresis. Proteins were transferred from SDS-polyacrylamide gels to nitrocellulose membranes and probed by Western blotting with various antibodies, followed by chemiluminescence detection (Bio-Rad). Several exposures were analyzed to determine the linear range of the chemiluminescence signals. Quantification was performed using the densitometry analysis mode of Image Lab software (Bio-Rad).

8. Denaturing immunoprecipitation for ubiquitination assay

Denaturing immunoprecipitation was performed as described previously [120]. Briefly, cells were lysed in denaturing buffer (50 mM Tris, pH 7.5, 150 mM NaCl, 1% Triton, 1% SDS, 1 mM Na_3VO_4, 10 mM NaF, 10 μM MG132) and boiled for 10 min.

Lysates were diluted 1:10 with the same buffer without SDS and incubated with the appropriate antibody overnight with rotation at 4 °C. Protein G-agarose (GE Healthcare Life Sciences) was added, and the beads-agarose were washed four times in lysis buffer (without SDS). Proteins were eluted at 95 °C in SDS loading buffer, separated by SDS-PAGE, transferred to nitrocellulose membrane, and probed by Western blotting with various antibodies, followed by chemiluminescence detection.

CHAPTER 3

"Hematopoietic and neural crest defects in zebrafish *shoc2* mutants:
a novel vertebrate model for Noonan-like syndrome"

Abstract

The extracellular signal-related kinase 1 and 2 (ERK1/2) pathway is a highly conserved signaling cascade with numerous essential functions in development. The scaffold protein Shoc2 amplifies the activity of the ERK1/2 pathway and is an essential modulator of a variety of signaling inputs. Germline mutations in Shoc2 are associated with the human developmental disease known as Noonan-like syndrome with loose anagen hair (NSLH). Clinical manifestations of this disease include congenital heart defects, developmental delays, distinctive facial abnormalities, reduced growth and cognitive deficits, along with hair anomalies. The many molecular details of pathogenesis of the Noonan-like syndrome and related developmental disorders, cumulatively called RASopathies, remains poorly understood. Mouse knockouts for Shoc2 are embryonic lethal, emphasizing the need for additional animal models to study the role of Shoc2 in embryonic development. Here, we characterize a zebrafish *shoc2* mutant, and show that Shoc2 is essential for development and that its loss is detrimental for neural crest development and for hematopoiesis.

Introduction: a novel vertebrate model for Noonan-like syndrome with loose anagen hair (NSLH).

Patients diagnosed with NSLH display abnormalities that are very broad phenotypically and often are more severe than patients with Noonan syndrome [153, 155, 166, 167], raising the questions of how mutations in Shoc2 contribute to a syndrome with a wide-spectrum phenotype, and what are the biological activities regulated by Shoc2-transmitted ERK1/2 signals. As a Shoc2 knockout in the mouse results in early embryonic lethality, additional animal models are needed to dissect the role of this important scaffolding protein during embryogenesis.

To investigate the role of Shoc2 in tissue development and morphogenesis, we have exploited the powerful zebrafish model (*Danio rerio*). Zebrafish were first introduced as a vertebrate model system in early 1980s and since have emerged as an important genetic system to study normal human development [168-174]. Molecular pathways in zebrafish are highly conserved and 70% of human genes have orthologues in zebrafish, suggesting that most human pathogenesis could be modeled in zebrafish [172]. Zebrafish have most of the vital organs seen in humans such as brain, central nervous system, kidney, pancreas, liver, intestine, heart, ear, nose, muscle, skin, blood, vasculature, cartilage, and bones. Other advantages that make zebrafish a powerful vertebrate model include fast early development on the order of a few days, ability to generate a large number of progeny, and the external development and transparency of zebrafish embryos which enables monitoring and high-resolution imaging of very early developmental events. Zebrafishes' external development allows them to be easily genetically manipulated. DNA, RNA, and morpholino can be readily injected into the

one-cell stage embryos [175]. Previous studies using zebrafish have played a key role in defining the core Ras-ERK1/2 pathway and have provided fundamental insights into the understanding of developmental abnormalities of other RASopathies [173, 176, 177].

The study presented in this chapter shows that both morpholino-mediated knockdown and CRISPR/Cas9 mutagenesis of Shoc2 in zebrafish results in multiple deficiencies during embryogenesis, including gross defects in blood cell differentiation and abnormal craniofacial development. Our observations that *shoc2* morphants and Shoc2 CRISPR/Cas9 mutants (crispants) have systemic defects in neural crest specification and hematopoiesis underscore the central role of Shoc2 in embryogenesis. Our finding that the loss of Shoc2 induces an array of developmental defects emphasizes its essential role in coordinating activities of the linear components of the ERK1/2 pathway. Moreover, we have developed and characterized a heritable model of Shoc2 that exhibits many of the clinical hallmarks associated with the RASopathies, which can now be used to decipher the molecular mechanisms underlying these diseases.

<center>**Results**</center>

1. Shoc2 in zebrafish

Bioinformatics searches identified one Shoc2 zebrafish orthologue that is highly homologous to human Shoc2 at the amino acid level, sharing 88% identity [111]. The zebrafish *shoc2* gene contains 9 exons, is located to chromosome 22 and predicts a 62.7-kDa protein of 561 amino acids. Comparison to the human Shoc2 protein sequences reveals significant conservation in the fold of the LRR domains, suggesting that these functional motifs have been conserved across evolution (**Figure 3.2**). To determine the temporal expression pattern of *shoc2,* we performed reverse transcription PCR (RT-PCR) using RNA templates obtained from embryos at 3, 6, 12, 24, 30, 48, and 72 hours post fertilization (hpf, **Figure 3.3**). RT-PCR confirmed that *shoc2* is maternally inherited and is expressed through all the analyzed time points. Shoc2 protein expression at early stages was confirmed using specific antibodies (**Figure 3.3**). We also examined the expression of *shoc2* by *whole-mount in situ* hybridization between the stages of 6 hpf and 2 dpf and found that *shoc2* is expressed ubiquitously during early development. Notably, at 24 hpf *shoc2* was expressed in the dorsal aorta and was detectable in the somite boundaries (**Figure 3.4**).

2. Morpholino knockdown of *shoc2*

To explore the function of Shoc2 during embryogenesis, we first used two different translation-blocking morpholino antisense (MOs) oligonucleotides to inhibit expression of *shoc2* at early stages of development (**Figure 3.5**). The effectiveness of

gene knockdown by these translation blocking MOs was confirmed by western blot analysis, and showed that the *shoc2* morpholino was highly efficient and its translation-blocking activity lasted through 3 dpf (**Figure 3.6**). Western blots of 3 dpf whole-embryo extracts derived from *shoc2* morphants also revealed a clear reduction of phospho-ERK1/2 in knockdown embryonic tissue, confirming that Shoc2 depletion leads to decreased levels of phosphorylated ERK1/2 in zebrafish (**Figure 3.6**). Both MOs produced similar phenotypes when injected into 1-cell-stage embryos (data not shown), and MO1 was used for all subsequent analyses. A standard control MO was used to control for non-specific phenotypes resulting from the microinjection procedure. Survival of MO-injected and un-injected embryos between 8 and 24 hpf was not significantly different across *shoc2* morphants (76.7±10.7%), control morphants (84.6±17.5%), and un-injected embryos (81.9±21.3%).

Control and *shoc2* MO-injected embryos were categorized based upon their morphology and developmental stage at 24 and 48 hpf using standard staging criteria [161]. At 24 and 48 hpf, morphological markers (including the presence or absence of a beating heart) were scored to determine the developmental stage. Nearly all embryos injected with the standard control MO were at the correct developmental stage at 24 hpf (98%) and showed no overt morphological changes. Among the *shoc2* morphants without developmental delay (90%), the body shape, head shape, and presence/absence of pericardial effusion were scored at 48 hpf, and the embryos were categorized as mild, moderate or severe. *Shoc2* morphants in the "mild" category displayed no developmental delay or overt morphological changes when compared to control morphants. This category represented a very small number of *shoc2* morphants (2%). *shoc2* morphants in

the "moderate" category were also at the correct developmental stage, but displayed mild body torqueing, with spinal curvature. Moderate category *shoc2* morphants also displayed mild brain malformation, large yolks, and kinked tails. The majority of *shoc2* morphants were categorized as "severe" and displayed a body torque with malformations of the tail and brain, and showed reduced circulation of blood cells within the dorsal aorta and posterior veins. We did not observe profound alterations in *shoc2* morphant heart structure; however, severe morphants did display a slightly faster, statistically significant heart rate at 72 hpf (**Figure 3.7**). All embryos in this category displayed enlarged yolks. This phenotype was observed in 94% of *shoc2* MO1 injected embryos (n>200, from 4 independent experiments). No pooling of red blood cells was observed at any site away from circulation in the *shoc2* morphants.

Since hematopoietic stem cells (HSCs) and angioblasts originate from shared pluripotent precursors, blood and blood vessel formation are closely related in early developmental stages [178]. Thus, we examined whether vascular angiogenesis was affected by Shoc2 knockdown. *Shoc2* MOs were injected into zebrafish embryos in which endothelial cells were marked by the expression of green fluorescent protein (*fli1a:EGFP)*, allowing for a more detailed analysis of vascular development [179]. At 22–48 hpf, the major vessels, such as dorsal aorta, caudal artery, posterior cardinal vein and caudal vein appeared normal, indicating normal vasculogenesis (not shown). However, at 72 hpf defective vasculature branching was visible with the most significant changes in the sub-intestinal vein (SIV; **Figure 3.8**). The SIV of 90% (n=61, from three independent experiments) of *shoc2* MO-injected embryos exhibited reduced size/number of vessel branches and/or ectopic blood vessels when compared to the basal defect level

44

of control embryos. Vascular defects did not appear to correlate directly with cardiac defects, as we observed embryos with vascular abnormalities that did not display major pericardial effusion or valvular insufficiency as assessed by a to-and-fro movement of blood within the heart.

The zebrafish hematopoietic system has been studied comprehensively. The genetic programs regulating the emergence of HSCs and blood development are largely conserved in mammals and zebrafish [174, 180, 181]. Zebrafish and mammals share major blood cell types that are generated from common lineages of HSCs and have two waves of hematopoiesis [181, 182]. The first wave, **primitive hematopoiesis**, occurs during early embryonic development and generates erythromyeloid progenitors (EMPs) that give rise to primitive erythrocytes and some primitive macrophages. The second wave, **definitive hematopoiesis**, gives rise to the HSCs that have the potential to both self-renew and generate all adult hematopoietic cell types [181, 182].

Primitive hematopoiesis of zebrafish occurs in two intraembryonic locations: the intermediate cell mass (ICM) and the anterior lateral mesoderm (ALM, **Figure 3.1**). Cells within the ICM differentiate into the endothelial cells of the trunk vasculature and proerythroblasts [183]. Concurrently, myelopoiesis is initiated in the ALM. Primitive erythropoiesis is regulated intrinsically by transcription factors expressed in erythroid cells and extrinsically by erythropoietin secreted from surrounding cells and tissues. The transcription factor *gata-1a* activates the expression of erythroid-specific genes to promote the production of erythrocytes and roughly, 300 *gata-1*-positive proerythroblasts in the ICM enter the circulation around 24 hpf and mature into erythrocytes. These primitive erythrocytes are morphologically different from adult zebrafish erythrocytes,

which have less cytoplasm and large elongated nuclei. Unlike mammalian erythrocytes that are nucleated only in their primitive wave and loose nucleus in the adult all zebrafish erythrocytes are nucleated. The primitive erythrocytes account for all circulating erythrocytes for the first 4 days post fertilization (dpf) [171, 174, 181-183].

Similar to cells in the ICM, the cells in the ALM contribute to both blood and vascular development and express transcription factors including *fli1a, gata-2, lmo2* and *scl* [174]. A subset of the cells in ALM expresses *pu.1,* a member of the ets family of transcription factors essential to the development of myeloid cells [184, 185].
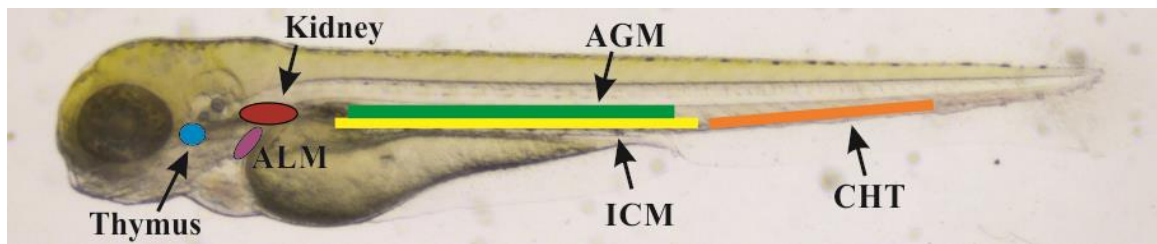
Figure 3.1 Hematopoietic ontogeny in the developing zebrafish embryo.
Primitive erythrocytes develop in the ICM while the primitive macrophages arise in ALM. Later, HSCs emerge in the AGM region, migrate to the CHT and eventually see the thymus and kidney. ICM- intermediate cell mass, ALM-anterior lateral mesoderm, AGM- aorta gonad mesonephros, CHT- caudal hematopoietic tissue, HSCs-hematopoietic stem cells.

The second wave, definitive hematopoiesis, takes place in the aorta-gonad-mesonephros (AGM, **Figure 3.1**). During definitive hematopoiesis, HSCs emerge from the ventral wall of the dorsal aorta (DA) of the AGM region. HSCs are responsible for the production of all mature blood cells (erythrocytes, granulocytes, monocytes, lymphocytes and thrombocytes) [174, 181, 183]. The involved transcription factors (i.e.

c-myb and *runx1*) and signaling pathways that regulate the formation of HSCs in a zebrafish are well conserved with mammals. After its emergence, the AGM progenitor cells first migrate to the caudal hematopoietic tissue (CHT, **Figure 3.1**) which is located posterior to the yolk extension and stay intermediately. HSCs then move to the thymus where the lymphocytes mature. Finally, HSCs reach their final destination, the kidney marrow, which is the human equivalent of bone marrow (**Figure 3.1**) [186]. In the kidney marrow, HSCs undergo unlimited self-renewal and also differentiate to produce all hematopoietic cell types throughout the zebrafish lifetime [182, 187].

To validate hematopoietic defects found in *shoc2* morphants , I utilized *o*-dianisidine staining to detect hemoglobin of erythropoietic cells [163, 188]. In control embryos, hemoglobin-positive cells were found soon after circulation started at 26 hpf, whereas *shoc2* MO-injected embryos completely lacked *o*-dianisidine staining (**Figure 3.9.A**). At 48-72 hpf erythrocytes in control embryo were robustly stained with *o*-dianisidine and were prominent in the ducts of Cuvier, over the yolk sac, while in *shoc2* MO-injected embryos we observed a marked decrease in the intensity of *o*-dianisidine staining. I then tested the specificity of MO-induced phenotypes by a mRNA rescue assay. When wild type (WT) human *shoc2* mRNA was co-injected with *shoc2* MO, a rescue of *shoc2* MO-induced defects in erythrocyte circulation defects was observed (**Figure 3.1.B and C**). Since the blood deficiencies were detected at the very early stages of hematopoiesis, I then tested whether other blood lineages were affected in *shoc2* morphants. Sudan Black B staining, which detects lipids in neutrophils and monocytes [189], was utilized to examine whether *shoc2* depletion affected the myeloid lineage. A significant reduction in the number of neutrophils in caudal hematopoietic tissue (CHT)

of *shoc2* morphants (93%, or 105/113 injected) in comparison with control-MO injected

embryos at 72 hpf was detected (**Figure 3.9.D**), indicating that the depletion of *shoc2*

causes defects in myelopoiesis. The cells positive for Sudan Black B staining were scored

in 5 somites at the CHT region after the yolk extension (**Figure 3.9.E**). Together, these

data suggest that Shoc2 is involved in general blood cell differentiation and possibly

plays a role in both the primitive and definitive waves of hematopoiesis [190].

3. Generation of zebrafish *shoc2* heritable mutants

Although MO injections readily permit transient knockdown of gene expression,

their efficacy is limited to the first few days post-fertilization. To gain a better

understanding of the roles of Shoc2-mediated ERK1/2 signals during development, as

well as allow for a quantitative phenotypic assessment, the CRISPR/Cas9 genome editing

approach was employed to develop stable lines of zebrafish harboring germline mutations

in *shoc2* [162]. Using this approach, I engineered sgRNA directing gene editing to

coding exons 2 and 3. Neither of the sites targeted by the sgRNAs overlapped with the

MO target sites (**Figure 3.10.A**). Multiple independent target-specific mutant alleles for

shoc2 were identified in the F1 generation (**Figure 3.10.B**). Mutations in the target region

were confirmed by both high resolution melting analysis and sequencing analysis (**Figure

3.11**). Each of the introduced mutations included a deletion and/or insertion within these

coding exons, introducing a frameshift and premature stop codon that would be expected

to truncate the Shoc2 protein. Zebrafish mutant lines harboring null mutations in exon 2

($shoc2^{\Delta 22}$) and 3 ($shoc2^{\Delta 14}$) were used in the following experiments. Both mutants carry

frame-shift mutations (c.357-378, del and c.671-684, del) that truncate the protein by 121

and 229 amino acids, respectively, predicting the loss of a large portion of Shoc2's LRR region (**Figure 3.12.A**). When *shoc2* mRNA was assessed in homozygous *shoc2^{Δ22}* and *shoc2^{Δ14}* mutants, a corresponding reduction in the size of the amplified fragments was detected (**Figure 3.12.B**). Protein expression analyses using an antibody to Shoc2 confirmed the loss of full-length Shoc2 in *shoc2^{Δ22}* and *shoc2^{Δ14}* alleles (**Figure 3.13**), while heterozygous Shoc2 alleles did not show decreases in Shoc2 protein (**Figure 3.14**). Importantly, we also observed decreased levels of pERK1/2 in *shoc2^{Δ22}* and *shoc2^{Δ14}* mutant larvae (**Figure 3.13**). To avoid potential off-target effects, *shoc2$^{Δ22/+}$* and *shoc2$^{Δ14/+}$* mutants were outcrossed to WT for three generations prior to the further study.

Zebrafish heterozygous for either *shoc2* mutant alleles were viable, fertile, and displayed no overt phenotypes. When heterozygous adults were in-crossed, no severe morphological defects were detected in the progeny prior to 5 dpf. However, at later stages of development, pleiotropic effects on larval morphology that became progressively severe were observed in the *shoc2$^{-/-}$* larvae. At 6 dpf, 90–100% of *shoc2^{Δ22}* and *shoc2^{Δ14}* mutant larvae developed edema of the heart cavity and along the trunk, yolk sac and yolk extension, around the eyes and became lethargic (**Figure 3.15**). The swim bladders of *shoc2^{Δ22}* and *shoc2^{Δ14}* larvae were underinflated and I observed a small but significant 1.25 fold increase in the heart beat of the severely edemic 6 dpf larvae when compared to WTs, the likely result of the increased edema at this stage. Further quantitative survival studies indicated that at 6 dpf, *shoc2^{Δ22}* and *shoc2^{Δ14}* larvae began to die, with none surviving beyond 9 dpf. All of WT and heterozygous larvae survived to 10 dpf and displayed the expected Mendelian ratio for homozygous WT vs. Heterozygous genotypes (1:2) (**Figure 3.16**). Similar severe edema was observed for the compound

mutant of *shoc2 $^{\Delta 22}$* and *shoc2 $^{\Delta 14}$* (**Figure 3.17**). Because the observed defects manifested themselves at 5-6 dpf, we hypothesize that the presence of maternally inherited *shoc2* allow *shoc2* crispants to develop somewhat normally during the first few days post fertilization. Taken together, these data demonstrate that loss of Shoc2 is detrimental to the embryonic zebrafish development.

4. Effects of Shoc2 mutants on neural crest development

Closer examination of *shoc2 $^{\Delta 22}$* and *shoc2 $^{\Delta 14}$* nulls indicated possible changes in craniofacial morphology. I found that at 6 dpf, *shoc2 $^{\Delta 22}$* and *shoc2 $^{\Delta 14}$* mutants were shorter in length than WT larvae, displayed smaller eye surface area, a narrow spinal cord, and had markedly abnormal craniofacial skeletons (**Figure 3.18.A, B, and D**). Morphological analyses of Alcian-Blue-stained samples revealed that *shoc2 $^{\Delta 22}$* mutants exhibited a prominent defect in Meckel's cartilage, which in *shoc2 $^{\Delta 22}$* mutants curved downwards and did not extend as far anteriorly as that of WT larvae. Additionally, we found that the ceratohyal cartilage of *shoc2* mutants were smaller and shifted farther posteriorly, or were missing entirely. To quantitatively evaluate the abnormality of the cartilage tissues, I analyzed the positional relationships between the Meckel's cartilage and the two ceratohyal cartilages, the length of ceratohyal arch, the angle between ceratohyals arch, and the total length of craniofacial cartilage structures (**Figure 3.18.C**). Significant changes were found in all of these parameters in *shoc2* mutants, indicating that Shoc2-mediated signaling is required for proper signal transmission during the development of the craniofacial structures.

Intramembranous (dermal) and cartilage bones appear during early larval development. By 6 dpf, three ossified teeth and a number of pharyngeal arches and other ossified bone structures can be visualized by Alizarin Red S staining, which detects calcific deposition by cells of an osteogenic lineage (**Figure 3.19**) [191]. I next tested whether bones form normally in homozygous *shoc2^{A22}* and *shoc2^{A14}* mutant larvae. Alizarin Red S staining demonstrated a strong reduction in calcification of craniofacial bones. We found that parasphenoid, notochord, and branchiostegal ray 1 and 2 were completely missing and opercle, ceratobranchial, and cleithrum bones were significantly deformed/delayed in *shoc2^{A22}* and *shoc2^{A14}* null mutants (**Figure 3.19 and 3.20**). Together, these data suggest that *Shoc2* also contributes to bone formation or remodeling.

Interestingly, mutations in *shoc2* also affected the pigmentation pattern of *shoc2* null larvae. At 6 dpf, WT larvae displayed a distinct uniform pattern of head and the lateral stripe melanophores (**Figure 3.21**). In contrast, *shoc2^{A22}* and *shoc2^{A14}* null larvae lost the regularity of melanophore patterning and presented with overlapping lentigines. The abnormal appearance of the melanophores in mutant larvae can be attributed to defects in patterning of regeneration and metamorphic melanophores, suggesting abnormal migration or differentiation of this lineage. Alternatively, this may be a result of a defective visual background adaption response due to the impairments in eye development. Collectively, these data suggest a defect in the development of the neural crest, which was corroborated by the findings that expression of the neural crest pluripotency marker *foxd3* was increased in *shoc2* null larvae (**Figure 3.22**). Additionally, high *shoc2* expression in the *sox10:RFP* positive cells isolated from the *Tg(sox10:RFP)* transgenic fish was detected (**Figure 3.23**), indicating that Shoc2 may

regulate neural crest specification in a cell-autonomous manner. Given the only known function of Shoc2 is to accelerate ERK1/2 signals, we conclude that altered expression of *foxd3* and neural crest cell development are the consequence of impaired Shoc2 function and resulting in decreased ERK1/2 activity.

5. Effects of Shoc2 mutants on hematopoiesis

Considering the blood phenotypes induced by the Shoc2 MO injections, I examined circulating blood in *shoc2$^{\Delta22}$* and *shoc2$^{\Delta14}$* null larvae. Consistent with the observations in the *shoc2* morphants, *o*-dianisidine staining revealed a significant decrease in erythropoietic cells in *shoc2$^{\Delta22}$* compared to WT larvae (**Figure 3.24.A**). Relative concentrations of hemoglobin were evaluated by the intensity of red color and scored in arbitrary units of intensity (a.u.i.) from 0 to 5, 0 being the weakest and 5 the strongest. The erythrocytes were scored in the ventral side of the head of the WT and *shoc2$^{\Delta22}$* null larvae (**Figure 3.24.B**). To determine whether macrophage and neutrophil numbers were affected, histochemical staining for myeloperoxidase (mpx, an enzyme characteristic of neutrophil primary granules) was performed (**Figure 3.24.C**). The mpx-positive cells located in 5 somites after the yolk extension were scored. Mpx-enzymatic activity assays detected a significant reduction in numbers of neutrophils in *shoc2$^{\Delta22}$* and *shoc2$^{\Delta14}$* null larvae when compared to the WT larvae (**Figure 3.24.D and 3.25**). The results of staining for mpx and hemoglobin indicate that the loss of Shoc2 abrogates differentiation of cells of different blood lineages. The observed changes were not likely due to the excessive apoptosis, since arcidine orange staining that visualizes apoptotic

52

cells showed no significant differences in $shoc2^{\Delta22}$ null larvae when compared to WT (data not shown).

I next explored possible mechanisms for how Shoc2 regulates the differentiation of specific blood lineages. The transcription factors *gata-1a*, *gata-2a, and pu.1* were reported to be early key factors in the process of primitive erythropoiesis and myelopoiesis. Quantitative transcription analysis using RNA isolated from WT, $shoc2^{\Delta22}$ and $shoc2^{\Delta14}$ larvae was performed. Expression levels of *gata-1a*, *gata-2a, mpx,* and *pu.1* were significantly lower in mutant larvae compared to WT larvae. Moreover, expression levels of other markers of blood lineages such as *l-plastin* (leukocytes,[192]), *rag-1* (B- and T-cells,[193]), *lck* (T-cells,[194]) were down-regulated approximately two-fold in *shoc2* mutants (**Figure 3.26**). Similar changes in expression of the relevant transcription factors were detected for $shoc2^{\Delta14}$ mutants (**Figure 3.27**). Therefore, the gene expression data indicate that loss of *shoc2* results in dysregulation of hematopoietic gene expression programs. Moreover, we found that *shoc2* is highly expressed in *gata1a:dsRed* cells isolated from *Tg(gata1a:dsRed)* transgenic embryos (**Figure 3.28**), indicating that *shoc2* is present in erythroid progenitor cells and therefore may regulate definitive hematopoiesis cell-autonomously.

Finally, I evaluated the morphology of circulating blood cells in detail in WT and *shoc2* mutants. Individual WT and mutant 6 dpf larvae were bled, and peripheral blood cells were deposited on slides by centrifugation and then stained using the May-Grünwald Giemsa method. The classification of normal teleost blood cells in various developmental stages is well-established [180]. Based on their distinct cell morphologies, we detected various sub-types of blood cells in both WT and mutant blood samples

(**Figure 3.29**). As expected, the majority of circulating cells were erythroid (**Figure 3.30**). The erythroid cells in zebrafish, similarly to the other teleosts, are elliptical and possess compact nuclei and cytoplasm filled with hemoglobin with typical size of 7-10µm [171]. Mutations in *shoc2* caused severe anemia, as significantly fewer erythrocytes were detected in the circulation (**Figure 3.30.A and B**). In addition, erythrocytes of *shoc2^{A22}* 6 dpf larvae were spherical, and had a considerably lower cell surface area as well as significantly smaller nuclei (**Figure 3.30B, C, and D**). Thus, based on general changes in blood cell numbers, loss of multiple blood lineages and altered erythrocyte surface area, the late pleiotropic phenotype of *shoc2^{A22}* larvae is associated with the loss of early ERK1/2 signals in hematopoiesis.

D. rerio Shoc2
aa 79-542

H. sap Shoc2
aa 79-553
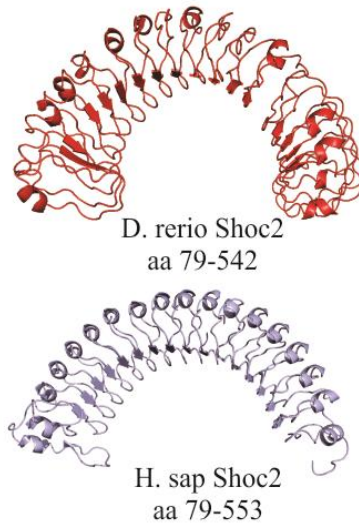
Figure 3.2 Homology models of zebrafish and human Shoc2, residues 79-561 and 79-582, respectively, were constructed using the published structure of Arabidopsis Flg22-FLS2-BAK1 immune complex (PDB id: 4MN8) and Leptospira interrogans LRR protein LIC11098 (PDB id: 4U08) as templates for zebrafish and human Shoc2 models correspondingly. The modeling was done using the I-TASSER server and figures were prepared using PyMol software.

(A)
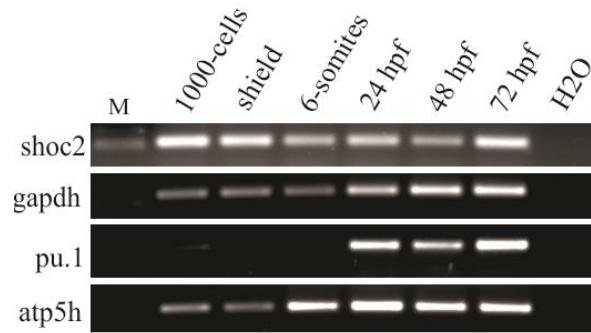
(B)
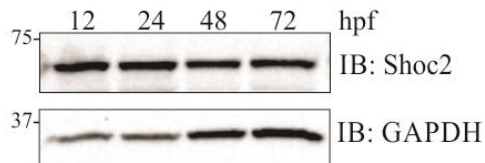
Figure 3.3 Shoc2 gene and protein expression in early development of zebrafish. **(A)** *shoc2* mRNA was detected using RT-PCR at the indicated times. *pu.1*, *atp5h* and *gapdh* were used as reference genes. *pu.1* was previously shown to express after 16 hpf. **(B)** Western blot analysis of zebrafish embryos. Embryos were harvested for immunoblotting at indicated time points. The expression of Shoc2 and GAPDH was analyzed using specific antibodies. GAPDH was used as a loading control.
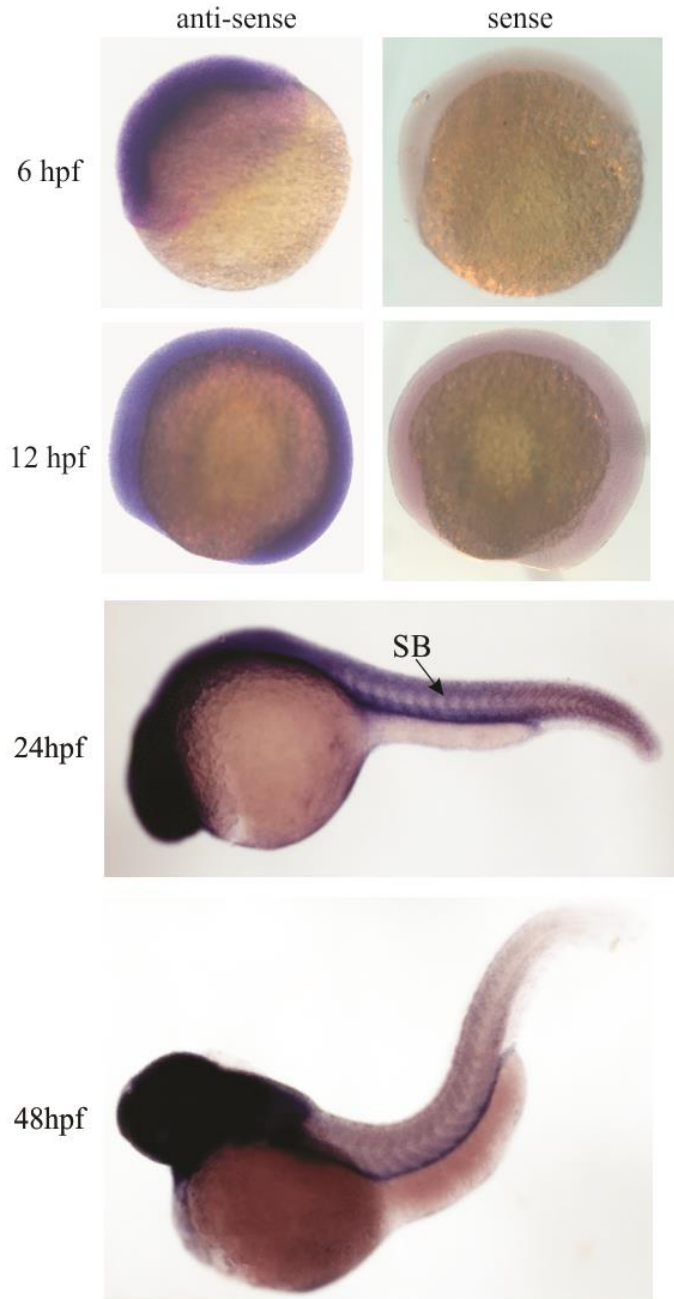
Figure 3.4 Expression pattern of *shoc2* in zebrafish embryonic development.
RNA *in situ* hybridization with antisense probes for Shoc2 in WT embryos at 6, 12, 24 and 48 hpf. An extensive anterior expression in the head region and the somite boundaries (black arrow) was observed at later stages (24 and 48 hpf). Images are in lateral views, anterior to the left.
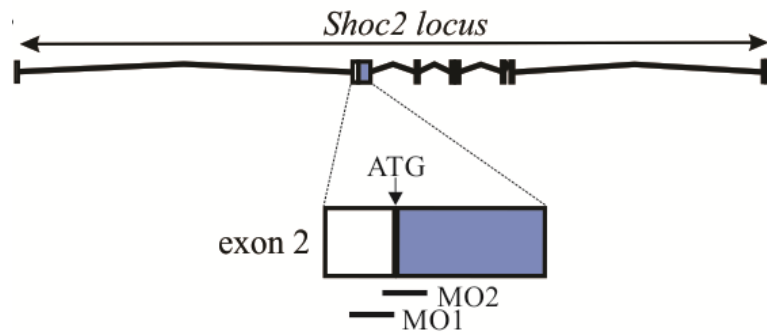
Figure 3.5 Schematic representation of Shoc2 loci and MO targeting sites.

Shoc2 intron-exon structure with two translation-blocking MOs targeting sites at exon 2 are depicted. MO- Morpholino.
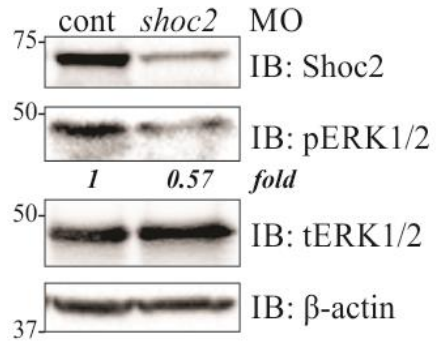
Figure 3.6 Western blot analysis of MO-injected embryos.

Embryos injected with *shoc2* and control MO were harvested for immunoblotting at 72 hpf. The expression of indicated proteins was analyzed using specific antibodies. β-actin was used as a loading control.

(A)

(B)

(C)
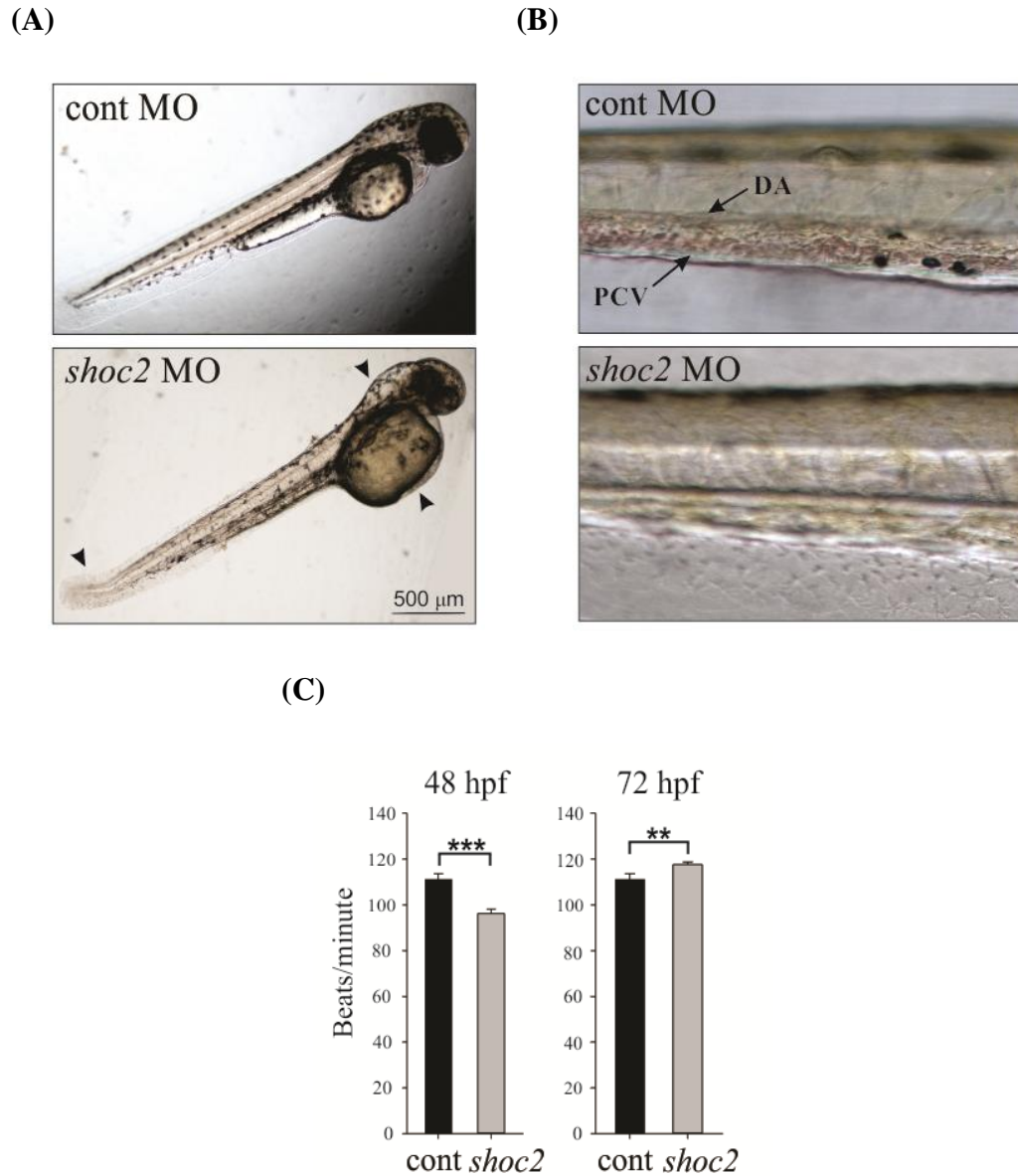
Figure 3.7 Characterization of *shoc2*-MO injected embryos. (A) Representative body images of control and *shoc2* morphants at 48 hpf. One-cell stage embryos were injected with the standard control MO and *shoc2* ATG MO1. The optimal dose for microinjection of MO was determined as that which resulted in specific defects but did not cause gross lethality or global defects. As shown, at 48 hpf, 70.4% (57 out of 81) of *shoc2* morphants displayed an enlarged hindbrain (arrowhead), enlarged yolk, and a posterior kink in the tail (arrow). **(B)** Representative body images of control and *shoc2* morphants at 72 hpf. *shoc2* MO-injected embryos showed reduced numbers of cells in circulation when compared to control embryos. **(C)** The cardiac heart rate of control and *shoc2* morphants

was measured at 48 and 72 hpf. Significant difference in heart rate was observed in *shoc2*-morphants when compared to WT. Error bars represent means with SEM. ***$p <$ 0.001 and **$p < 0.05$ (Student's t-test). MO- morpholino, hpf- hours post fertilization, M- DNA marker, PVC- posterior cardinal vein, DA- dorsal aorta.

(Experiments performed by Marie Forbes-Osborne and analyzed by HyeIn Jang)
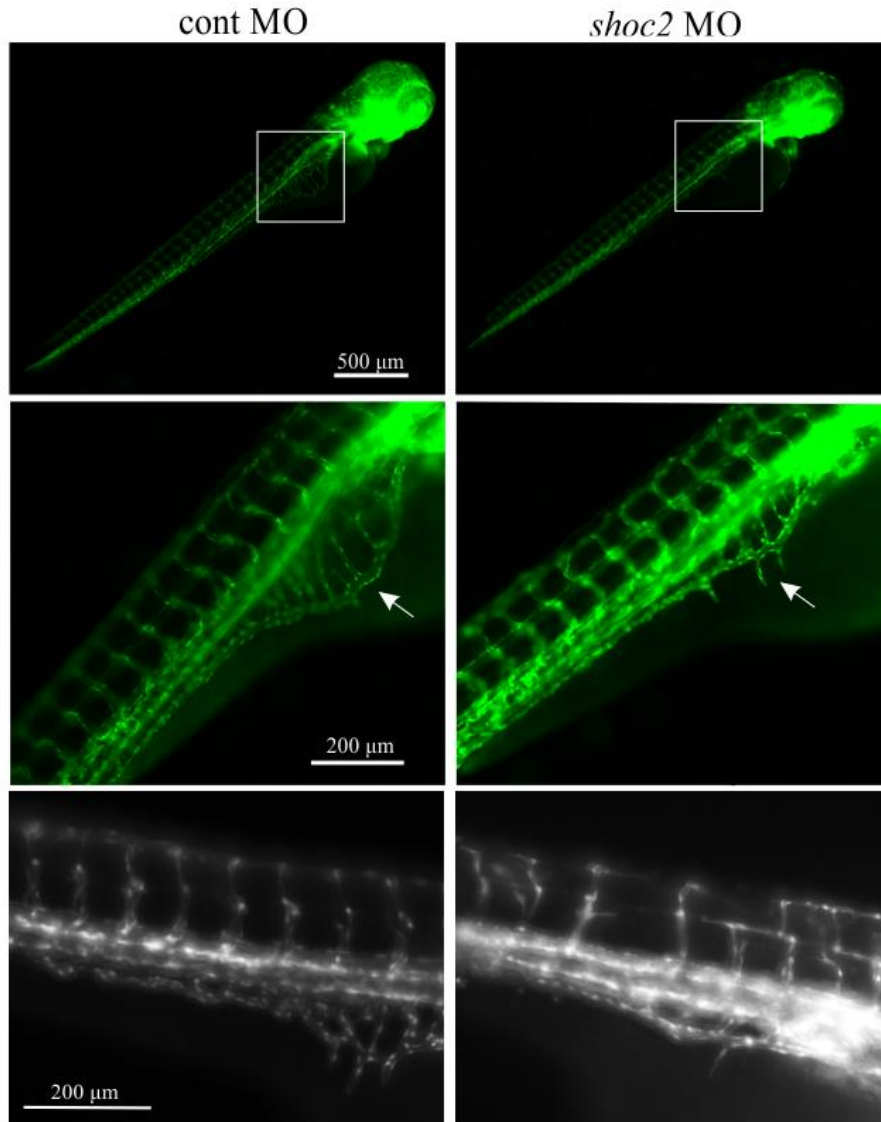
Figure 3.8 Disruption of zebrafish *shoc2* results in vasculature defects.
fli1a:EGFP embryos were injected with control or *shoc2* MO. Control embryo showed well-organized inter-segmental vessels, while embryos injected with *shoc2* MO showed aberrant trunk blood vessels and disorganized sub-intestinal vein, indicated by arrow. All embryos shown in lateral view with anterior to the right and dorsal to the top. Images are taken at 3 dpf.

(A)

	26 hpf	48 hpf	72 hpf
cont MO			
shoc2 MO			

(B)

48 hpf

cont MO

shoc2 MO

shoc2 MO + *hshoc2* mRNA

(C)

(D)

72 hpf

cont MO

shoc2 MO

(E)

number of cells/field

***

n=20

n=22

cont MO   shoc2 MO
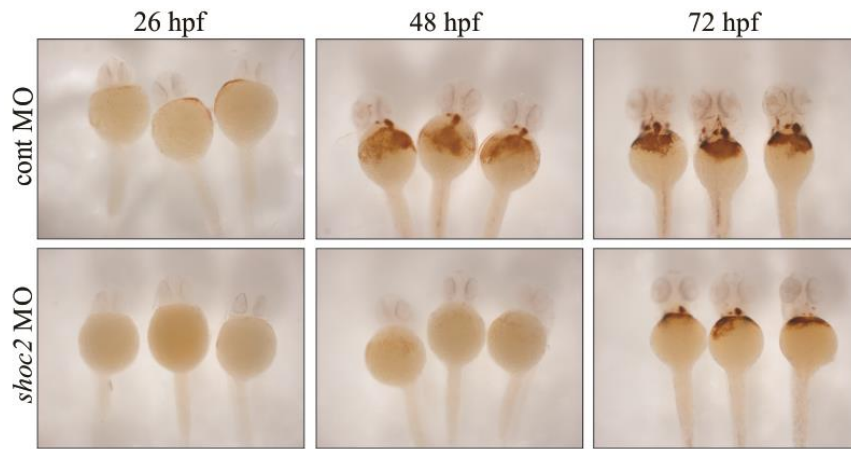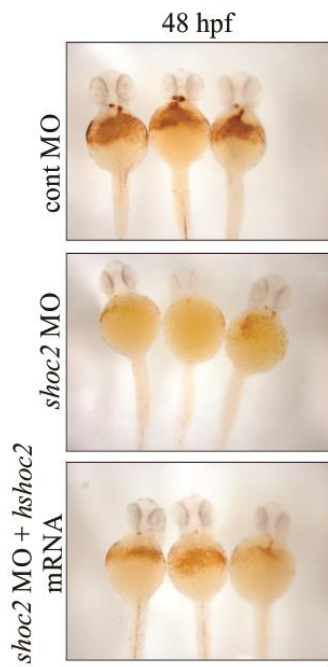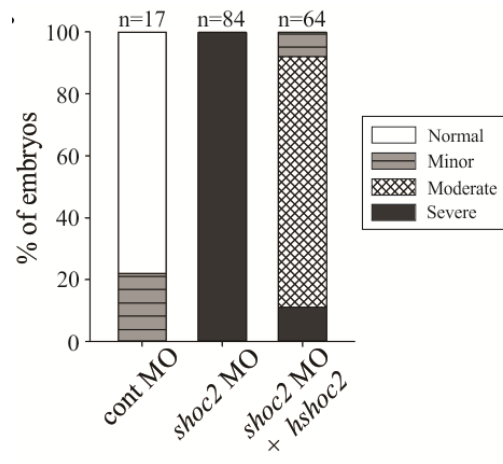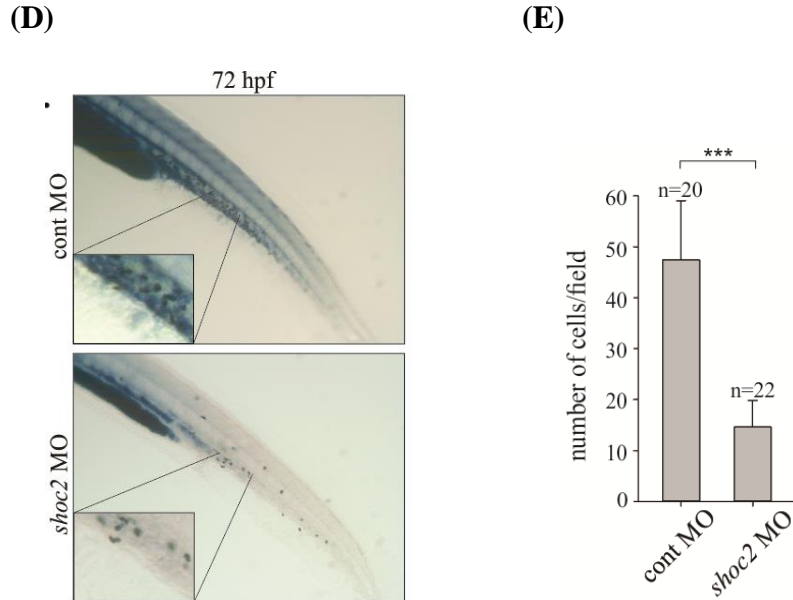
Figure 3.9 Number of erythropoietic and myelopoietic cells are affected in *shoc2*
MO injected embryos. (A) *o*-dianisidine staining of hemoglobin in control and *shoc2*
MO injected embryos at the indicated times (26, 48, and 72 hpf). In control embryos,
hemoglobin-positive cells were found on the yolk sac soon after circulation starting at 26
hpf, *shoc2* morphants lacked staining completely. At 48 hpf the number of *o*-dianisidine
positive cells was severely reduced in *shoc2* morphants in comparison to control. **(B)**
Injection of human *shoc2* mRNA in *shoc2* morphants. The data show rescue of
hemoglobin phenotypes at 48 hpf. **(C)** Analysis of hemoglobin staining presented in (B).
o-dianisidine positive area in the region of yolk and tail was assessed based on
hemoglobin staining intensity. Number of embryos analyzed: 48 hpf cont-MO injected
embryos, n=17; 48 hpf *shoc2* MO, 5.24 ng/embryo, n=84; 48 hpf *shoc2* MO, 5.24
ng/embryo plus 100 pg/embryo human *shoc2* mRNA, n=64. **(D)** Sudan Black B staining
of myelopoietic cells (neutrophils) in control- and *shoc2*-MO injected embryos at 72 hpf.
Significant reduction in circulating neutrophils was found in *shoc2* morphants (93%, or
105/113 injected). Insets show neutrophils in clumps in the CHT. Three biological
replicates were performed for all experiments. **(E)** Analysis of Sudan Black B staining
presented in D. Sudan Black B-positive cells were counted within the 5 somites of CHT
region. Error bars represent means with SEM. ****p* < 0.001 (Student's t-test). hpf- hours
post fertilization, MO- morpholino, CHT- caudal hematopoietic tissue.

(A)

(B)
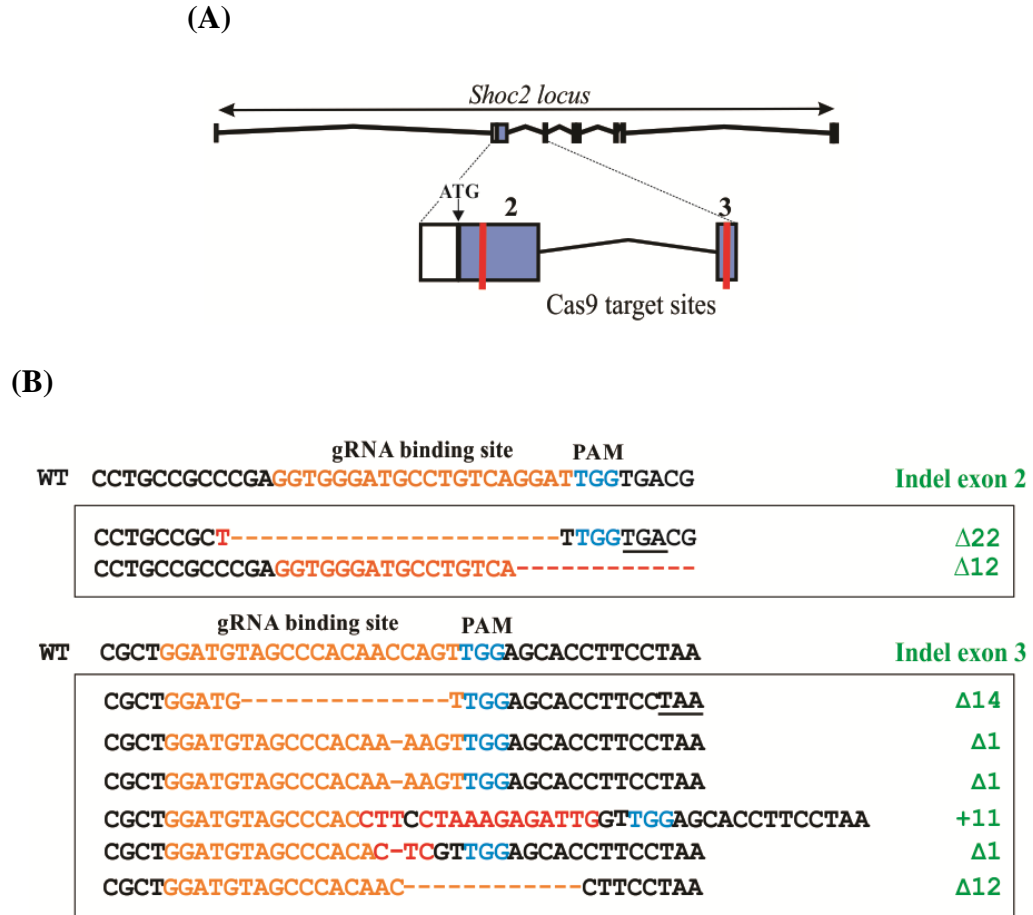
Figure 3.10 Heritable mutations of the Shoc2 gene.

(A) Zebrafish *Shoc2* genomic locus on chromosome 22 with the DNA cleavage positions (in exon 2 and exon 3 indicated by the red bars).

(B) Details of the F1 offspring genotypes. The F1 genotypes contain deletions (dashes) and insertions (red letters) at the *shoc2* gRNA and #2 sites (orange letters) near proto-spacer adjacent motif sequences (blue letters). The numbers of deleted or inserted base pairs and resultant frameshift mutations are indicated. The premature stop codons are underlined.

(A)
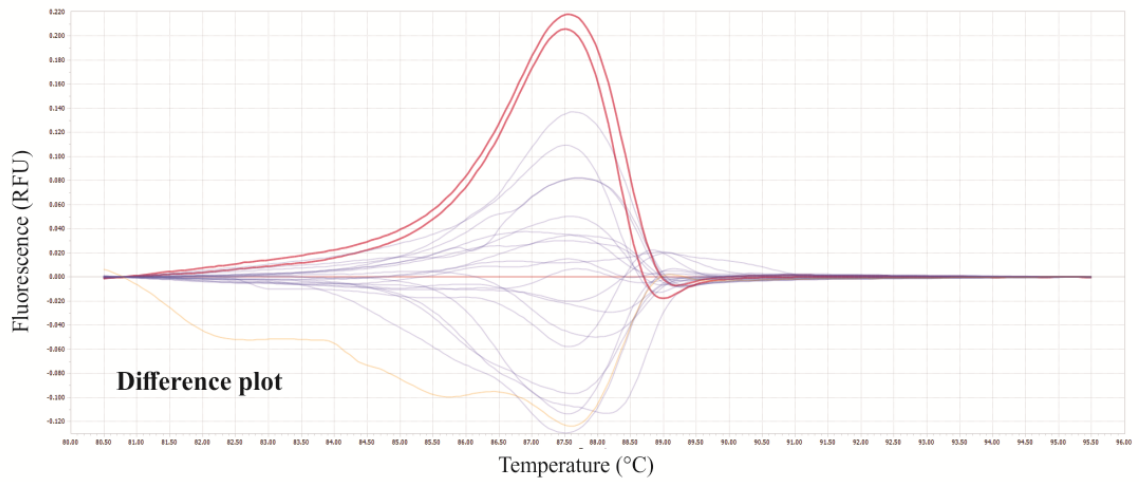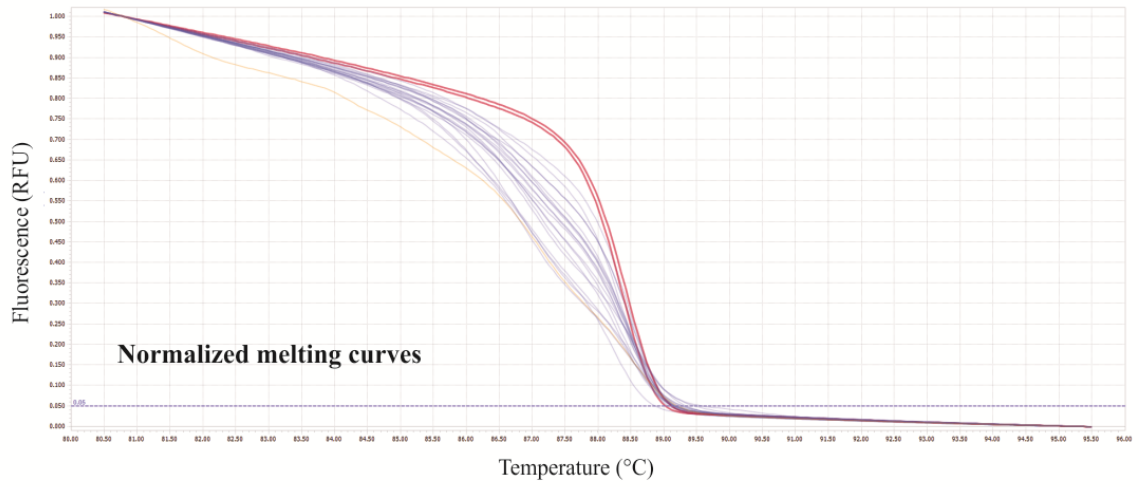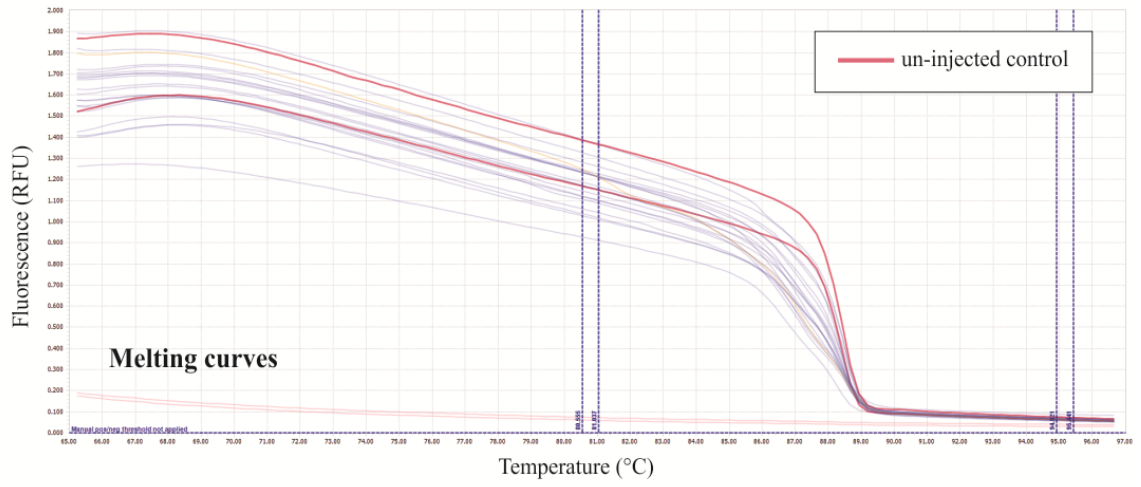
(B)
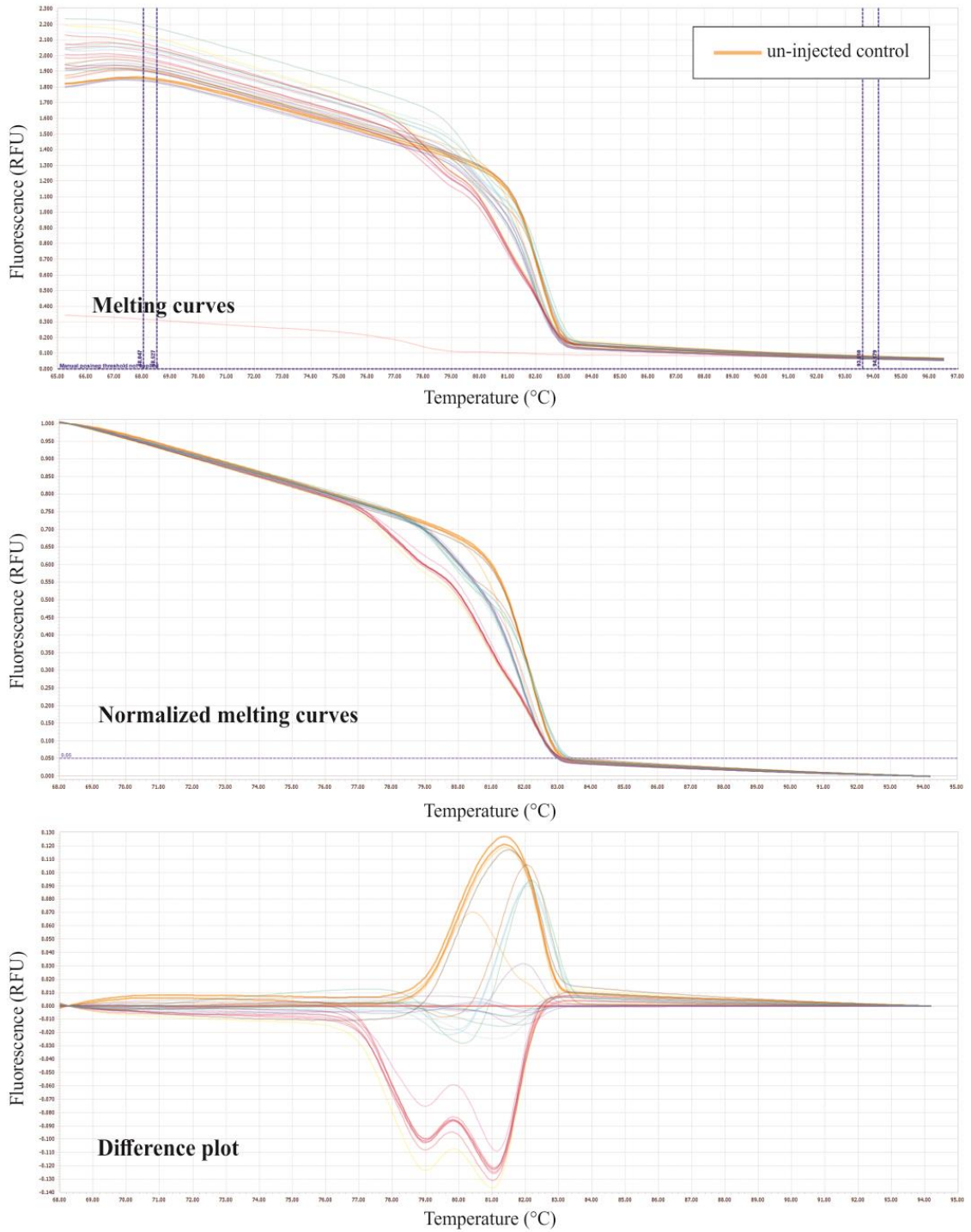
Figure 3.11 Detection of *shoc2* mutant alleles in individual *shoc2* sgRNA/Cas9 injected embryos.

The HRMA curve discriminates WT and mutant alleles. The genomic DNA was prepared from individual 1 day-post-injected embryos. The LightCycler® 480 High Resolution Melting Master and LightCycler® 96 system were used. The curves of embryos injected with *shoc2* sgRNA/Cas9 targeting exon 2 **(A)** and exon 3 **(B)** were shifted and irregular, indicating the presence of insertions/deletions.

(A)
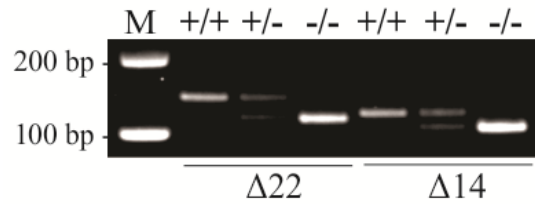
(B)
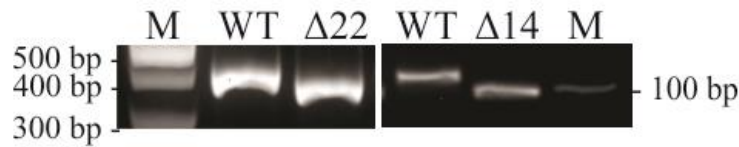
Figure 3.12 PCR analysis detecting *shoc2^Δ22* and *shoc2^Δ14* alleles.

(A) PCR analysis of genomic DNA allows for sensitive detection of WT and *shoc2^Δ22* and *shoc2^Δ14* mutant alleles in individual larvae (F3 generation). Acrylamide gel electrophoresis shows PCR amplicons of WT, heterozygous and homozygous *shoc2^Δ22* and *shoc2^Δ14* carriers. **(B)** RT-PCR analysis allows for sensitive detection of WT and *shoc2^Δ22* and *shoc2^Δ14* mutant RNA in individual larvae. Acrylamide gel electrophoresis shows PCR amplicons of WT, heterozygous and homozygous *shoc2^Δ22* and *shoc2^Δ14* carriers. M- DNA marker.
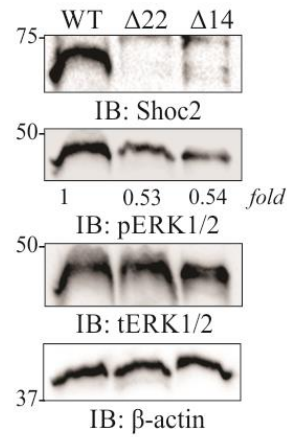
Figure 3.13 Immunoblot analysis of WT, *shoc2^Δ22* and *shoc2^Δ14* larvae.
Larvae were harvested for immunoblotting at 6 dpf. Protein expression was analyzed using specific antibodies. β-actin was used as a loading control.
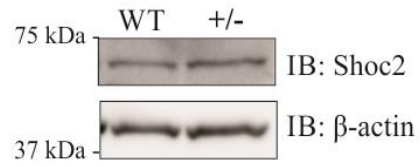
Figure 3.14 Expression of Shoc2 in WT and *shoc2^{Δ22+/-}* zebrafish.

Western blot analysis detects unaltered expression of Shoc2 protein in adult WT and *shoc2^{Δ22+/-}* zebrafish.
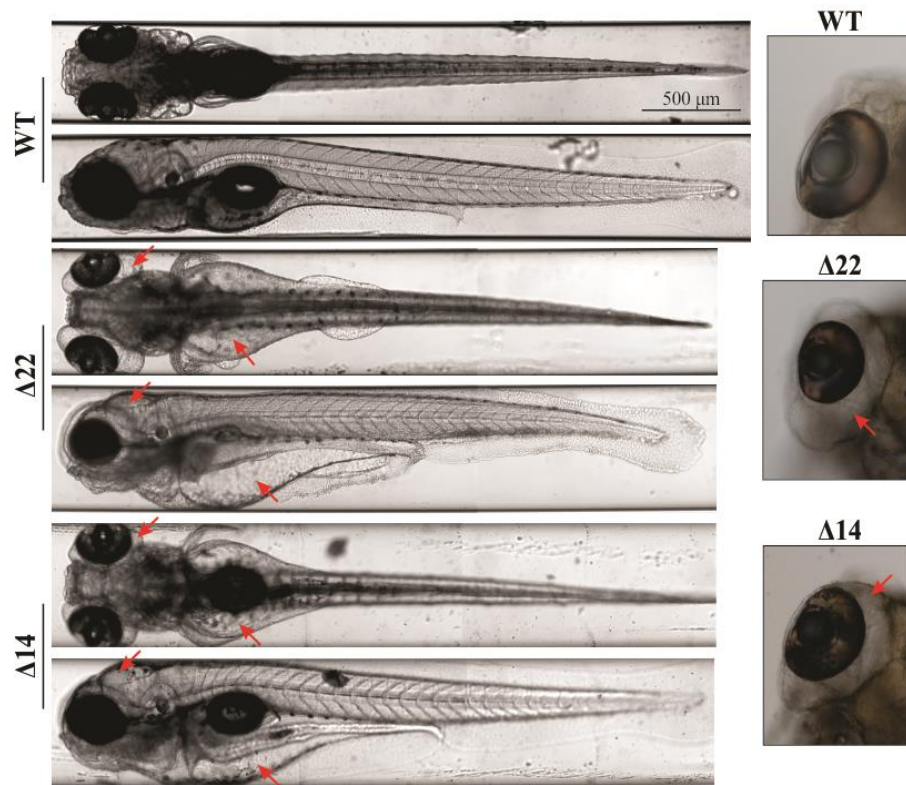
Figure 3.15 Late pleiotropic phenotype of *shoc2^{Δ22}* and *shoc2^{Δ14}* crispants.
Severe edema between the trunk and the yolk sac and yolk extension, heart and kidney, and underinflated yolk of 6 dpf *shoc2^{Δ22}* and *shoc2^{Δ14}* crispants are indicated with red arrows. Insets show severe eye edema of *shoc2^{Δ22}* and *shoc2^{Δ14}* crispants. Larvae are shown in dorsal or lateral view. Larvae were positioned and imaged live with the Vertebrate Automated Screening Technology (VAST) platform (Union Biometrica) [195]. Larvae were anaesthetized with 0.2 mg/mL tricaine prior to being loaded into the sample reservoir. Dorsal and lateral images were acquired at a >70% minimum similarity from the pattern-recognition algorithm. High-resolution frontal and posterior images were stitched together using Adobe Photoshop CS6. For each larva shown, 3.5-fold magnified views of the eye region are displayed.
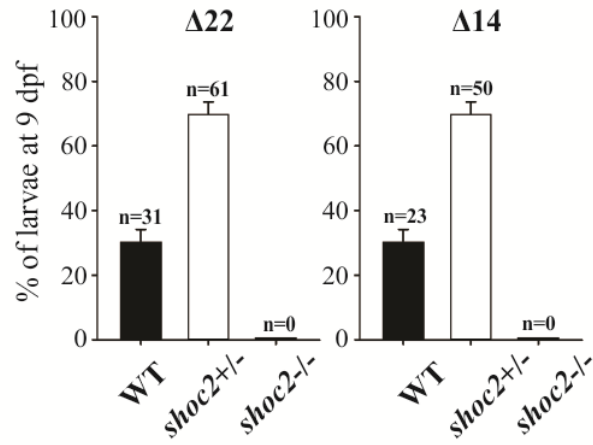
Figure 3.16 PCR analysis of genomic DNA of *shoc2^{Δ22}* and *shoc2^{Δ14}* inbred larvae at 9 dpf. Progeny of three independent inbreeding experiments using heterozygous *shoc2^{Δ22}* and *shoc2^{Δ14}* fish were genotyped. All survival larvae were genotyped as either WT or heterozygous carriers of the *shoc2^{Δ22}* and *shoc2^{Δ14}* crispant allele. Three biological replicates were performed for both alleles.

(A)

(B)
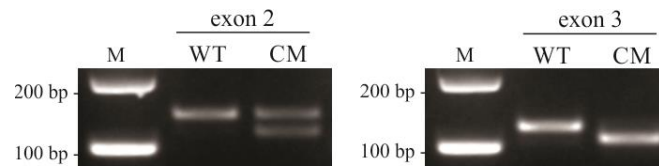
Figure 3.17 *shoc2^Δ22^-shoc2^Δ14^* **compound mutants develop edemic phenotype.**
*shoc2^Δ22+/-^* and *shoc2^Δ14+/-^* adult fish were crossed to generate *shoc2^Δ22^-shoc2^Δ14^*
compound mutants. **(A)** Images of 6 dpf compound crispants show edemic phenotype
similar to the observed in *shoc2^Δ22^* and *shoc2^Δ14^* crispants. Red arrows indicate edema
around the eye, heart/yolk region of the larva. **(B)** PCR analysis of genomic DNA
confirms the deletions in both alleles: exon2 with 22 bp deletion and exon3 with 14 bp
deletion. M- DNA Marker. CM- compound mutant.

(Experiments performed by Rebecca Norcross and analyzed by HyeIn Jang)

(A)

WT

500 μm

Δ22

WT

Δ22

250 μm

(B)

pq
ch
mk
an
mk
pq
et
cb1
cb2
cb3
cb4
po
hs
A ↔ P

WT

250 μm

Δ22
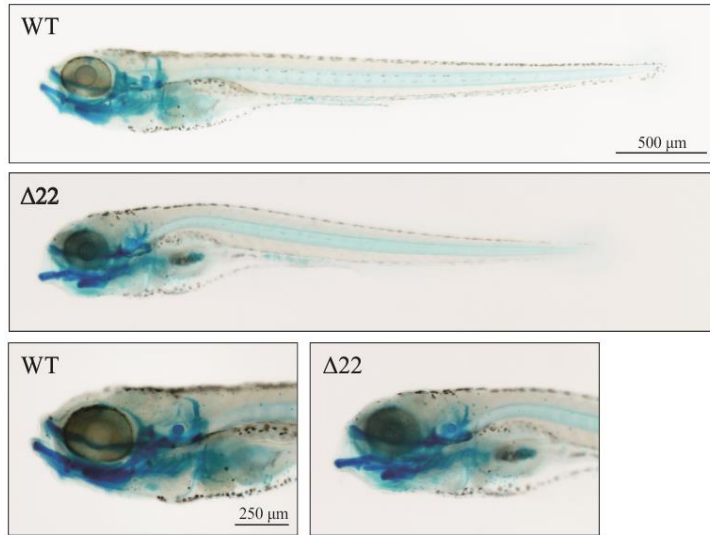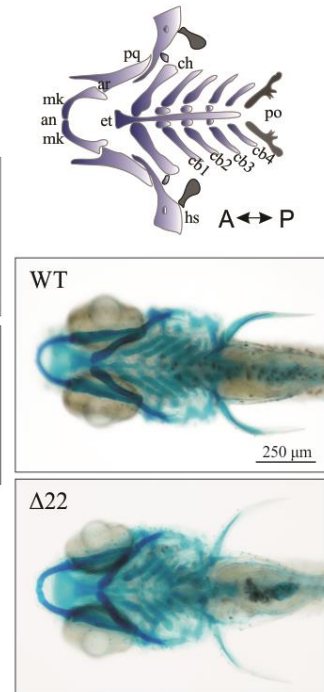
(C)
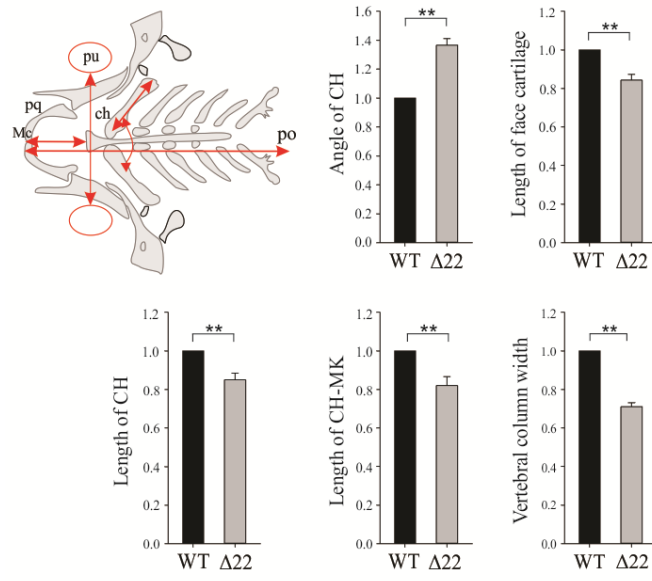
(D)
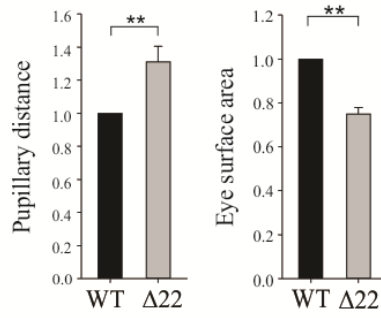
Figure 3.18 *shoc2* loss leads to defects in craniofacial cartilage specification and differentiation.

(A) Lateral and ventral views of a 6 dpf WT and *shoc2^{Δ22}* crispant larvae after Alcian blue staining. Mutant larvae show significant changes in head cartilage.

(B) Schematic representation of the different head cartilage elements in ventral view of 6 dpf. anterior limit (an), articulation (ar), ceratobranchial pairs 1 to 4 (cb1-4), ceratohyal (ch), ethmoid plate (et), hyosymplectic (hs), Meckel's cartilage (mk), palatoquadrate (pq), posterior limit (po).

(C) Schematic representation of parameters quantified; length of ceratohyal (CH) and CH to Meckel's cartilage (mk), angle of CH, pupillary distance (pu), eye surface area, width of vertebral column and length of total face cartilage (red arrows) were measured for morphometry. Y-axes on graphs indicate the fold change of *shoc2^{Δ22}* crispants compared to WT.

(D) Measured distance between the eyes and the eye surface area of 6 dpf WT and *shoc2^{Δ22}* crispant larvae. Three biological replicates were performed for all experiments (n= 20/group). (**$p < 0.05$, Student's *t*- test). Error bars represent means with SEM. A- anterior, P- posterior.
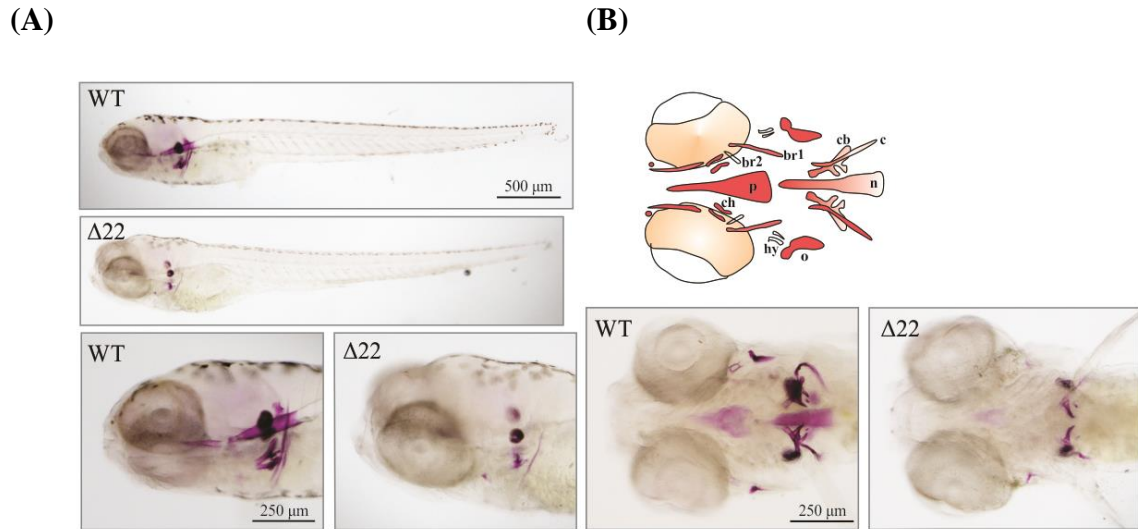
Figure 3.19 Bone development is impaired in *shoc2^Δ22* crispant larvae.

(**A**) Lateral view of a 6 dpf WT and *shoc2^Δ22* crispant larvae detected by Alizarin Red S staining. Mutant larvae show significant differences in cranial bone formation.

(**B**) Schematic representation of the different cranial bone elements detectable at 6 dpf: branchiostegal ray 1 and ray 2 (br1 and br2), notochord (n), opercle (o), parasphenoid (p) and ceratobranchial 5 (cb). Ventral view of 6 dpf WT and *shoc2^Δ22* larvae stained with Alizarin Red S. Detected changes include defects in ossification of parasphenoid, ceratohyal, branchiostegal rays, opercle, ceratohyal and notochord. Three biological replicates were performed for all experiments (n= 30/group).
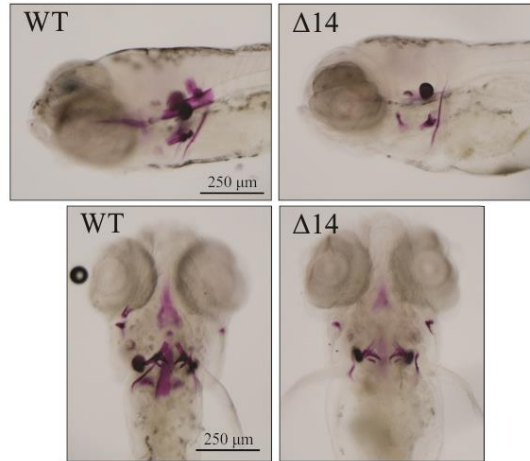
Figure 3.20 Bone development is impaired in *shoc2^Δ14* crispant larvae.

Lateral and ventral view of a 6 dpf WT and *shoc2^Δ14* crispant larvae detected after Alizarin Red S staining. Mutant larvae show significant differences in cranial bone formation.

(A)
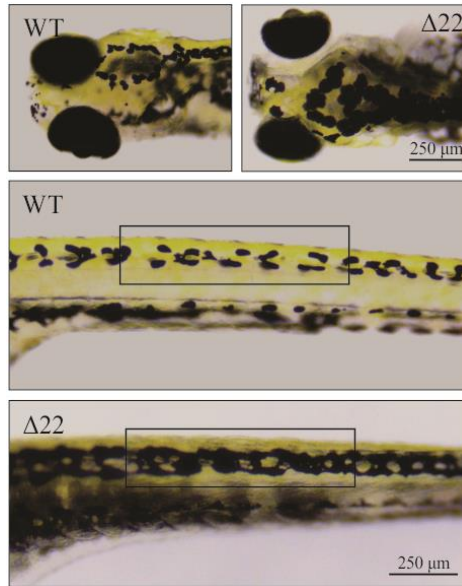
(B)

Figure 3.21 Pigmentation pattern of *shoc2* null larvae.

Dorsal (head) and lateral (trunk) views of 6 dpf larvae showing melanophores in WT and *shoc2^{Δ22}* **(A)**, and *shoc2^{Δ14}* **(B)** crispants. *shoc2^{-/-}* mutants presented with closed gaps in pigmentation pattern of head and lateral stipe (brackets) melanophores when compared with WT controls.
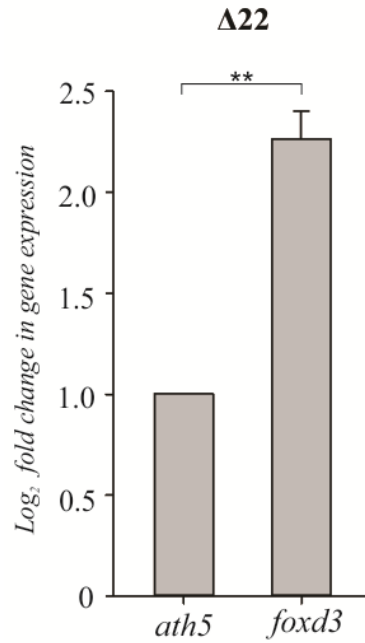
Figure 3.22 Levels of *foxd3* mRNA expression quantified by qPCR.

The data are presented as the fold change of the mRNA levels in WT larvae versus the mRNA levels in mutant larvae. *ath5* is a control mRNA. The results represent an average of three biological replicas. Error bars indicate means with SEM. **p < 0.05 (Student's t-test).
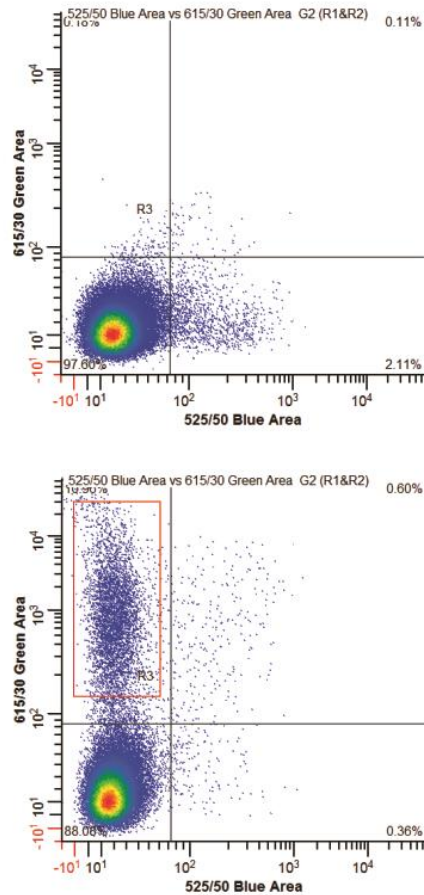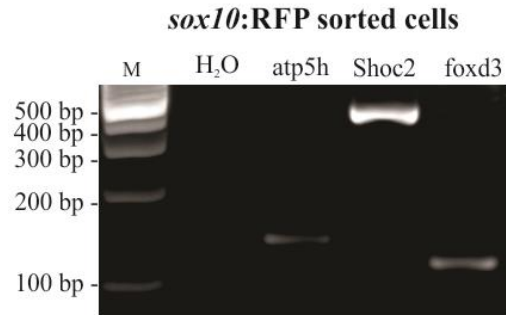
Figure 3.23 *shoc2* expressed in neural crest cells.

sox10:RFP positive cells were isolated from the transgene adult fish using flow cytometry. FACS profile of *sox10:RFP* are shown. Red boxes indicate the collected cell populations. Total RNA was isolated and RT-PCR was performed. RT-PCR detected *shoc2* in both *sox10*-positive flow-sorted cells. *foxd3* is included to confirm the specificity of flow sorting. M- DNA Marker.

(A)

(B)

(C)

(D)

85
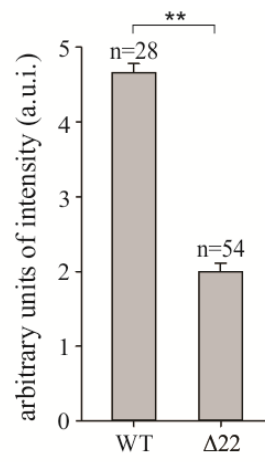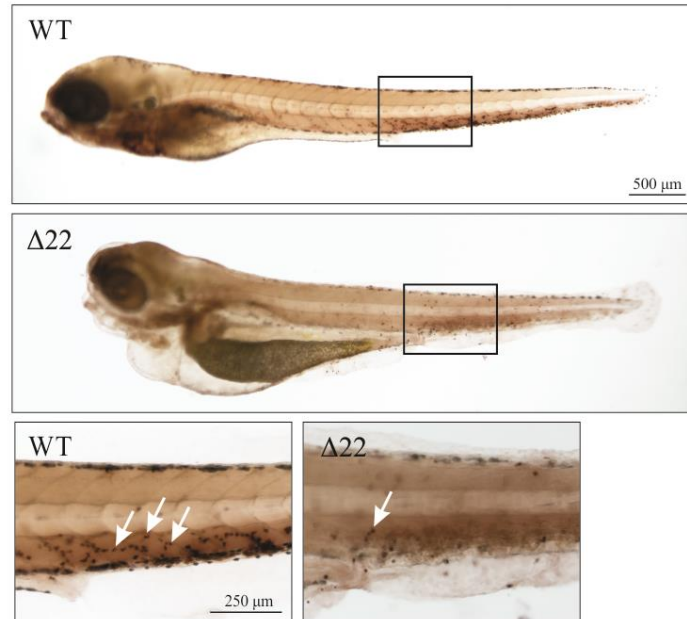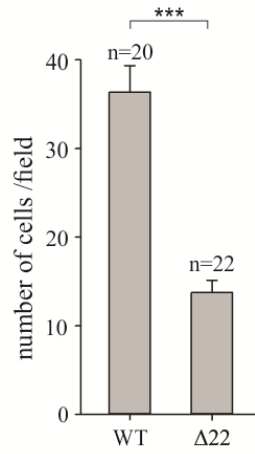
Figure 3.24 Impaired hematopoiesis in *shoc2^{Δ22}* crispant larvae.

(A) *o*-dianisidine staining detecting hemoglobin of erythropoietic cells in control and *shoc2^{Δ22}* larvae at 6 dpf. In control, larvae hemoglobin-positive cells were found on the yolk sac and tail while *shoc2^{Δ22}* crispants showed significantly decreased number of cells. Images are shown in lateral and ventral view.

(B) Quantitative analysis of the number of erythropoietic cells in circulation. Relative intensity of hemoglobin staining was scored in arbitrary units of intensity 0 to 5, 0 being the weakest and 5 the strongest. **$p < 0.05$ (Student's t-test).

(C) Histochemical staining for mpx enzyme activity in WT and *shoc2^{Δ22}* at 6 dpf. Larvae are shown in lateral view with the anterior to the left. The images are representative of ≥ 20 larvae in each group. The staining was repeated with similar results for three independent experiments. Arrows point to mpx-positive cells.

(D) The number of mpx-positive cells within the indicated box (5 somites). Error bars represent means with SEM. ***$p < 0.001$ (Student's t-test).
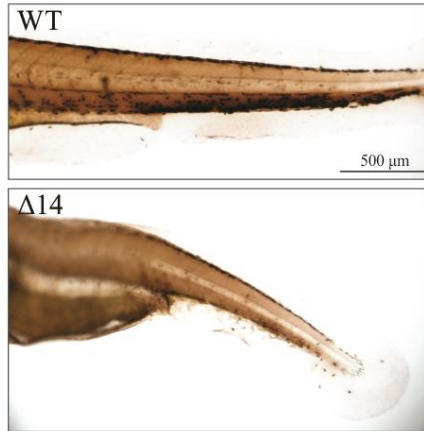
Figure 3.25 Histochemical staining for mpx enzyme activity in 6 dpf WT and
shoc2^{Δ14} **crispants.** Larvae are shown in lateral view with the anterior to the left. The
images are representative of ≥ 20 larvae in each group. The staining was repeated with
similar results for three independent experiments.
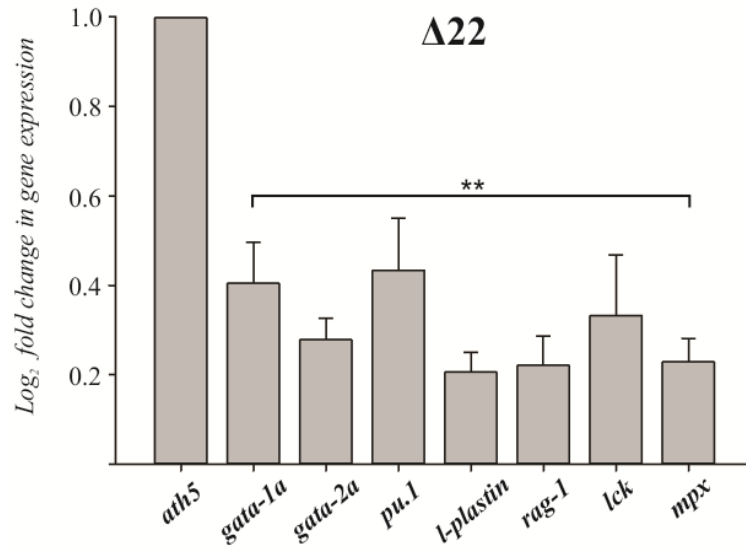
Figure 3.26 Loss of *shoc2* causes a reduction in the expression of blood cell markers.
qPCR analysis of blood lineage markers. Total RNA was extracted from 6 dpf WT and
mutant larvae and levels of mRNA expression were quantified by qPCR. The data are
presented as the fold change of the mRNA levels in WT larvae versus the mRNA levels
in mutant larvae. *ath5* is a control mRNA. The results represent an average of three
biological replicas. Error bars indicate means with SEM. **p < 0.05 (Student's t-test).
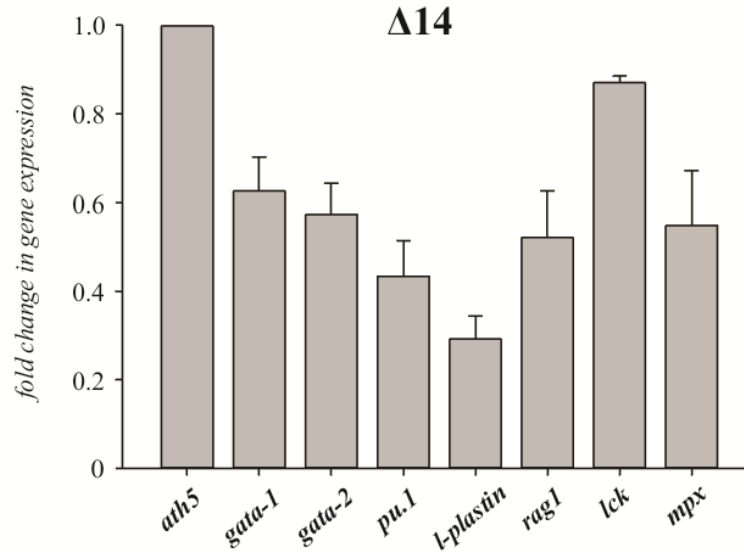
Figure 3.27 Loss of *shoc2* causes a reduction in the expression of blood cell markers.
The relative changes in the expression of hematopoietic markers were evaluated in
shoc2^{Δ14} crispants. Total RNA was extracted from 6 dpf WT and mutant larvae and levels
of mRNA expression were quantified by qPCR. The data are presented as the fold change
of the mRNA levels in WT larvae versus the mRNA levels in mutant larvae. *ath5* is a
control mRNA. The results represent an average of three biological replicas. Error bars
indicate means with SEM. **p < 0.05 (Student's t-test).
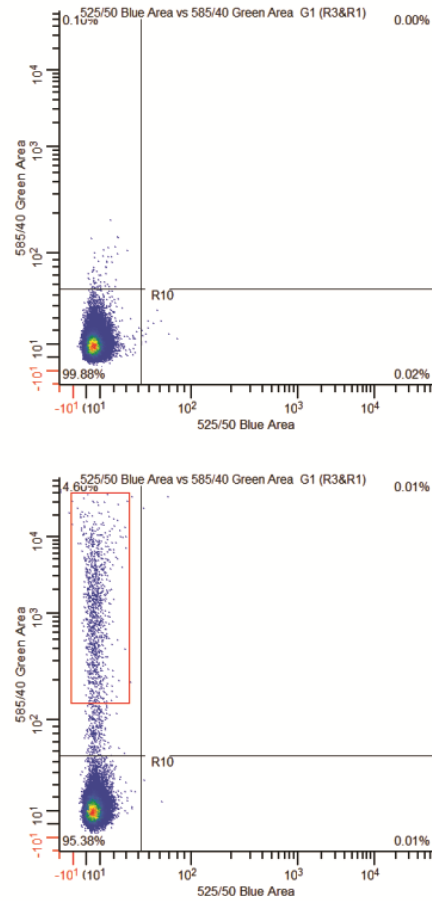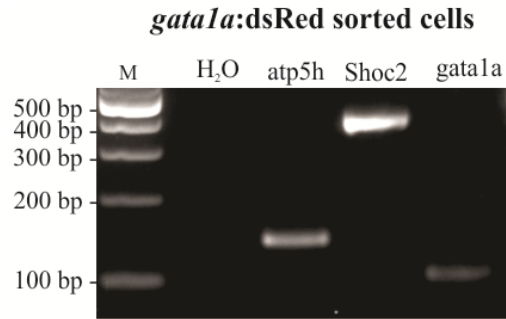
Figure 3.28 *shoc2* **is expressed in hematopoietic cells.**

gata1a:dsRed positive cells were isolated from adult fish using flow cytometry. FACS profile of *gata1a:dsRed* is shown. Red box indicates the collected cell populations. Total RNA was isolated and RT-PCR was performed. RT-PCR detected *shoc2* in flow-sorted cells. *gata1a* was included to confirm the specificity of flow sorting. M- DNA Marker.

(A)

(B)
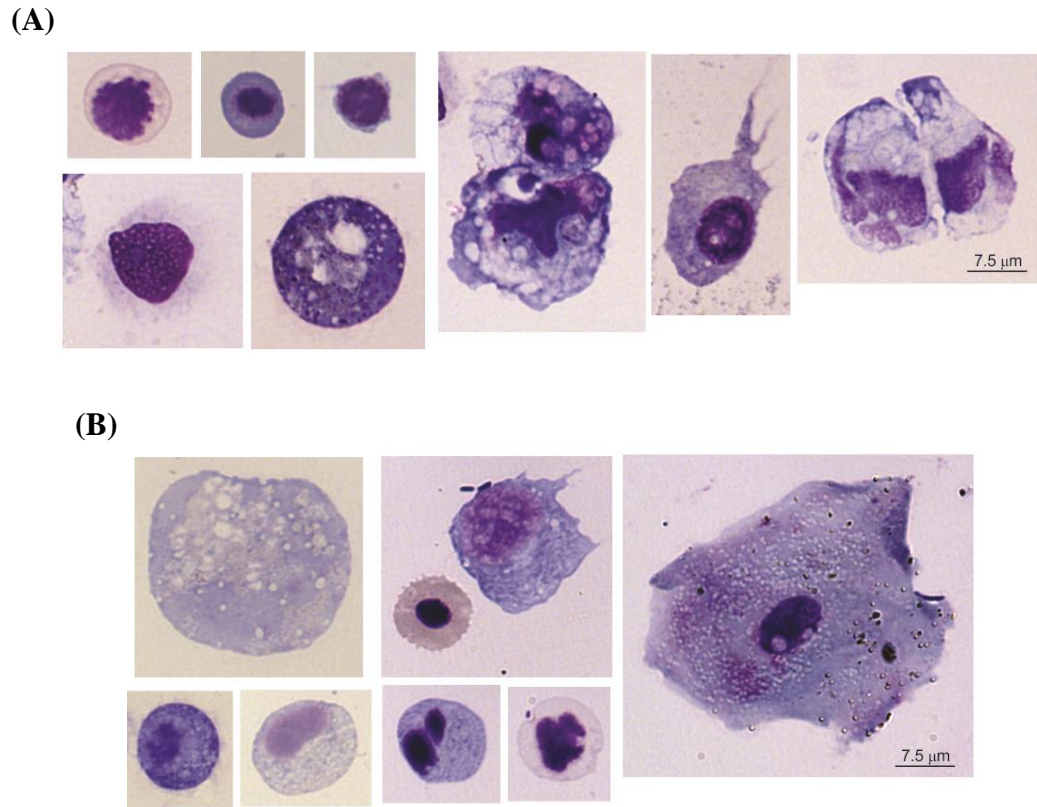
Figure 3.29 Blood cell types found in 6 dpf larvae.

Peripheral blood cells from **(A)** WT and **(B)** *shoc2^{Δ22}* larvae at 6 dpf stained with May-Grünwald Giemsa. Blood cells isolated from six WT or six *shoc2^{Δ22}* larvae were cytospun onto a coated slide and stained. Various blood cell subtypes were detected in both WT and *shoc2^{Δ22}* larvae.

(A)
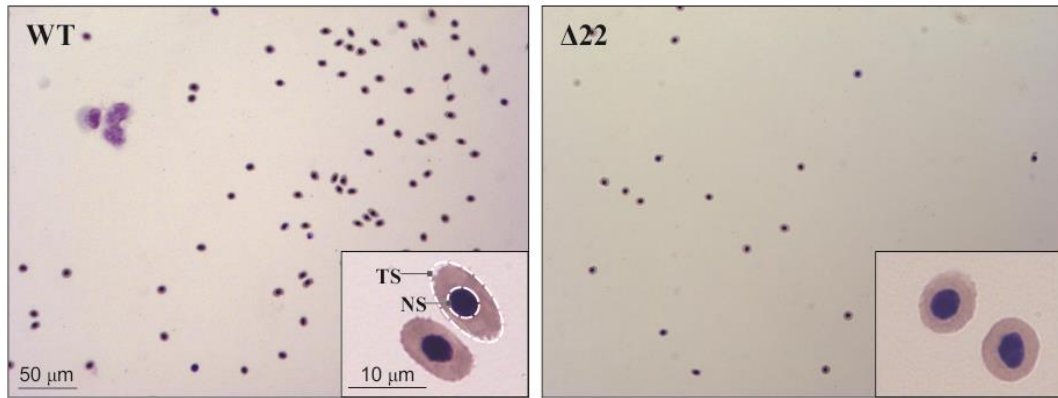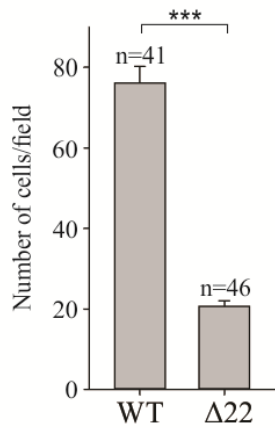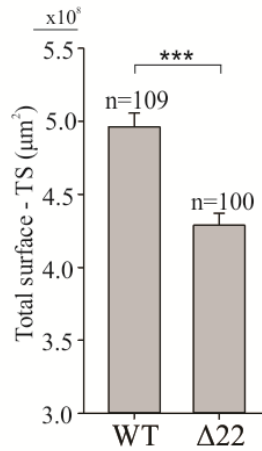
(B)   **(C)**   **(D)**
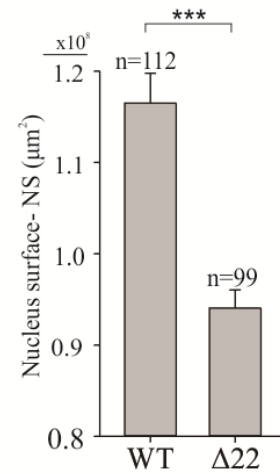
Figure 3.30 Loss of *shoc2* causes a reduction in the number of circulating blood cells.

(A) Cytology of blood cells from WT and *shoc2$^{\Delta22}$* larvae at 6 dpf. Peripheral blood cells isolated from six WT or six *shoc2$^{\Delta22}$* larvae were cytospun onto a coated slide and stained by the May-Grünwald Giemsa method. The *shoc2$^{\Delta22}$* larvae had significantly lower numbers of blood cells than WT larvae. Erythrocytes from 6 dpf WT larvae show the typical elliptical morphology, while the *shoc2$^{\Delta22}$* cells were smaller and more circular in shape. Images were taken with a Leica DFC 7000 T camera with a 100x oil objective and 10x eyepiece.

(B) Total number of blood cells from samples in (A) is shown. The results represent an average of three biological replicas. n represents a number of fields used for scoring.

(C) Total surface area and **(D)** surface area of nuclei of erythrocytes from WT and *shoc2* knockout cells were measured and graphed. All calculations were performed using the morphometry mask statistics modules of the Slidebook 6.0 software. The results represent an average of three biological replicas. Error bars represent means with SEM. ***$p < 0.001$ (Student's t-test).

	M	WT	Δ22	Δ14	Forward primer	Reverse primer
atp5h	200 bp				5'-TGCCATCTCAGCAAAACTTG-3'	5'-CACAGGCTCAGGAACAGTCA-3'
l-plastin	300 bp / 200 bp				5'-GTCGATGTGGATGGGAACGG-3'	5'-CCCTCCTCGGAGTATGAGTGC-3'
gata-1a	200 bp / 100 bp				5'-AAGATGGGACAGGCCACTA-3'	5'-TGCTGACAATCAGCCTCTTTT-3'
mpx	300 bp / 200 bp				5'-TTCTTTTTGTGGTGGGCTGC-3'	5'-CTCCCGTGTCTTTCGAGCTG-3'
gata-2a	100 bp				5'-AACAATCGGGCTGTGGACAA-3'	5'-AGCACTCCAATCCTGCGTTT-3'
pu.1	300 bp				5'-CAGAGCTACAAAGCGTGCAG-3'	5'-GCAGAAGGTCAAGCAGGAAC-3'
lck	300 bp / 200 bp				5'-ACAATTTGGCAGCACATGTCTTT-3'	5'-GGCAGTTACACTGGTCACAC-3'
rag-1	300 bp / 200 bp				5'-CCAGGTGAAGACATTTGCCG-3'	5'-ATTACGCAGAGTGTGCAGGG-3'
foxd3	200 bp / 100 bp				5'-TTGACGCTCAGTGGAATC-3'	5'-TCTTGACGAAGCAGTCGT-3'

Table. 1. RT-PCR of hematopoietic and non-hematopoietic genes.

RT-PCR of cells and WT, *shoc2^{Δ22}* and *shoc2^{Δ14}* larvae. Genes are indicated to the left; *atp5h* is used as a reference gene. Primer sequences are to the right of each gene.

Chapter 4

Title:
Shoc2 couples the E3 ligase HUWE1 with VCP/p97
to control ERK1/2 signaling

Abstract

The pivotal role of the scaffolding protein Shoc2 in controlling ERK1/2 signals is underscored by its role in the pathogenesis of Noonan-like developmental syndrome. However, the molecular mechanisms regulating signal transmission via this intricate signaling module remain unclear. Here we identify that Shoc2 scaffold, through its leucine repeats rich domain, brings together the hexameric AAA+ ATPase VCP/p97 and the E3 ligase HUWE1 to modulate the levels of the HUWE1-mediated allosteric ubiquitination of Shoc2 and RAF-1. Abrogated activity of VCP/p97 ATPase leads to the increased presence of HUWE1 in the Shoc2 complex, followed by augmented Shoc2/RAF-1 ubiquitination and altered RAF-1 phosphorylation. We found that in fibroblasts from patients with Inclusion Body Myopathy with Paget's disease of bone and Frontotemporal Dementia (IBMPFD) that harbor germline mutations in VCP/p97, the levels of Shoc2 ubiquitination and ERK1/2 phosphorylation are imbalanced. This study provides a mechanistic basis for the critical role of VCP/p97 in regulating the ERK1/2 pathway and reveals a previously unrecognized function of the ERK1/2 pathway in the pathogenesis of IBMPFD.

Introduction

During the past decade, a solid body of literature has demonstrated the functional significance of the molecular chaperone Valosin-containing protein (VCP) also known as p97 or Cell Division Cycle 48 (cdc48) in yeast [196, 197]. VCP is an *A*TPase *A*ssociated with a variety of cellular *A*ctivities (AAA+) –ATPase protein motor protein that is expressed in the cytosol, membrane-bound organelles (Golgi, ER, endosomes), and in the nucleus. Best known for its function in endoplasmic reticulum associated protein degradation (ERAD), VCP is involved in various cellular processes regulating a perplexing range of cellular functions. VCP helps remove misfolded proteins at different locations to protect the cell from protein stress, eliminate regulatory proteins in various intracellular signaling pathways including those that govern chromatin remodeling, DNA replication and repair, and facilitate proteasome-independent degradation in the lysosome by controlling protein sorting in the endocytic pathway and by regulating autophagy. [198-200]. Overall, VCP has emerged as a central and important element of the ubiquitin system with the majority of VCP substrates being ubiquitinated [201, 202]. Ubiquitination can be simply described as a three-step process catalyzed by three classes of enzymes: ubiquitin activating enzyme E1, ubiquitin conjugating enzyme E2, and ubiquitin ligase E3 which confers substrate specificity. Well-known for their role in protein degradation, ubiquitin marks have also been shown to contribute to the mechanisms regulating cellular signaling cascades and catalytic activities of signaling proteins [203, 204].

The incredible diversity of VCP functions is achieved through a multitude of regulatory co-factors that dictate subcellular localization, oligomeric state of VCP, and substrate specificity [202, 205-209]. Importantly, VCP/p97 functions as an unfoldase, or "segregase" in processes such as DNA replication, nuclear and Golgi membrane assembly, and non-proteasomal degradation through macroautophagy and the endolysosomal pathway [197]. The molecular mechanisms underlying the "segregase" activity of the ring-shaped hexameric VCP assembly rely on the conformational changes induced by ATP binding and hydrolysis by the two ATPase domains D1 and D2 that follow the N-terminal domain (**Figure 4.1.A**) [197]. VCP forms stacked hexameric rings formed by the D1 and D2 domains with the N-domain on the outside of the D1 ring. This structural arrangement of domains allows the N-domain of VCP to interact with different cofactors. The AAA+ modules (D1 and D2) encompass the consensus Walker A and Walker B motifs that are critical for ATP binding and ATP hydrolysis, respectively. ATP hydrolysis in D2 seems to generate the main force of ATPase activity, while D1 participates in substrate binding and stabilizes unfolded proteins [197, 210, 211]. It is believed that the conformational changes of the VCP molecule driven by ATPase activity generate mechanical movement that is responsible for the VCP function [196, 211]. VCP itself contains an intrinsic ubiquitin-binding site in its N-domain with low affinity for ubiquitin. Similarly, many cofactors of VCP also bear ubiquitin-binding domains [201, 202, 206]. These additional ubiquitin binding sites enhance the affinity of VCP for ubiquitinated substrates [197]. It has been shown that all thirteen mammalian UBX (Ubiquitin regulatory X) domain-containing proteins serve as cofactors for VCP and

recruit substrates to VCP and regulate their fate [202]. Moreover, it has been established that VCP interacts with several single RING-and HECT-domain E3 ligases [212, 213].

As VCP governs critical steps in ubiquitin-dependent protein quality control and intracellular signaling pathways, it is not surprising that defects in VCP and its binding partners contribute to various diseases [196, 214, 215]. Germline mutations in VCP cause an autosomal dominant and fatal familial multi-systemic disease, Inclusion Body Myopathy with early-onset Paget disease and Frontotemporal Dementia (IBMPFD, OMIM #167320) that is characterized by incomplete penetrance of three main features: disabling muscle weakness, osteolytic bone lesions consistent with Paget's disease, and frontotemporal dementia [196, 215, 216]. A majority of IBMPFD-associated VCP/p97 mutants alter structural orientation between the VCP N- and D1 domains, thus altering the recognition by cofactors and/or ATPase activity [196, 215]. At the cellular level, IBMPFD is characterized by the impairments in protein degradation and accumulation of the ubiquitinated protein aggregates as well as several other cellular defects, but the molecular basis underlying these cellular abnormalities remains elusive. Currently, there is no cure for IBMPFD and the only treatment offered to patients merely alleviates the disease symptoms.

Being a key mediator of several major protein homeostasis processes, VCP has also emerged as an attractive target for anti-cancer therapy [217, 218]. Recent advances in developing of a selective ATP-competitive inhibitor has given rise to a small-molecule compound, CB-5083, that induces a strong antitumor response in solid tumors and is currently being evaluated in clinical trials [218-223].

In this study, we have found that VCP/p97 modulates signals of the canonical extracellular signal-regulated kinase (ERK1/2) pathway transduced by remodeling the Shoc2-scaffolding module. Earlier studies in Galperin lab showed that Shoc2 assembles an intricate scaffolding complex that incorporates canonical signaling enzymes (i.e. Ras, RAF-1 and the catalytic subunit of protein phosphatase 1c (PP1c)) as well as the proteins of the ubiquitin machinery, the E3 ligase HUWE1 and AAA+ ATPase PSMC5 [116, 120]. Together these proteins create an elegant mechanism that both accelerates and fine-tunes the amplitude of the ERK1/2 signals in a spatially-defined manner. Specifically, in the Shoc2 module, the E3 ligase HUWE1 catalyzes the ubiquitination of Shoc2 and RAF-1 to provide a negative-feedback mechanism that modulates activity of the ERK1/2 pathway. Consequently, PSMC5 triggers an essential redistribution of the Shoc2 complexes to late endosomes/multivesicular bodies (LE/MVBs) where HUWE1 is sequestered from the scaffolding complex [116, 120]. Here, I demonstrate that VCP/p97 is critical for the proper remodeling of the Shoc2 signaling complex and a subsequent tuning of the ERK1/2 signals via the Shoc2–Ras–RAF-1 complex. We provide evidence that in Noonan-like patients, Shoc2 aberrantly localized to the plasma membrane is inaccessible to VCP/p97, preventing proper complex remodeling. Importantly, our findings demonstrate that the alterations in Shoc2 ubiquitination and ERK1/2 phosphorylation are important elements of IBMPFD pathology.

Results

1. VCP/p97 is a novel partner in the Shoc2 scaffold module

Earlier studies in the Galperin lab identified several proteins of the ubiquitin machinery including the previously reported E3 ligase HUWE1 and the AAA+ ATPase PSMC5 as interacting partners of Shoc2. This yeast two-hybrid screen of the human adult/fetal heart library also detected the twenty-nine cDNA prey fragments covering amino acids 180-390 of the 97 kDa AAA+ ATPase VCP/p97. All of the isolates extended over the carboxyl-terminus of the N domain and part of the D1 domain connected by the inter-domain linker (N-D1) of VCP (**Figure 4.1.A**).

To validate the Shoc2 and VCP interaction, we co-expressed glutathione *S*-transferase (GST)-fused Shoc2 (GST-Shoc2) and GFP-tagged VCP (VCP-GFP) in HEK 293FT cells. VCP was detected in the GST immunoprecipitate, indicating the association of VCP and Shoc2 (**Figure 4.1.B**). HA-tagged M-Ras/Shoc2 immunoprecipitation was used as a positive control [110, 120]. Co-immunoprecipitation of endogenous Shoc2 with VCP, PSMC5 and ectopically expressed YFP-M-Ras from HEK 293FT cells showed that these proteins form a quaternary complex (**Figure 4.1.C**). Since VCP is often associated with the recognition of ubiquitinated substrates [224], we utilized a previously characterized Shoc2 7KR (seven Lys mutated to Arg) mutants in which ubiquitination is reduced 70- 80% compared to that of WT Shoc2 [120]. Immunoprecipitation experiments were performed using Cos1 cells stably expressing either WT or the 7KR mutant of Shoc2-YFP and depleted of endogenous Shoc2 [120]. The presence of VCP in the Shoc2 7KR mutant immunoprecipitate decreased dramatically, indicating that VCP recognizes ubiquitinated Shoc2 (**Figure 4.1.D**). To map the interaction region of Shoc2 with VCP,

we utilized an HA-tagged VCP with tagRFP (tRFP)-tagged Shoc2 mutants generated in our previous studies [111]. The immunoprecipitation assay revealed that the leucine rich repeats 12-14 (aa 347-417) of Shoc2 mediate the association with VCP (**Figure 4.2**). Interestingly, this region of Shoc2 was earlier reported as the binding domain of HUWE1 (**Figure 4.2.E**) [120]. Together, these results demonstrate that VCP is a previously unrecognized interacting partner in the Shoc2–Ras–RAF-1 signaling scaffold complex.

2. VCP/p97 and Shoc2 colocalize on late endosomes and/or multivesicular bodies

The Shoc2 multi-protein complexes are targeted to endosomes upon activation of the ERK1/2 pathway [122]. To delineate what role VCP plays in cellular distribution of the Shoc2 module, we analyzed the localization of Shoc2-VCP complexes using complementary methods of subcellular fractionation and fluorescence microscopy (**Figure 4.3**). A crude endosomal (late and early endosomes) fraction (CE) of Cos1 cells were enriched using a discontinuous sucrose density gradient centrifugation at the 8/35% interface of the gradient [165]. The distribution of key markers of early endosomes (EEA1/Rab5) and plasma membrane (Na^+/K^+-ATPase) indicates that CE as well as Golgi and endoplasmic reticulum (G/ER) fractions were free of any significant amount of plasma membranes (**Figure 4.3.A**). We found that VCP can readily precipitate Shoc2 from the recovered CE protein interface, indicating that VCP is redistributed to the endosomes together with Shoc2 (**Figure 4.3.B**). The total amount of homogenate was comparable to the amount of total lysate used in immunoprecipitation experiments in **Figure 4.1**. Furthermore, we examined localization of VCP-GFP in cells stably depleted of endogenous Shoc2 and expressing Shoc2-tRFP together with the oligomeric PSMC5

(GST-PSMC5) that triggers Shoc2 recruitment to late endosomes/multivesicular bodies (LE/MVBs) [116]. Immunofluorescence microscopy revealed that the majority of Shoc2-tRFP- and GST-PSMC5 positive vesicles contained VCP-GFP as well (**Figure 4.3.C**). Many of the Shoc2-tRFP/GST-PSMC5/VCP-GFP-positive vesicles often contained the multi-membrane intra-luminal branches characteristic of large multivesicular bodies (MVBs) and in some instances reached 4-5 μm in size, probably as a result of membrane fusion induced by the accumulation of Shoc2-PCMC5 complexes. These vesicular structures were previously characterized as the late endosomal compartments [116, 122]. Interestingly, the ATPase activity deficient QQ mutant of VCP (E305Q, E578Q) was also easily detectable on the Shoc2-PSMC5 positive endosomes (**Figure 4.3.C**), suggesting that enzymatic activity of VCP has no effect on Shoc2 complex subcellular distribution. To support this assumption, I analyzed the endosomal distribution of the Shoc2 7KR mutant. I found that while deficient in VCP association, the Shoc2 7KR mutant can be recruited to endosomes as effectively as its WT counterpart (**Figure 4.4.A and B**).

Next, I explored the subcellular localization of the Shoc2-VCP complexes utilizing a Shoc2 S2G mutant found in patients with Noonan-like syndrome [152]. This S2G substitution in Shoc2 results in the aberrant N-terminal myristoylation and a plasma membrane targeted protein. VCP was not detectable in the Shoc2 immunoprecipitates obtained from the stable cells depleted of endogenous Shoc2 and expressing the S2G Shoc2-tRFP mutant (**Figure 4.3.D**), indicating that Shoc2-VCP complexes are formed in a spatially-defined manner. Findings in **Figure 4.3.D** were confirmed by the immunofluorescence microscopy (**Figure 4.3.E**). To confirm that correct spatial distribution of the Shoc2 complex is required for the Shoc2-VCP association, I utilized

the Shoc2 Δ21-C mutant lacking the PSMC5 binding domain and deficient in its ability to recruit the Shoc2 complexes to the endosomal compartment [116]. Results in **Figure 4.3.F** show that this mutant was impaired in its ability to associate with VCP as well. Given that the Shoc2 Δ21-C mutant is markedly over-ubiquitinated [116], this data indicated that endosomal localization of VCP is essential for the remodeling of the Shoc2 complex.

3. VCP modulates ubiquitination of Shoc2 in the complex on endosomes

To delineate mechanisms underlying the remodeling activity of VCP in the Shoc2 complex, we evaluated whether the ATPase activity of VCP was involved in the assembly of the Shoc2 module. ATPase activity deficient QQ mutant of VCP (amino residues) and VCP ATP-competitive chemical inhibitor CB-5083 were utilized [219-222]. Of note, cell treatment with CB-5083 has no effect on the levels of the proteins in the Shoc2 complex (**Figure 4.5**). CB-5083 was reported to not inhibit the ATPase activity of PSMC5 [219]. When examining the Shoc2-VCP interaction in cells expressing either the WT or QQ mutant of VCP-GFP, we detected increased amount of the VCP QQ mutant in the complex with Shoc2 (**Figure 4.6.A**). Similarly, increased amounts of VCP were found in GST-Shoc2 precipitate from cells treated with the CB-5083 inhibitor (**Figure 4.6.B**). Next, I assessed the interaction of Shoc2 with its other interacting partners in cells treated with CB-5083, RAF-1, PSMC5 and HUWE1. Interestingly, while the loss of ATPase activity had no effect on the ratio of RAF-1 and PSMC5 in the Shoc2 complex, we found increased amounts of VCP and the E3 ligase HUWE1 associated with Shoc2 in cells treated with CB-5083 (**Figure 4.6.C**). Given that the Shoc2 recognition

domains by VCP and HUWE1 overlap, I then explored the possibility that VCP and HUWE1 bind to the scaffold competitively. Indeed, in the cells depleted of HUWE1, increased amounts of VCP immunoprecipitated with Shoc2 (**Figure. 4.6.D**). These results suggest that VCP may potentially compete with HUWE1 and that ATPase activity of VCP plays an important role in the assembly/disassembly or "segregation" of the Shoc2 signaling module.

The E3 ligase HUWE1 mediates ubiquitination of Shoc2 and RAF-1 [120], thus our data strongly indicates that the ATPase activity of VCP may regulate the levels of the Shoc2 and RAF-1 ubiquitination catalyzed by HUWE1. In order to examine this scenario, we treated the cells with CB-5083 and examined the ubiquitination of Shoc2 and RAF-1. As expected, the levels of Shoc2 (**Figure 4.7.A**) and RAF-1 (**Figure 4.7.B**) ubiquitination were increased significantly either in cells treated with CB-5083 or cells expressing the VCP QQ mutant (**Figure 4.8**).

Studies in the Galperin lab have previously established that HUWE1-mediated Shoc2 ubiquitination is induced upon EGFR activation and its time-course closely follows the ERK1/2 phosphorylation curve (**Figure 4.7.C**, lanes 1-4) [120]. Conversely, in cells treated with CB-5083, ubiquitination of Shoc2 sustained irrespective of the EGFR activation status (**Figure 4.7.C**, lanes 6-8). Subsequently, CB-5083 treatment led to the accumulation of VCP and HUWE1 in the Shoc2 immunoprecipitate from the endosomal fractions (**Figure 4.7.D**). The levels of the ubiquitinated Shoc2 precipitated from the endosomal fraction of the cells treated with CB-5083 were also significantly higher than in control cells, while the overall ubiquitination of the proteins in the CE fraction was comparable (**Figure 4.7.E**).

Surprisingly, these experiments also revealed that the amplitude of phosphorylated ERK1/2 in cells treated with CB-5083 was higher than in control cells. These findings were inconsistent with the previously understood role of Shoc2-ubiquitination as being a negative-feedback mechanism to reduce ERK1/2 activation [120]. Thus, I examined the activation of the RAF-1 kinase coupled with Shoc2 scaffold. Phosphorylation of RAF-1 at Ser338 was compared in Shoc2 precipitates from the cells treated with CB-5083 or control cells. As shown in **Figure 4.7.F**, in control cells, phosphorylation of the Shoc2-bound RAF-1 increased 2-fold in response to EGFR stimulation. However, in the cells treated with CB-5083, no changes in RAF-1 phosphorylation were observed even though total levels of phospho-ERK1/2 were higher in the inhibitor treated cells. Given the multitude of VCP-controlled cellular functions, it is possible that loss of the VCP-ATPase activity deregulates negative feedback loops targeting other components of the ERK1/2 network, or rather, induces activation of ERK1/2 via the alternative signaling loop or kinases other than RAF-1. Teasing apart precise loops that activate ERK1/2 upon CB-5083 inhibition will require further investigation. Nevertheless, we conclude that in the Shoc2 scaffolding module, VCP is likely to regulate HUWE1-mediated Shoc2 ubiquitination by sequestering the E3 ligase HUWE1 from the complex. Taken together, these data suggests that VCP is recruited to the endosomal compartment together with Shoc2 where it exerts its mechanoenzyme activity to remodel the Shoc2 scaffolding complex, regulate the Shoc2-routed RAF-1/ERK1/2 activation, and possibly "reactivate" the Shoc2 complex.

4. The Shoc2/ERK1/2 nexus in IBMPFD pathogenesis

IBMPFD-causing mutations have significant effects on substrate processing [225]. Hence, we tested whether the most-common disease-related mutation of VCP (Arg155His) [197, 214, 215] affects levels of Shoc2 ubiquitination. Expression of the VCP R155H mutant in Cos 1 cells led to increased levels of Shoc2 ubiquitination, while expression of its WT counterpart rather had an opposite effect on ubiquitination of Shoc2 (**Figure 4.9.A**). Finally, to analyze the VCP-Shoc2 interaction under the pathologically relevant conditions, we utilized cultured primary fibroblasts from three IBMPFD patients expressing VCP proteins altered in the mutational hotspot, R155H. Fibroblasts from two healthy relatives were used as controls. The levels of Shoc2 ubiquitination were significantly higher in immunoprecipitates from lysates of IBMPFD fibroblasts when compared to lysates from healthy fibroblasts (**Figure 4.9.B**). I also observed that steady-state levels of phospho-ERK1/2 were significantly higher in IBMPFD fibroblasts, which was reminiscent of the results in **Figure 4.7.C and F**, cell treatment with VCP inhibitor. This data further indicates that aberrations in VCP function might trigger compensatory network responses that are no longer under the tight fine-tuning of the Shoc2 scaffold.

To confirm this hypothesis, we depleted Shoc2 in IBMPFD fibroblasts and examined the phospho-ERK1/2 response (**Figure 4.9.C**). As expected, siRNA depletion of Shoc2 in normal fibroblasts led to a dramatic decrease in ERK1/2 phosphorylation. However, in IBMPFD fibroblasts loss of Shoc2 had no effect on ERK1/2 phosphorylation. Our results indicate that when in complex with Shoc2, VCP facilitates tuning of the appropriate levels of ERK1/2 phosphorylation.

106

(A)
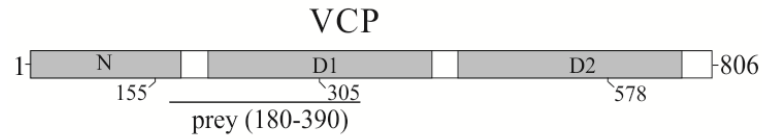
(B)
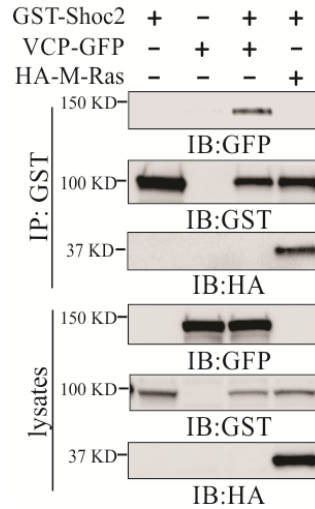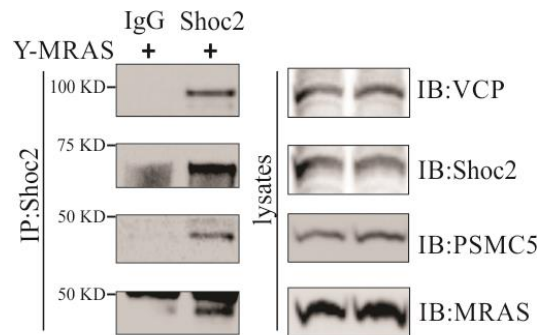
(C) **(D)**
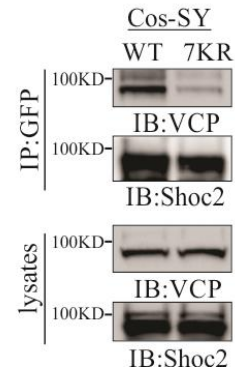
Figure 4.1 Shoc2 interacts with VCP.

(A) A schematic diagram depicting the domains of VCP protein. The position of mutants used in this study well as the prey region of VCP (aa180-390) obtained in the yeast two-hybrid screening is shown. N- N-terminus domain, D1 and D2- ATPase domain.

(B) 293FT cells were co-transfected with VCP-GFP, HA-M-Ras or GST-Shoc2. VCP-GFP and HA-M-Ras were immunoprecipitated and analyzed by immunoblotting using anti-HA, -GFP or -GST antibodies.

(C) Co-immunoprecipitation of endogenous Shoc2, VCP and PSMC5 and ectopically expressed YFP-M-Ras. Shoc2, VCP, PSMC5, and M-Ras antibodies were used to detect VCP, PSMC5 and M-Ras in Shoc2 immunoprecipitates, and in total lysates of 293FT cells.

(D) GFP-tagged VCP was immunoprecipitated from Cos cells depleted of endogenous Shoc2 and stably expressing either YFP-tagged Shoc2 or 7KR mutant Shoc2. VCP and Shoc2 were detected in GFP immunoprecipitates and lysates using anti-VCP and anti-Shoc2 antibodies.

(A)

		Shoc2-VCP binding
WT	N [1] LRR [C] 582	+
N-LRR9	1 [299]	−
N-LRR11	1 [346]	−
N-LRR15	1 [440]	+
LRR12-C	347 [582]	+
LRR12-14	347 [417]	+
LRRΔ12-14	1 [582]	−
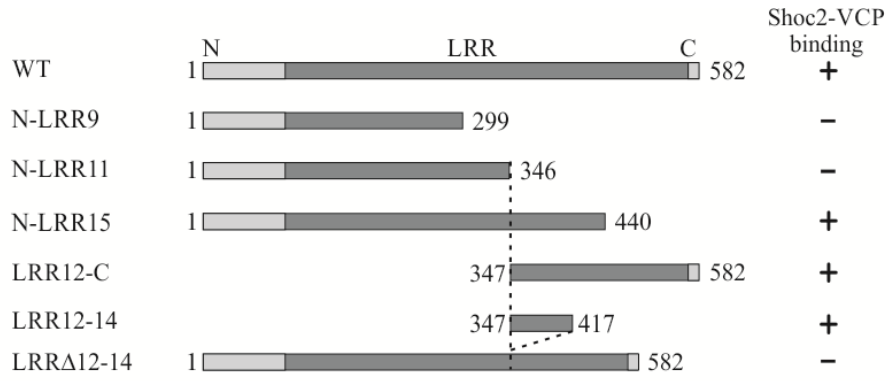
(B)
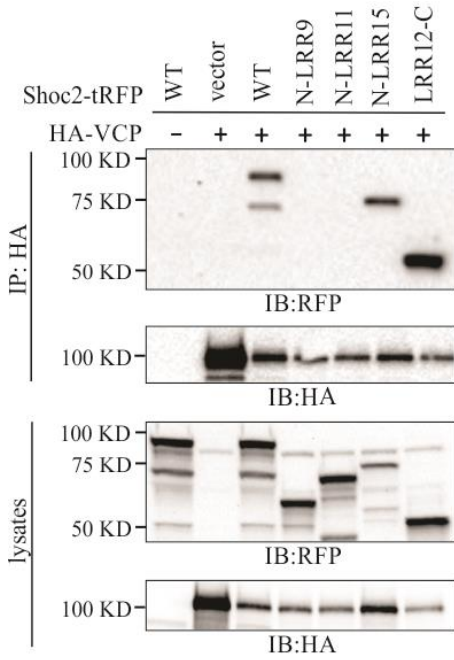
(C)
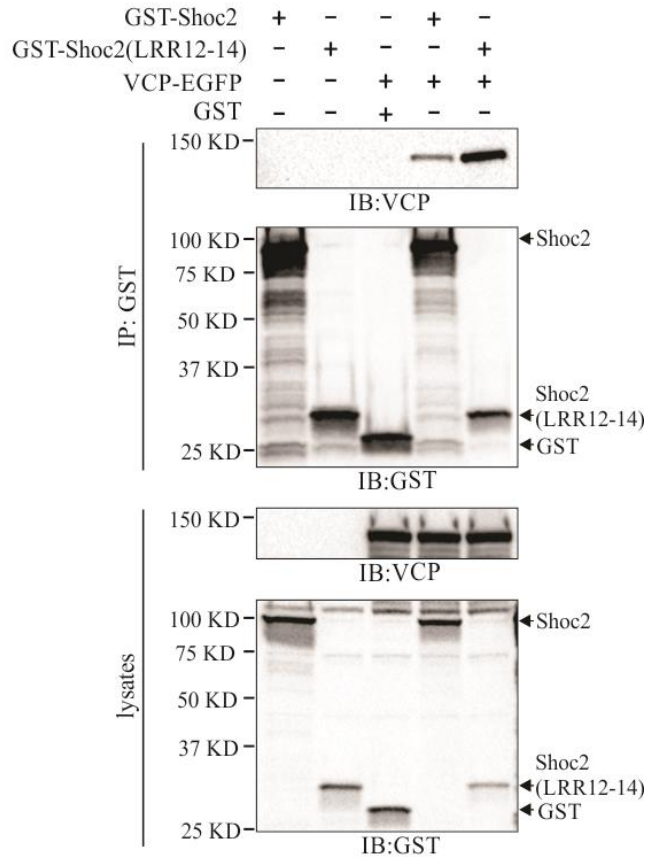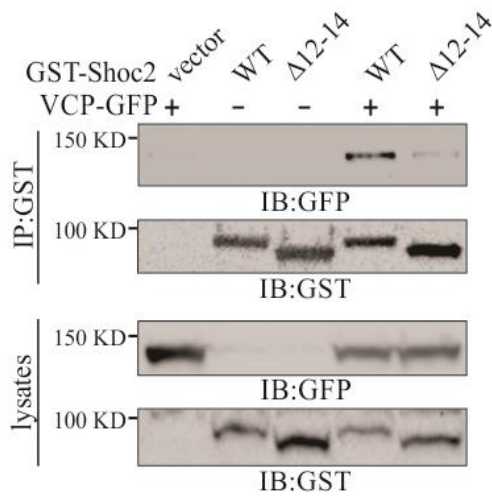
(D)   **(E)**
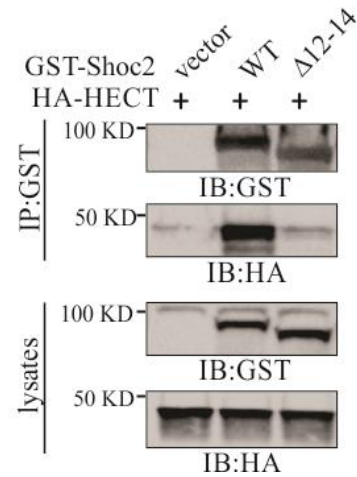
Figure 4.2 Mapping the interacting domains of VCP and Shoc2.

(A) Schematic representation of the Shoc2 truncated mutants. LRR, leucine-rich repeats.

(B) HEK 293FT cells were co-transfected with HA-VCP and Shoc2-tRFP truncated mutants depicted in **(A)**. HA-VCP was immunoprecipitated and immunoprecipitates were analyzed by immunoblotting using anti-HA and -RFP antibodies.

(C and D) HEK 293FT cells were co-transfected with VCP-GFP and Shoc2-GST WT or truncated mutant LRR12-14 **(C)**, or Δ12-14 **(D)** depicted in **(A)**. GST-Shoc2 was immunoprecipitated and analyzed by immunoblotting using anti-GST and -VCP antibodies.

(E) HEK 293FT cells were co-transfected with GST-Shoc2 (WT or Δ12-14) and HA-tagged HECT domain of HUWE1. GST-Shoc2 was immunoprecipitated and immunoprecipitates were analyzed by immunoblotting using anti-GST and -HA antibodies.

(Panel (D) and (E) were generated by EunRyoung Jang)
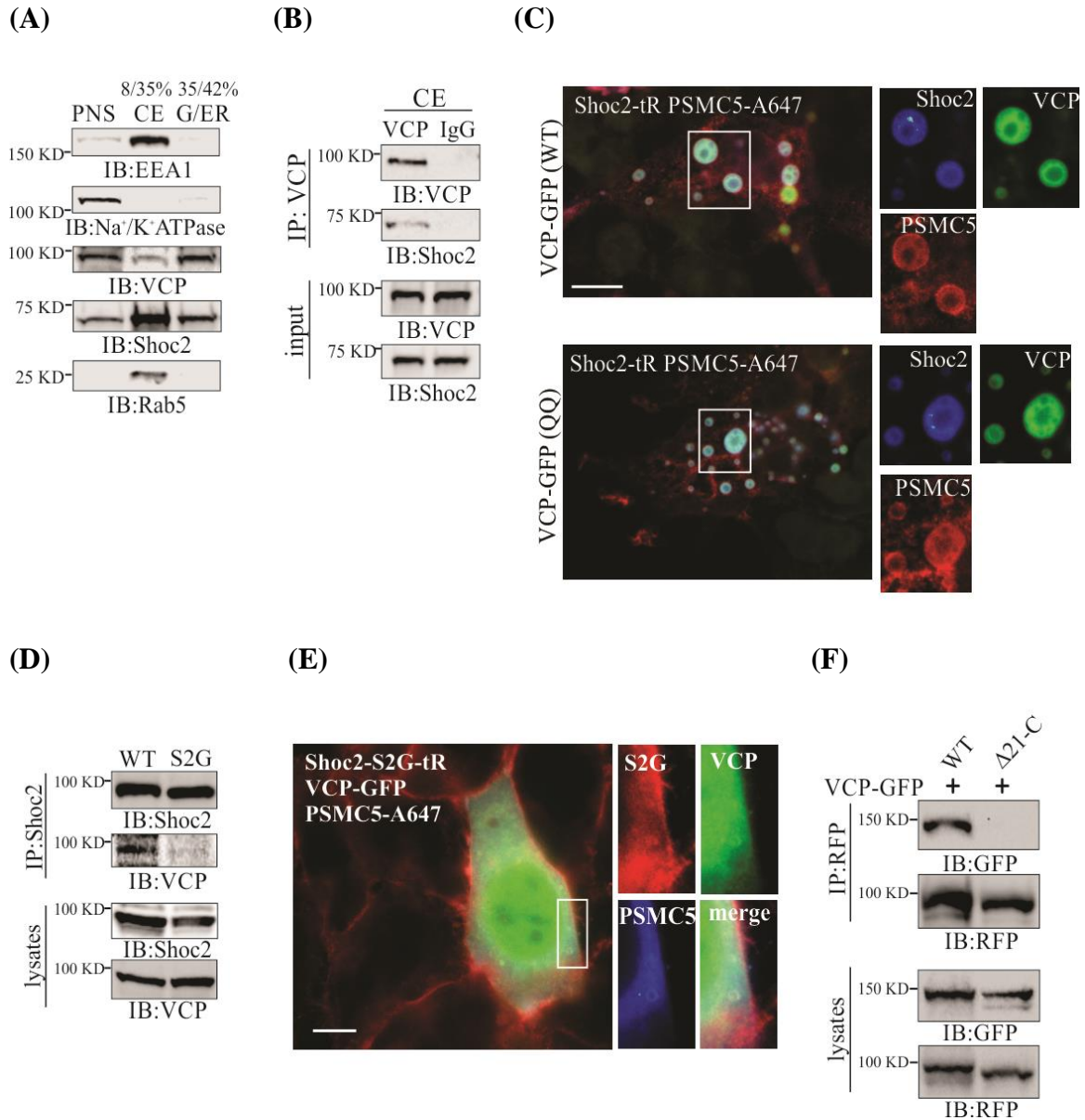
Figure 4.3. VCP is in complex with Shoc2 on endosomes.

(A) Post-nuclear supernatants (PNS) from Cos 1 cells were layered on 8-42% sucrose gradients and subjected to ultracentrifugation. The indicated proteins were identified by immunoblotting (IB) using specific antibodies in crude endosome (CE) or Golgi and endoplasmic reticulum (G/ER) fractions.

(B) VCP was immunoprecipitated from the crude endosomal fraction and analyzed by using specific anti-VCP and Shoc2 antibodies.

(C) Cos-SR cells expressing VCP-GFP (WT or QQ mutant) and GST-PSMC5 were fixed, immunostained for GST, followed by immunofluorescence microscopy. Insets

show high magnification images of the region indicated by white rectangles. Scale bars: 10 μm.

(D) Shoc2 was immunoprecipitated from Cos-SR cells depleted of endogenous Shoc2 and stably expressing WT or S2G mutant Shoc2-tRFP. The immunoprecipitates were analyzed with anti-VCP, and -Shoc2 antibodies.

(E) Cos1 cells stably expressing the Shoc2-S2G mutant (Shoc2-S2G-tR) were transfected with GST–PSMC5 and VCP-GFP. GST–PSMC5 was immunostained with anti-GST antibody. Cells were fixed and followed by immunofluorescence microscopy. Insets show high magnification images of the regions of the cell indicated by white rectangles. Scale bars: 10 μm.

(F) Cos1 cells depleted of endogenous Shoc2 and stably expressing either full-length Shoc2-tRFP (WT) or the mutant of Shoc2 (Δ21-C) were transfected with VCP-GFP. Shoc2 was immunoprecipitated (IP) using anti-RFP antibodies. The immunoprecipitates were analyzed by immunoblotting (IB) using anti-RFP and -GFP antibodies.

(Panel (D) and (F) were generated by EunRyoung Jang)

(A)

(B)
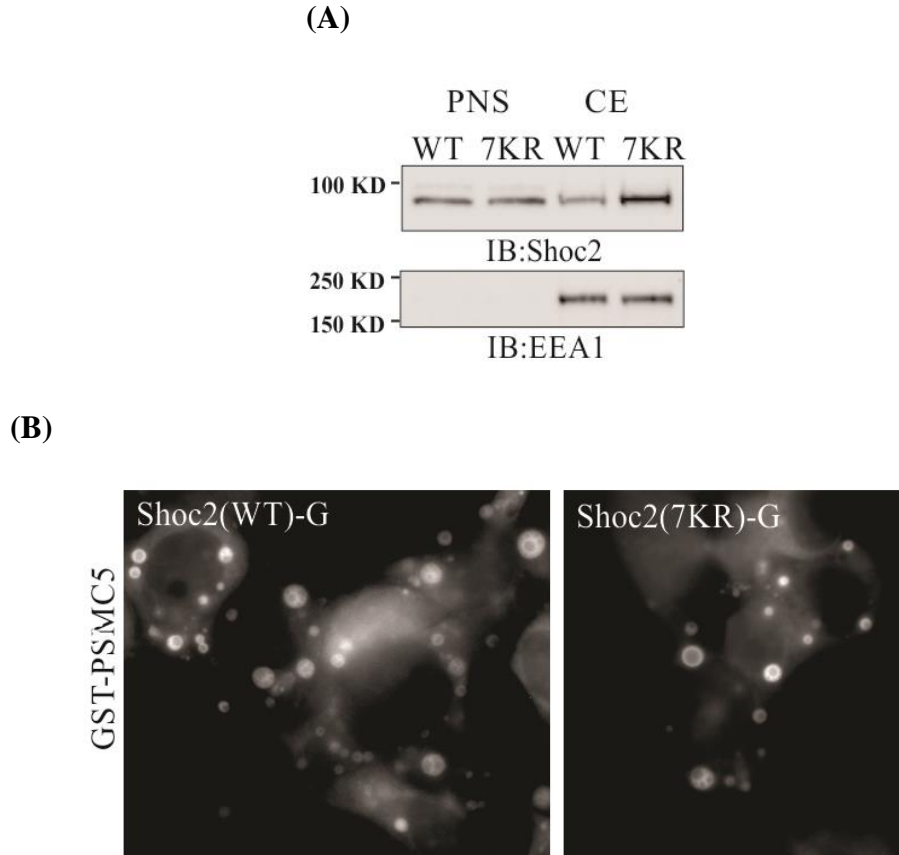
Figure 4.4 Endosomal distribution of the Shoc2 7KR mutant.

(A) Post-nuclear supernatants (PNS) from Cos1 cells stably expressing either WT Shoc2-YFP or the Shoc2-7KR mutant were layered on 8-42% sucrose gradients and subjected to ultracentrifugation to collect crude endosomal subcellular fractions (CE). Western blot analysis was performed and the expression of the indicated proteins was analyzed using specific antibodies.

(B) Cos1 cells stably expressing either WT Shoc2-YFP or the Shoc2-7KR mutant were transiently transfected with GST-PSMC5 and imaged with fluorescence microscope.
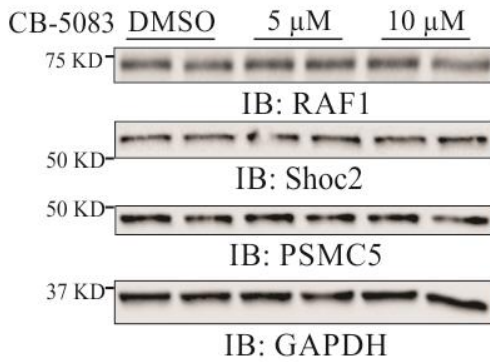
Figure 4.5 VCP does not regulate degradation of Shoc2 and Shoc2's interacting partners. Cos 1 cells were treated with the vehicle (DMSO) or two different doses of VCP-ATPase inhibitor CB-5083 for 48 h and subjected to western blot analysis. Blots were probed for RAF-1, Shoc2, PSMC5, and GAPDH.
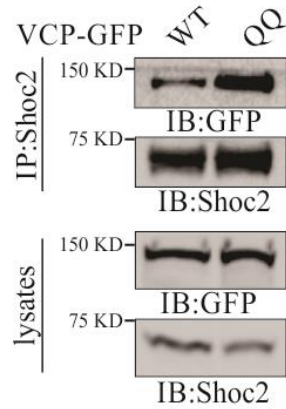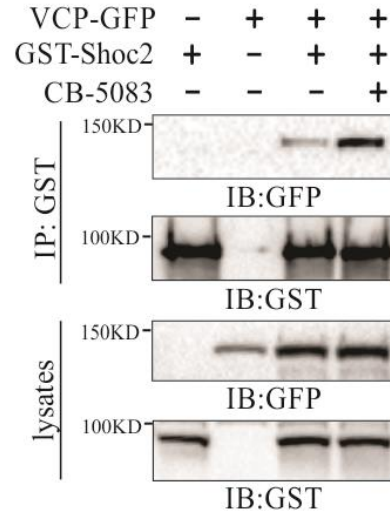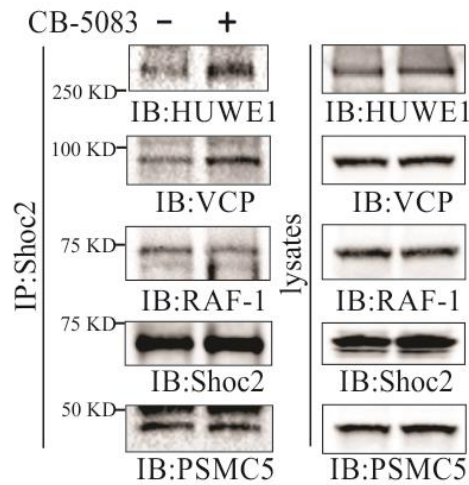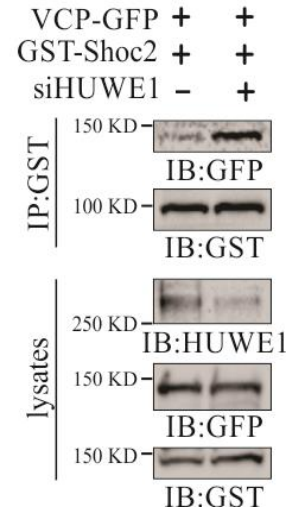
Figure 4.6 ATPase activity of VCP is necessary to modulate the interaction of Shoc2 with HUWE1.

(A) Endogenous Shoc2 was immunoprecipitated from HEK 293FT cells transfected with wild-type (WT) or catalytically inactive (QQ) mutant of VCP-GFP using anti-Shoc2 antibody. The immunoprecipitates were analyzed by immunoblotting using anti-GFP and -Shoc2 antibodies.

(B) HEK 293FT cells were co-transfected with VCP-GFP and GST-Shoc2. Cells were then treated with the vehicle (DMSO) or 5 µM of CB-5083 for 4 hr. GST-Shoc2 immunoprecipitates were analyzed using anti-GST and -GFP antibody antibodies.
(C) Endogenous Shoc2 was immunoprecipitated from Cos1 cells treated with vehicle (DMSO) or 5 µM of CB-5083 for 4 hr. The immunoprecipitates were analyzed by immunoblotting using anti-VCP, -HUWE1, RAF-1, -Shoc2, and -PSMC5 antibodies.
(D) GST-Shoc2 was immunoprecipitated from HEK 293FT cells co-transfected with VCP-GFP and GST-Shoc2 and depleted in HUWE1. The immunoprecipitates were analyzed using anti-GFP, and -GST antibodies.

(Panel (A), (C) and (D) were generated by EunRyoung Jang)

(A)

CB-5083   −   +

IP: Shoc2
IB:Ub
250 KD
150 KD
100 KD

IB:Shoc2
75 KD

lysates
IB:Ub
250 KD
150 KD
100 KD

IB:Shoc2
75 KD

(B)

CB-5083   −   +

IP:RAF-1
IB:Ub
250 KD
150 KD
100 KD

IB:RAF-1
75 KD

lysates
IB:Ub
250 KD
150 KD
100 KD

IB:RAF-1
75KD

(C)

DMSO   CB-5083
EGF   0   7   15   30   0   7   15   30   min

IP:Shoc2
IB:Ub
250 KD
150 KD
100 KD

IB:Shoc2
75 KD

lysates
IB:Ub
250 KD
150 KD
100 KD

IB:Shoc2
75 KD

IB:pERK1/2
50 KD

(D)

CE
CB-5083   −   +

IP:Shoc2
IB:HUWE1
250 KD
IB:VCP
100 KD
IB:Shoc2
75 KD

input
IB:HUWE1
250 KD
IB:VCP
100 KD
IB:Shoc2
75 KD
IB:Rab5
25 KD

(E)

CE
CB-5083   −   +

IP:Shoc2
IB:Ub
250 KD
150 KD
100 KD
IB:Shoc2
75 KD

input
IB:Ub
250 KD
150 KD
100 KD
75 KD
IB:Shoc2
75 KD

(F)

GST-Shoc2 + YFP-RAF-1

DMSO   CB-5083
EGF   −   +   −   +

IP:GST
IB:pRAF-1 (S338)
100 KD
IB:RAF-1
100 KD
IB:GST
100 KD

lysates
IB:RAF-1
100 KD
IB:GST
100 KD
IB:pERK1/2
50 KD

(G)

DMSO   CB-5083

Fold change of pRAF-1
2.5
2.0
1.5
1.0
0.5

EGF   −   +   −   +

117

Figure 4.7 VCP controls levels of ubiquitination of Shoc2 and affects RAF-1/ERK1/2 activation.

(A-B) Endogenous Shoc2 **(A)** or RAF-1 **(B)** were immunoprecipitated from denatured cell lysates of Cos1 cells treated with 5 µM of CB-5083 for 4 h. Shoc2 and RAF-1 ubiquitination was detected by immunoblotting using anti-ubiquitin (Ub) antibody.

(C) Cos1 cells were serum-starved for 16 h, treated with 5 µM of CB-5083 for 4 h, and then stimulated with EGF (0.2 ng/ml) for 7, 15 and 30 min. Endogenous Shoc2 was precipitated from denatured cell lysates using anti-Shoc2 antibodies and its ubiquitination was detected with anti-ubiquitin (Ub) antibody. Immunoblots were analyzed with anti-Shoc2, -Ub, and -pERK1/2 antibodies. The results in each panel are representative of those from three independent experiments.

(D) Crude endosomal (CE) subcellular fractions were prepared from Cos1 cells treated with vehicle (DMSO) or 5 µM of CB-5083 for 4 h. Endosomal Shoc2 was immunoprecipitated and analyzed using indicated antibodies. Rab5 was used as a loading control.

(E) Shoc2 was precipitated from denatured endosomal fractions prepared in (D) using anti-Shoc2 antibodies. Shoc2 ubiquitination was detected with anti-Ub antibody.

(F) Cos1 cells were transfected with GST-Shoc2 and YFP-RAF-1. At 48 h post-transfection, the cells were serum-starved for 16 h and treated with vehicle (DMSO) or 5 µM of CB-5083 for 4 h and then stimulated with EGF (0.2 ng/ml) for 7 min. Shoc2 was immunoprecipitated using anti-GST antibody. Immunoblots were analyzed with anti-p-RAF-1, -RAF-1, -GST, and -pERK1/2 antibodies. Blots from the multiple experiments were analyzed. Bars represent the mean ± S.E. (n=3) for pRAF-1 normalized to the value for GAPDH in arbitrary units (P<0.01, by Student's t-test).

The results in each panel are representative of those from three independent experiments.

(Panel (C) and (D) were generated by EunRyoung Jang)
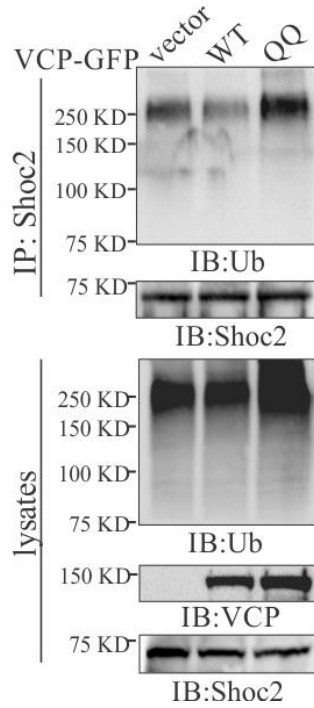
Figure 4.8 Ubiquitination of Shoc2 is altered in VCP mutant (E305Q, E578Q) expressing Cos1 cells. Endogenous Shoc2 was precipitated from the denatured cell lysates of Cos1 cells expressing vector, WT, or R155H mutant of VCP-GFP mutant. Shoc2 ubiquitination was detected with anti-Ub antibody.
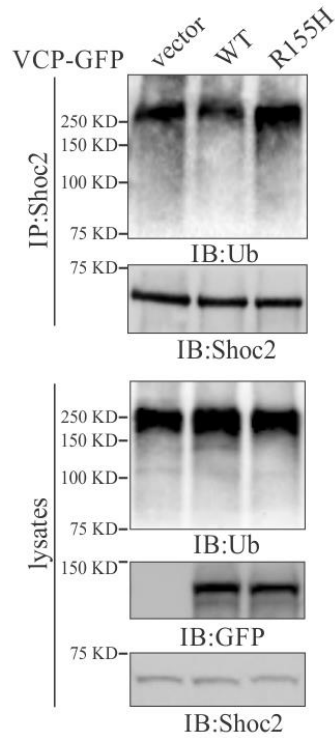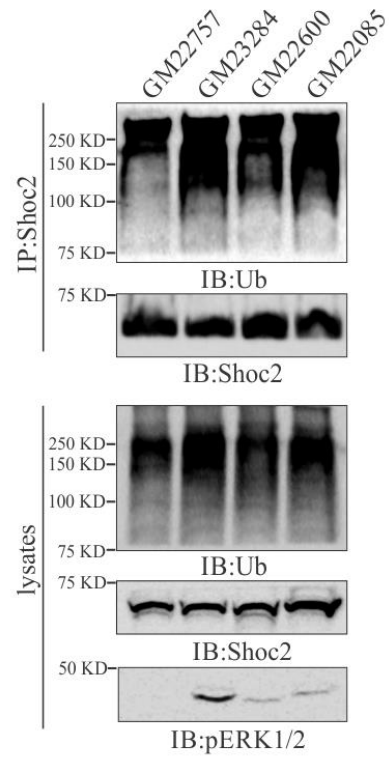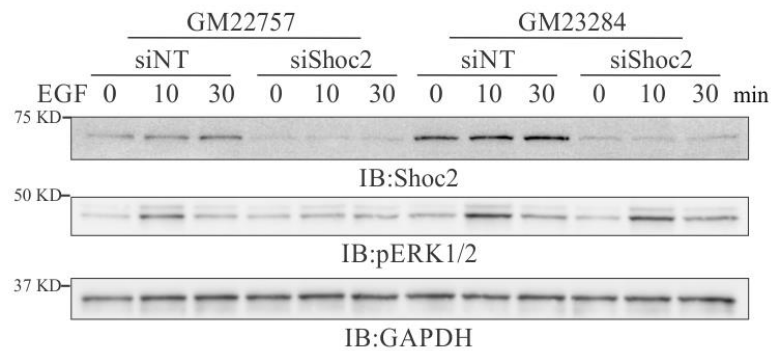
Figure 4.9 Ubiquitination of Shoc2 is altered in fibroblasts from IBMPFD patients.
(A) Endogenous Shoc2 was precipitated from the denatured cell lysates of Cos1 cells expressing WT and R155H mutant of VCP-GFP. Shoc2 ubiquitination was detected with anti-Ub antibody.

(B) Endogenous Shoc2 was immunoprecipitated from the denatured lysates of primary fibroblast using anti-Shoc2 antibodies. GM23284, GM22600, GM22085 – fibroblasts harboring VCP R155H mutation, GM22757- normal control. Shoc2 ubiquitination was detected with anti-Ub antibody. pERK1/2 was analyzed using specific pERK1/2 (p42/44) antibodies.

(C) Primary fibroblasts from (B) were transfected with non-targeting (NT) siRNA or Shoc2 (siShoc2) siRNAs. Cells were serum-starved for 16 h and then stimulated with EGF (0.2 ng/ml) for 0, 10, and 30 min. Immunoblots were analyzed with anti-pERK1/2, -Shoc2, and -GAPDH antibodies. Blots from the multiple experiments were analyzed. Bars represent the mean ± S.E. (n=3) for pERK1/2 normalized to the value for GAPDH in arbitrary units (P<0.01, by Student's t-test).

The results in each panel are representative of those from three independent experiments.

(Panel (A) and (B) were generated by EunRyoung Jang)

Chapter 5

Discussion and Future Directions

The work presented in this dissertation was performed with the goal of defining the physiological function of Shoc2-routed ERK1/2 signals in embryonic development and revealing new insights into the molecular mechanisms underlying Shoc2-mediated ERK1/2 signaling. This dissertation is comprised of two interconnected research projects discussed in two separate chapters. In chapter 3, I described the work that utilized a zebrafish vertebrate model and demonstrated that Shoc2 is critical in early embryonic development and its loss results in a number of developmental deficiencies, including profound loss of blood cells and delay in development of multiple neural crest lineages.

In chapter 4, I characterized the novel interacting partner within the Shoc2 scaffolding module, AAA+ ATPase VCP. Studies in this chapter show that VCP activity is a critical element in the mechanisms remodeling the Shoc2 signaling complex and fine-tuning the ERK1/2 signals. Importantly, these studies also demonstrate that the alterations in Shoc2 ubiquitination and ERK1/2 phosphorylation are important elements of the IBMPFD pathology.

1. The physiological function of Shoc2 in development

Given the early embryonic lethality of shoc2 knock-out mice and causative effects of Shoc2 mutations in NSLH syndrome, we hypothesized that Shoc2 is critical for normal development. However, the biological targets of the Shoc2-mediated ERK1/2 signals are

not clear. Transient depletion of Shoc2 in zebrafish using *shoc2*-specific MO allowed us to observe the profound effect Shoc2 depletion has on very early developmental stages. We found that the depletion of Shoc2 in early stage embryos causes defects in blood cell development, vasculature development and ERK1/2 activation. The results obtained using MO prompted us to generate a heritable zebrafish *shoc2* knockout utilizing the most rapidly developing genetic methodology- CRISPR/Cas9 editing. CRISPR/Cas9 genetic editing can be easily applied to virtually any genome of interest by a customizable short RNA guide targeting Cas9 endonuclease [226]. Using this methodology, a number of germline-transmitting CRISPR/Cas9 *shoc2* mutant lines were successfully generated. In the studies summarized above, I have utilized two genetically-modified zebrafish lines harboring either 22 bp deletion in exon 2 or 14 bp deletion in exon 3. Similar to mice knockouts, our findings demonstrate that a systemic deficit of Shoc2 in zebrafish critically impairs a number of developmental functions and is lethal [227]. Interestingly, unlike s*hoc2* knockout mice, our *shoc2* CRISPR/Cas9 zebrafish knockout did not present with apparent changes in cardiac function or pericardial effusions, although further studies are needed to analyze possible subtle heart malformations. Yi and colleagues observed that conventional *shoc2*$^{-/-}$ (*sur-8* in mice) knockout mice die due to an early stage embryonic lethality and partial absorption of mutant embryos at E8.5 [121]. The conditional deletion of the *shoc2* gene in endothelial cells displayed multiple cardiac defects, smaller body size, subcutaneous edema in their dorsal body, fetal lung congestion and did not survive past E14.5. These *shoc2*-deficient mice had abnormalities in transposition of the great arteries, a ventricular septal defect, and double outlets of the right ventricle and right aortic arch and defects of heart valve

morphogenesis. Surprisingly, no obvious change in the level of activated ERK1/2 or two other MAP kinases, JNK and p38, were detected in *shoc2* null endothelial cells, possibly indicating the non-autonomous role for Shoc2 in the endothelial cells.

A key finding of this study is that the abrogated expression of Shoc2 in zebrafish embryos results in a rapid manifestation of a robust phenotype that exhibits hallmarks of human RASopathies, further supporting the likelihood of conservation in Shoc2 signaling targets between human and zebrafish. Remarkably, severe edema, anemia, and arrhythmia observed in *shoc2* null larvae were reminiscent of fetal hydrops- a serious fetal condition previously reported in several cases of newborns heterozygous for the S2G missense mutation in Shoc2. In patients molecularly diagnosed with Shoc2's NSLH mutation, fetal hydrops presented as fluid accumulation in fetal compartments, pleural and pericardial effusion, skin edema, leukocytosis, and thrombocytopenia [123, 166, 228].

Craniofacial defects detected in Shoc2 null larvae are another well-recognized component of the pleiotropic spectrum of RASopathy phenotypes [229]. The striking abnormalities in the development of cartilage, bone ossification, and the patterning of pigment cells in *shoc2* null zebrafish larvae indicate an essential role for Shoc2 in the specification of neural crest-derived tissues. In addition to craniofacial cartilage, bone and melanocytes, smooth muscle, blood vessels, peripheral and enteric neurons, and glia are all derived from a temporary group of highly migratory multipotent stem cells that delaminate from the neural tube early in embryogenesis [230, 231]. Importantly, several of the RASopathy hallmarks, such as craniofacial birth defects are usually attributed to the defects in neural crest cell development. Augmented expression of the transcription

factor *foxd3* found in *shoc2* knockouts provides insights into the possible underlying mechanisms downstream of the Shoc2-ERK1/2 module and is in-line with the canonical function of the Ras/ERK1/2 pathway in neural crest specification and migration [232]. High levels of *sox10* or *foxD3* in embryonic stem cells and neural crest cells have been shown to promote multi-potentiality and the levels of *these* transcription factors change dramatically with cell specification [233-235]. Hence, it is possible that suppression of Shoc2-mediated ERK1/2 signals promotes the maintenance of pluripotent progenitor cells due to increased *foxD3* levels, or other related transcription factors, consequently delaying neural crest differentiation and migration. Interestingly, lentiviral depletion of Shoc2 in neuronal progenitor cells (NPCs) resulted in misbalanced differentiation and proliferation of NPCs [115]. Although these studies did not formally demonstrate a requirement for Shoc2-ERK1/2 activity in stem cell specification, they showed that Shoc2 may act as an anti-differentiation factor that may regulate ERK1/2 signals controlling NPCs for proliferation and self-renewal. However, other Shoc2-ERK1/2 dependent mechanisms, such as selective integration of signals mediated by BMP, TGFβ, FGF or EGF cannot be excluded [236]. Even though several signaling pathways are involved in the development of neural crest-derived tissues [236], our data indicate that the changes observed in *shoc2* null animals attest to a lack of functional redundancy with other members of the ERK1/2 pathway and/or contribute to the expression of different sets of transcriptional downstream targets. Our data in **Figure 3.23** show that *shoc2* is highly expressed in *sox10*-positive cells, indicating its cell autonomous functions in neural crest cells. Future studies in cells isolated from neural crest lineages will facilitate the identification of molecules upstream and downstream of the Shoc2-ERK1/2 module

and are likely to reveal novel functions of Shoc2 in neural crest development. The exact details of how Shoc2-ERK1/2 signals affect neural crest specification remain to be elucidated. Future studies utilizing CRISPR/Cas9 mutants transgenic for the neural crest markers *sox10:RFP* or *foxD3:GFP* will help determine the Shoc2-ERK1/2 signals regulating motility of the neural crest cells or the transcriptional programs regulating their specification.

Occasionally, RASopathy patients are diagnosed with an aggressive myeloproliferative disorder resembling a rare hematologic malignancy in children termed Juvenile myelomonocytic leukemia (JMML) [237, 238]. Some JMML symptoms such as anemia and thrombocytopenia are reminiscent of the robust loss of circulating blood cells we observed in the Shoc2 crispants and, based on our data in **Figure 3.28**, is likely due to the autonomous function of Shoc2 in hematopoietic cells.

The findings that *shoc2* crispants did not have a preferential loss of a particular blood lineage (**Figure 3.30**) support our hypothesis that Shoc2-ERK1/2 signals are universally critical for the production or expansion of progenitors rather than the differentiation of a particular blood lineage at the very early stages of hematopoiesis. The balance between primitive erythroid and myeloid cell production is primarily governed by equilibrium of the expression of the transcription factor *gata-1* and *pu.1* [184, 185, 190, 239]. Loss of *gata-1* expression in zebrafish embryos results in transformation of erythroid precursors into myeloid precursors with myeloid expansion at the expense of total number of erythroid cells [239]. Our data in **Figure 3.26** and **3.27**, showing that the loss of Shoc2 causes a reduction in expression of both *gata-1* and *pu.1* further supports

our hypothesis that Shoc2-ERK1/2 signals are responsible for the production/expansion of blood progenitors.

Based on earlier studies demonstrating that Shoc2 transduces ERK1/2 cell motility signals [240], it is tempting to speculate that Shoc2-deficient hematopoietic progenitors are impaired in their ability to migrate to the environment that supports their maturation. Alternatively, the loss of Shoc2 may abrogate the signals potentiating the maturation of these cells. To test this notion, CRISPR/Cas9 mutants transgenic for c-*myb:eGFP* or *cd41:GFP*, markers widely utilized to visualize hematopoietic stem and progenitor cells, will be particularly beneficial. These transgenic zebrafish lines will allow tracing the development of HSCs in real time as well as the analysis of fundamental transcriptional programs of HSCs in *shoc2* null fish.

Alterations in the expression of the Shoc2 binding partners, Ras and RAF-1, in zebrafish are found to cause phenotypes partially overlapping with those observed in *shoc2* mutants [241, 242]. Yet, the robust phenotype observed for *shoc2* nulls in which expression of Ras and RAF signaling proteins is unaltered suggests that the Shoc2 scaffold is critical for Ras-RAF signal transmission, underscoring its role as a "master organizer" and also emphasizes the critical role of the Shoc2-routed ERK1/2 signal.

One of the advantages of using zebrafish is the ability to annotate the pathogenicity and biological activity of human disease-causing alleles. As a future study, it will be interesting to determine the effect of RASopathy mutations and Shoc2 ubiquitination in zebrafish development.

In summary, a novel zebrafish model was developed to identify a previously unrecognized role of Shoc2 in vasculogenesis, in the specification of neural crest cells, and in hematopoiesis. This study not only emphasizes a critical role for Shoc2 in the morphogenesis of embryonic tissues, but also underscores the advantages of our zebrafish model for dissecting the contribution of individual regulatory components of the ERK1/2 pathway. The zebrafish $shoc2^{-/-}$ model will be very instrumental in identifying the implications of the multiple Shoc2 protein interactions through *in vivo* structure-function analysis. Our model will further help elucidate molecular mechanisms underlying Shoc2-related pathologies, help track the molecular changes that take place when Shoc2 is not transmitting ERK1/2 signals, as well as determine the roles of target genes downstream of the Shoc2 scaffolding module in a number of developmental processes.

2.1 VCP is a part of the Shoc2-Ras-RAF-1 signaling complex

Studies presented here are the first to identify the AAA+ ATPase VCP as a player in the ERK1/2 cascade and provide new insight into the mechanism modulating ubiquitination of Shoc2 and RAF-1 and the subsequent transmission of the signals through the Shoc2 scaffolding complex. I show compelling evidence that VCP is an integral partner in the Shoc2 signaling module. Results in **Figure 4.1** and **4.2** demonstrate that a pool of endogenous VCP is found in the multimolecular complex with Shoc2 and its known molecular partners HUWE1, M-Ras, PSMC5 and RAF-1, and that leucine-rich repeats 12 to 14 of Shoc2's LRR domain are sufficient for the recognition of Shoc2 by VCP [110, 111, 116, 119, 120]. This data also shows that VCP is associated with ubiquitinated Shoc2 (**Figure 4.1.D**). Prior work demonstrated that VCP is associated with

a set of adaptor proteins that recruit or modify substrates [202, 206-209, 224, 225, 243-247]. Thus, it is unlikely that VCP recognizes Shoc2 without the assistance of a cofactor. Future studies using an unbiased mass-spectrometry approach would be instrumental in defining other molecular determinants of the complex, including a cofactor mediating the VCP and Shoc2 recognition and, possibly, additional components of the VCP-related machinery in the Shoc2 complex.

Our findings of overlap in the VCP's and HUWE1's Shoc2 recognition site at the LRR 12-14 provided a critical clue into the possible function of VCP in the Shoc2 complex, implying that VCP might compete with the E3 ligase for Shoc2 binding. Therefore, we postulated that in the Shoc2 complex, mechano-activity of VCP is exerted to "sequester" the E3 ligase HUWE1 from the Shoc2 scaffolding complex in order to modulate levels of the ubiquitin conjugated to Shoc2 and tune the signals transmitted via the Shoc2 module. This hypothesis was consistent with the observations that perturbations in ATPase activity of VCP lead to changes in the stoichiometric ratio of VCP and HUWE1 in the Shoc2 complex and altered both levels and dynamics of Shoc2 ubiquitination. This hypothesis is also in agreement with the core biochemical activity of VCP to segregate protein components from multiprotein complexes or multimolecular structures [196, 197]. The precise mechanism by which VCP exerts its "segregase" activity is not known, but the most accepted hypothesis is that VCP grabs onto the ubiquitinated polypeptide to be segregated and initiates it unfolding. Thus, it is conceivable that in the Shoc2 complex VCP also acts as "segregase" that unfolds ubiquitinated substrate. However, which one of the proteins in the Shoc2 complex is a "true" substrate that undergoes unfolding is not clear. Along with

Shoc2 and RAF-1, the E3 ligase HUWE is also marked by ubiquitin as the HECT domain of HUWE1 catalyze self-ubiquitination in the process of Ubiquitin transmission [120].

Assuming that Shoc2 is the "true" substrate of VCP, a number of outcomes for this segregation activity in the complex are possible. For instance, in addition to the sequestration of HUWE1 from the complex, Shoc2 unfolding may also result in the loss of RAF-1 or in an orientation of RAF-1 that would be unfavorable for signal transmission. These scenarios require further studies using methodologies that can reconstitute remodeling events of the Shoc2 scaffolding complex *in vitro*. Overall, we have yet to determine whether VCP-induced changes in the composition of the Shoc2 complex ultimately lead to changes in Shoc2 conformation, actual dissociation of HUWE1 from the complex or other related events of the complex remodeling.

Irrespective of the specific aspects of the Shoc2 complex remodeling, this study provides novel, exciting knowledge on how the ubiquitin machinery regulates signal transition. Previous work revealed that ubiquitin conjugates are utilized to control the Ras-ERK1/2 signal transduction differentially [217]. Ubiquitination stabilizes the association of H-Ras with endosomes and its ability to activate the ERK1/2 pathway [248]. K-Ras and H-Ras are each shown to be activated by mono-ubiquitination but via distinct molecular mechanisms. While mono-ubiquitination of K-Ras has an inhibitory effect on GAP-mediated hydrolysis, mono-ubiquitination of H-Ras enhances GTP-GDP exchange [248-250]. In addition to studies in the Galperin lab demonstrating that ubiquitin conjugates control the activation status of the RAF-1 kinase, others reported that RAF-1 stability and degradation are controlled by the ubiquitin-proteasome system [120]. Additional equally interesting examples are known, but the comprehensive picture

of how ubiquitination is involved in the regulation of the ERK1/2 signaling cascade is far from being complete.

Furthermore, results presented here are in agreement with the earlier observations demonstrating that Shoc2 ubiquitination is controlled in a spatially restricted manner [116]. Much like the E3 ligase HUWE1 and AAA+ ATPase PSMC5, VCP was found in complex with wild-type Shoc2 when targeted to the endosomal membranes. In contrast, VCP failed to recognize the aberrantly targeted to the plasma membrane Shoc2 S2G RASopathy mutant (**Figure 4.3.D and E**). Inhibition of VCP activity by CB-5083 caused an increased ubiquitination of the endosome-localized Shoc2, further emphasizing the role endosomes play in supporting the specific micro-environmental requirement for the regulation of signaling [96]. MP1/p14 (or LAMTOR2-LAMTOR3), β-arrestin, and flotillin-1 are adaptor proteins that utilize endocytic compartments as spatially confined intracellular platforms to control both intensity and specificity of signals transduced through these complexes [7, 25, 77, 85-89, 251].

The processing of VCP substrates is contingent on the binding of K48- and K11-conjugated ubiquitin chains by VCP and/or its adaptor [252]. The Galperin lab previously showed that Shoc2 contains K48- and K-63 ubiquitin chains [120]. Further work *in vitro* and *in vivo* studies are needed to determine the exact requirements and the nature of ubiquitin chains required for the interaction with VCP.

Importantly, we observed that the inhibition of VCP activity by CB-5083 leads to a consistent increase in the phospho-ERK1/2 response to stimuli (**Figure 4.7.C and F**). This prompted a hypothesis that the abnormal function of VCP not only affects the regulatory mechanisms within the Shoc2 complex but also deregulates a tightly

controlled ERK1/2 signaling network and affects the balance through multiple branches of the network.

2.2 Functional implications of VCP-modulated ubiquitination of Shoc2

Results of this study showed that loss of VCP activity alters the amplitude of RAF-1 kinase phosphorylation (**Figure 4.7.F**), indicating that VCP provides an additional control over the amplitude of the ERK1/2 signals transmitted via the Shoc2 module. Thus, somewhat not surprisingly, we found that in primary fibroblasts collected from patients diagnosed with IBMPFD and harboring the R155H mutation, levels of Shoc2 ubiquitination and phospho-ERK1/2 were dysregulated.

VCP has been identified as a causative gene of the dominantly inherited syndrome IBMPFD, a neuro-degenerative multi-systemic disorder with cognition defects [196, 253]. The R155H substitution is the most prevalent, but the precise effect of this hot-spot mutation on VCP's ATPase activity is still a subject for active investigation [216]. Several studies argue that this mutation has no effect on VCP structure and is leading to an elevated ATPase activity as an indirect consequence of a decoupling of substrate binding from mechanochemical transduction in the D2 domain of VCP [254]. Overall, the mechanisms of IBMPFD pathogenesis are not fully understood [196, 197].

My work shows that Shoc2 accelerates ERK1/2 activity upon pathway stimulation in primary fibroblasts obtained from healthy individuals (**Figure 4.9.C**). However, in primary fibroblasts harboring a VCP (R155H) mutation, levels of Shoc2-conjugated ubiquitin and phospho-ERK1/2 were elevated (**Figure 4.9.C**). Importantly, Shoc2 depletion had no effect on EGF-induced activation of ERK1/2 in IBMPFD, further

supporting our hypothesis that Shoc2-ERK1/2 signals are part of a tightly controlled and

balanced larger signaling network and that deregulation in the Shoc2-ERK1/2 axis

triggers imbalanced ERK1/2 activity. Importantly, this study is the first to suggest a

possible involvement of aberrant ERK1/2 signaling in the pathogenesis of IBMPFD.

Future studies will aid in understanding the full extent of the mechanisms causing this

disease.
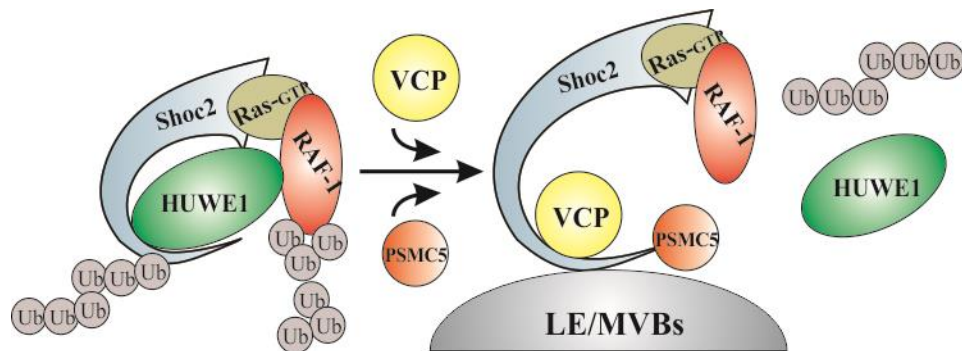
Figure 5.1 Schematic model of VCP's function in Shoc2-mediated ERK1/2 signals.
HUWE1 mediates ubiquitination of Shoc2 and RAF-1 that negatively regulates the RAF-1 activity. Subsequently, PSMC5 facilitates the redistribution of the ubiquitinated Shoc2 complex to endosomes where VCP drives the remodeling of the Shoc2 module by disengaging HUWE1 as a matter of "reactivating" the Shoc2 signaling module for the next signal transmission.

To summarize, we propose a model that is based on what is currently understood

for the mechanisms modulating the Shoc2-mediated ERK1/2 signals (**Figure 5.1**). This

model postulates that ERK1/2 pathway activation is followed by HUWE1-mediated

ubiquitination of Shoc2 and RAF-1, causing adjustments in the amplitude of ERK1/2

signaling. Thereafter, PSMC5 facilitates the recruitment of the Shoc2 complex to

endosomes where VCP possibly sequesters or "segregates" HUWE1 from the Shoc2

complex, possibly aiding in the "reactivation" of the Shoc2 signaling module.

To provide further support for this model, it is necessary to examine the activation of RAF-1 that is in complex with Shoc2 on endosomes. Future studies should investigate where the Shoc2-Ras-RAF-1 complexes are formed when proteins of the ubiquitin machinery (HUWE1, PSMC5, and VCP) incorporate into the complex and what triggers the Shoc2-VCP interaction.

In summary, the studies presented in this dissertation identified an unexpected physiological role for the Shoc2-transmitted ERK1/2 signals in hematopoiesis and neural crest development. They also added another layer to our understanding of the mechanisms controlling transmission of the ERK1/2 signals through the Shoc2 scaffolding complex. Together these results have a potential to open up new avenues for the development of better therapeutic strategies for the treatment of RASopathies and IBMPFD.

Appendix

List of Acronyms and Abbreviations

ALM	Anterior lateral mesoderm
AGM	Aorta-gonad-mesonephros
AAA+ ATPase	ATPase-associated with diverse cellular activities
bp	Base pair
JNK	c-Jun N-terminal kinase
CFC	Cardio-facio-cutaneous syndrome
CHT	Caudal hematopoietic tissue
CRISPR	Clustered regularly interspaced short palindromic repeats
Cas9	CRISPR-associated protein 9
CE	Crude endosome
dpf	Days post fertilization
DNA	Deoxyribonucleic acid,
DA	Dorsal aorta
EEA1	Early endosome antigen 1
ERAD	Endoplasmic reticulum associated protein degradation
EGFP	Enhanced green fluorescent protein
EGF	Epidermal growth factor
EGFR	Epidermal growth factor receptor
Erbin	Erbb2 interacting protein
EMPs	Erythromyeloid progenitors
ERK	Extracellular signal-regulated kinase
FGF	Fibroblast growth factor receptor
FGFR	Fibroblast growth factor receptor
FACS	Fluorescence activated cell sorting
GST	Glutathione-S-transferase
GAPDH	Glyceraldehyde 3-phosphate dehydrogenase
G/ER	Golgi/Endoplasmic reticulum
GFP	Green fluorescent protein
HUWE1	HECT, UBS and WWE domain containing 1
HA	Hemagglutinin
HSCs	Hematopoietic stem cells
HRMA	High resolution melting analysis
HPLC	High-performance liquid chromatography
hpf	Hours post fertilization
IP	Immunoprecipitation
IBMPFD	Inclusion body myopathy with paget's disease of bone and frontotemporal dementia

ICM	Intermediate cell mass
IQGAP1	IQ motif-containing GTPase activating protein 1
JMML	Juvenile myelomonocytic leukemia
kDa	Kilo dalton
KSR	Kinase suppressor of Ras
LE/MVBs	Late endosomes/Multivesicular bodies
LRR	Leucine-rich repeat
MP1	MAPK kinase 1 partner
MAPKAPK	MAPK-activated protein kinase
MAPK	Mitogen-activated protein kinase
MEK	Mitogen-activated protein kinase kinase
MO	Morpholino
NGF	Nerve growth factor
NCCs	Neural crest cells
NF1	Neurofibromatosis type 1
NS	Noonan syndrome
NSLH	Noonan syndrome with loose anagen hair
NSML	Noonan syndrome with multiple lentigines
PFA	Paraformaldehyde
PTU	Phenyl thiourea
PCR	Polymerase chain reaction
PVC	Posterior cardinal vein
PSMC5	Proteasome 26S subunit ATPase 5
PP1c	Protein phosphatase 1c
qPCR	Quantitative PCR
RTK	Receptor tyrosine kinase
RFP	Red fluorescent protein
RT-PCR	Reverse transcript PCR
RNA	Ribonucleic acid
SCRIB	Scribbled homolog
sgRNA	Single guide RNA
siRNA	Small interfering RNA
SH2	Src homology 2
SIV	Sub-intestinal vein
UPS	ubiquitin-proteasomal system
VCP	Valosin-containing protein
VAST	Vertebrate automated screening technology
WT	Wild-type

References

1. Roskoski, R., Jr., *ERK1/2 MAP kinases: structure, function, and regulation.* Pharmacol Res, 2012. **66**(2): p. 105-43.
2. Ramos, J.W., *The regulation of extracellular signal-regulated kinase (ERK) in mammalian cells.* Int J Biochem Cell Biol, 2008. **40**(12): p. 2707-19.
3. Katz, M., I. Amit, and Y. Yarden, *Regulation of MAPKs by growth factors and receptor tyrosine kinases.* Biochim Biophys Acta, 2007. **1773**(8): p. 1161-76.
4. Schulze, W.X., L. Deng, and M. Mann, *Phosphotyrosine interactome of the ErbB-receptor kinase family.* Mol Syst Biol, 2005. **1**: p. 2005 0008.
5. Zarich, N., et al., *Grb2 is a negative modulator of the intrinsic Ras-GEF activity of hSos1.* Mol Biol Cell, 2006. **17**(8): p. 3591-7.
6. Margolis, B. and E.Y. Skolnik, *Activation of Ras by receptor tyrosine kinases.* J Am Soc Nephrol, 1994. **5**(6): p. 1288-99.
7. Wortzel, I. and R. Seger, *The ERK Cascade: Distinct Functions within Various Subcellular Organelles.* Genes Cancer, 2011. **2**(3): p. 195-209.
8. Marshall, C.J., *Specificity of receptor tyrosine kinase signaling: transient versus sustained extracellular signal-regulated kinase activation.* Cell, 1995. **80**(2): p. 179-85.
9. Ebisuya, M., K. Kondoh, and E. Nishida, *The duration, magnitude and compartmentalization of ERK MAP kinase activity: mechanisms for providing signaling specificity.* J Cell Sci, 2005. **118**(Pt 14): p. 2997-3002.
10. Murphy, L.O. and J. Blenis, *MAPK signal specificity: the right place at the right time.* Trends Biochem Sci, 2006. **31**(5): p. 268-75.
11. Pouyssegur, J., V. Volmat, and P. Lenormand, *Fidelity and spatio-temporal control in MAP kinase (ERKs) signalling.* Biochem Pharmacol, 2002. **64**(5-6): p. 755-63.
12. Mor, A. and M.R. Philips, *Compartmentalized Ras/MAPK signaling.* Annu Rev Immunol, 2006. **24**: p. 771-800.
13. Lloyd, A.C., *Distinct functions for ERKs?* J Biol, 2006. **5**(5): p. 13.
14. Traverse, S., et al., *EGF triggers neuronal differentiation of PC12 cells that overexpress the EGF receptor.* Curr Biol, 1994. **4**(8): p. 694-701.
15. Morrison, D.K. and R.J. Davis, *Regulation of MAP kinase signaling modules by scaffold proteins in mammals.* Annu Rev Cell Dev Biol, 2003. **19**: p. 91-118.
16. Chuderland, D. and R. Seger, *Protein-protein interactions in the regulation of the extracellular signal-regulated kinase.* Mol Biotechnol, 2005. **29**(1): p. 57-74.
17. Vaudry, D., et al., *Signaling pathways for PC12 cell differentiation: making the right connections.* Science, 2002. **296**(5573): p. 1648-9.
18. Wang, B., et al., *Erk1/2 promotes proliferation and inhibits neuronal differentiation of neural stem cells.* Neurosci Lett, 2009. **461**(3): p. 252-7.
19. Li, Z., M.H. Theus, and L. Wei, *Role of ERK 1/2 signaling in neuronal differentiation of cultured embryonic stem cells.* Dev Growth Differ, 2006. **48**(8): p. 513-23.

20. Murphy, L.O., J.P. MacKeigan, and J. Blenis, *A network of immediate early gene products propagates subtle differences in mitogen-activated protein kinase signal amplitude and duration.* Mol Cell Biol, 2004. **24**(1): p. 144-53.

21. Stork, P.J., *ERK signaling: duration, duration, duration.* Cell Cycle, 2002. **1**(5): p. 315-7.

22. Langeberg, L.K. and J.D. Scott, *Signalling scaffolds and local organization of cellular behaviour.* Nat Rev Mol Cell Biol, 2015. **16**(4): p. 232-44.

23. Plotnikov, A., et al., *The MAPK cascades: signaling components, nuclear roles and mechanisms of nuclear translocation.* Biochim Biophys Acta, 2011. **1813**(9): p. 1619-33.

24. Yoon, S. and R. Seger, *The extracellular signal-regulated kinase: multiple substrates regulate diverse cellular functions.* Growth Factors, 2006. **24**(1): p. 21-44.

25. Yao, Z. and R. Seger, *The ERK signaling cascade--views from different subcellular compartments.* Biofactors, 2009. **35**(5): p. 407-16.

26. Wainstein, E. and R. Seger, *The dynamic subcellular localization of ERK: mechanisms of translocation and role in various organelles.* Curr Opin Cell Biol, 2016. **39**: p. 15-20.

27. Jaaro, H., et al., *Nuclear translocation of mitogen-activated protein kinase kinase (MEK1) in response to mitogenic stimulation.* Proc Natl Acad Sci U S A, 1997. **94**(8): p. 3742-7.

28. Lenormand, P., et al., *Growth factors induce nuclear translocation of MAP kinases (p42mapk and p44mapk) but not of their activator MAP kinase kinase (p45mapkk) in fibroblasts.* J Cell Biol, 1993. **122**(5): p. 1079-88.

29. Shaul, Y.D. and R. Seger, *The MEK/ERK cascade: from signaling specificity to diverse functions.* Biochim Biophys Acta, 2007. **1773**(8): p. 1213-26.

30. Adachi, M., M. Fukuda, and E. Nishida, *Nuclear export of MAP kinase (ERK) involves a MAP kinase kinase (MEK)-dependent active transport mechanism.* J Cell Biol, 2000. **148**(5): p. 849-56.

31. Agudo-Ibanez, L., P. Crespo, and B. Casar, *Analysis of Ras/ERK Compartmentalization by Subcellular Fractionation.* Methods Mol Biol, 2017. **1487**: p. 151-162.

32. Mendoza, M.C., E.E. Er, and J. Blenis, *The Ras-ERK and PI3K-mTOR pathways: cross-talk and compensation.* Trends Biochem Sci, 2011. **36**(6): p. 320-8.

33. Kholodenko, B.N., J.F. Hancock, and W. Kolch, *Signalling ballet in space and time.* Nat Rev Mol Cell Biol, 2010. **11**(6): p. 414-26.

34. Aksamitiene, E., A. Kiyatkin, and B.N. Kholodenko, *Cross-talk between mitogenic Ras/MAPK and survival PI3K/Akt pathways: a fine balance.* Biochem Soc Trans, 2012. **40**(1): p. 139-46.

35. Roberts, P.J. and C.J. Der, *Targeting the Raf-MEK-ERK mitogen-activated protein kinase cascade for the treatment of cancer.* Oncogene, 2007. **26**(22): p. 3291-310.

36. Kim, E.K. and E.J. Choi, *Pathological roles of MAPK signaling pathways in human diseases.* Biochim Biophys Acta, 2010. **1802**(4): p. 396-405.

37. Tidyman, W.E. and K.A. Rauen, *The RASopathies: developmental syndromes of Ras/MAPK pathway dysregulation.* Curr Opin Genet Dev, 2009. **19**(3): p. 230-6.

38.   Tidyman, W.E. and K.A. Rauen, *Mutational and functional analysis in human Ras/MAP kinase genetic syndromes.* Methods Mol Biol, 2010. **661**: p. 433-47.

39.   Durrant, D.E. and D.K. Morrison, *Targeting the Raf kinases in human cancer: the Raf dimer dilemma.* Br J Cancer, 2018. **118**(1): p. 3-8.

40.   Holderfield, M., et al., *Targeting RAF kinases for cancer therapy: BRAF-mutated melanoma and beyond.* Nat Rev Cancer, 2014. **14**(7): p. 455-67.

41.   Chang, F., et al., *Signal transduction mediated by the Ras/Raf/MEK/ERK pathway from cytokine receptors to transcription factors: potential targeting for therapeutic intervention.* Leukemia, 2003. **17**(7): p. 1263-93.

42.   Safaee Ardekani, G., et al., *The prognostic value of BRAF mutation in colorectal cancer and melanoma: a systematic review and meta-analysis.* PLoS One, 2012. **7**(10): p. e47054.

43.   Davies, H., et al., *Mutations of the BRAF gene in human cancer.* Nature, 2002. **417**(6892): p. 949-54.

44.   Mercer, K., et al., *Expression of endogenous oncogenic V600EB-raf induces proliferation and developmental defects in mice and transformation of primary fibroblasts.* Cancer Res, 2005. **65**(24): p. 11493-500.

45.   Prior, I.A., P.D. Lewis, and C. Mattos, *A comprehensive survey of Ras mutations in cancer.* Cancer Res, 2012. **72**(10): p. 2457-67.

46.   Barretina, J., et al., *The Cancer Cell Line Encyclopedia enables predictive modelling of anticancer drug sensitivity.* Nature, 2012. **483**(7391): p. 603-7.

47.   Shepherd, C., I. Puzanov, and J.A. Sosman, *B-RAF inhibitors: an evolving role in the therapy of malignant melanoma.* Curr Oncol Rep, 2010. **12**(3): p. 146-52.

48.   Roos, W.P., et al., *B-Raf inhibitor vemurafenib in combination with temozolomide and fotemustine in the killing response of malignant melanoma cells.* Oncotarget, 2014. **5**(24): p. 12607-20.

49.   Varga, A., et al., *RAF1/BRAF dimerization integrates the signal from RAS to ERK and ROKalpha.* Sci Signal, 2017. **10**(469).

50.   Derdas, S.P., et al., *Expression analysis of B-Raf oncogene in V600E-negative benign and malignant tumors of the thyroid gland: correlation with late disease onset.* Med Oncol, 2013. **30**(1): p. 336.

51.   Heneberg, P., *[Advances in clinical treatment of malignant melanoma: B-RAF kinase inhibition].* Klin Onkol, 2011. **24**(4): p. 256-64.

52.   Fernandez-Medarde, A. and E. Santos, *Ras in cancer and developmental diseases.* Genes Cancer, 2011. **2**(3): p. 344-58.

53.   Jindal, G.A., et al., *RASopathies: unraveling mechanisms with animal models.* Dis Model Mech, 2015. **8**(9): p. 1167.

54.   Bustelo, X.R., et al., *RAS GTPase-dependent pathways in developmental diseases: old guys, new lads, and current challenges.* Curr Opin Cell Biol, 2018. **55**: p. 42-51.

55.   Rauen, K.A., *The RASopathies.* Annu Rev Genomics Hum Genet, 2013. **14**: p. 355-69.

56.   Good, M.C., J.G. Zalatan, and W.A. Lim, *Scaffold proteins: hubs for controlling the flow of cellular information.* Science, 2011. **332**(6030): p. 680-6.

57.   Whitmarsh, A.J. and R.J. Davis, *Structural organization of MAP-kinase signaling modules by scaffold proteins in yeast and mammals.* Trends Biochem Sci, 1998. **23**(12): p. 481-5.

58.   Burack, W.R. and A.S. Shaw, *Signal transduction: hanging on a scaffold.* Curr Opin Cell Biol, 2000. **12**(2): p. 211-6.

59.   Brown, M.D. and D.B. Sacks, *Protein scaffolds in MAP kinase signalling.* Cell Signal, 2009. **21**(4): p. 462-9.

60.   Kranz, J.E., B. Satterberg, and E.A. Elion, *The MAP kinase Fus3 associates with and phosphorylates the upstream signaling component Ste5.* Genes Dev, 1994. **8**(3): p. 313-27.

61.   Choi, K.Y., et al., *Ste5 tethers multiple protein kinases in the MAP kinase cascade required for mating in S. cerevisiae.* Cell, 1994. **78**(3): p. 499-512.

62.   Marcus, S., et al., *Complexes between STE5 and components of the pheromone-responsive mitogen-activated protein kinase module.* Proc Natl Acad Sci U S A, 1994. **91**(16): p. 7762-6.

63.   Printen, J.A. and G.F. Sprague, Jr., *Protein-protein interactions in the yeast pheromone response pathway: Ste5p interacts with all members of the MAP kinase cascade.* Genetics, 1994. **138**(3): p. 609-19.

64.   Elion, E.A., *Pheromone response, mating and cell biology.* Curr Opin Microbiol, 2000. **3**(6): p. 573-81.

65.   Elion, E.A., *The Ste5p scaffold.* J Cell Sci, 2001. **114**(Pt 22): p. 3967-78.

66.   Elion, E.A., *Ste5: a meeting place for MAP kinases and their associates.* Trends Cell Biol, 1995. **5**(8): p. 322-7.

67.   Bhattacharyya, R.P., et al., *The Ste5 scaffold allosterically modulates signaling output of the yeast mating pathway.* Science, 2006. **311**(5762): p. 822-6.

68.   Kornfeld, K., D.B. Hom, and H.R. Horvitz, *The ksr-1 gene encodes a novel protein kinase involved in Ras-mediated signaling in C. elegans.* Cell, 1995. **83**(6): p. 903-13.

69.   Therrien, M., et al., *KSR, a novel protein kinase required for RAS signal transduction.* Cell, 1995. **83**(6): p. 879-88.

70.   Sundaram, M. and M. Han, *The C. elegans ksr-1 gene encodes a novel Raf-related kinase involved in Ras-mediated signal transduction.* Cell, 1995. **83**(6): p. 889-901.

71.   Xing, H., K. Kornfeld, and A.J. Muslin, *The protein kinase KSR interacts with 14-3-3 protein and Raf.* Curr Biol, 1997. **7**(5): p. 294-300.

72.   Roy, F. and M. Therrien, *MAP kinase module: the Ksr connection.* Curr Biol, 2002. **12**(9): p. R325-7.

73.   Roy, F., et al., *KSR is a scaffold required for activation of the ERK/MAPK module.* Genes Dev, 2002. **16**(4): p. 427-38.

74.   Stewart, S., et al., *Kinase suppressor of Ras forms a multiprotein signaling complex and modulates MEK localization.* Mol Cell Biol, 1999. **19**(8): p. 5523-34.

75.   Nguyen, A., et al., *Kinase suppressor of Ras (KSR) is a scaffold which facilitates mitogen-activated protein kinase activation in vivo.* Mol Cell Biol, 2002. **22**(9): p. 3035-45.

76. Razidlo, G.L., et al., *Phosphorylation regulates KSR1 stability, ERK activation, and cell proliferation.* J Biol Chem, 2004. **279**(46): p. 47808-14.

77. Meister, M., et al., *Mitogen-Activated Protein (MAP) Kinase Scaffolding Proteins: A Recount.* Int J Mol Sci, 2013. **14**(3): p. 4854-84.

78. Frodyma, D., et al., *Coordinating ERK signaling via the molecular scaffold Kinase Suppressor of Ras.* F1000Res, 2017. **6**: p. 1621.

79. Kortum, R.L. and R.E. Lewis, *The molecular scaffold KSR1 regulates the proliferative and oncogenic potential of cells.* Mol Cell Biol, 2004. **24**(10): p. 4407-16.

80. Neilsen, B.K., et al., *KSR as a therapeutic target for Ras-dependent cancers.* Expert Opin Ther Targets, 2017. **21**(5): p. 499-509.

81. McKay, M.M., A.K. Freeman, and D.K. Morrison, *Complexity in KSR function revealed by Raf inhibitor and KSR structure studies.* Small GTPases, 2011. **2**(5): p. 276-281.

82. Revelli, J.P., et al., *Profound obesity secondary to hyperphagia in mice lacking kinase suppressor of ras 2.* Obesity (Silver Spring), 2011. **19**(5): p. 1010-8.

83. Henry, M.D., et al., *Obesity-dependent dysregulation of glucose homeostasis in kinase suppressor of ras 2-/- mice.* Physiol Rep, 2014. **2**(7).

84. Pearce, L.R., et al., *KSR2 mutations are associated with obesity, insulin resistance, and impaired cellular fuel oxidation.* Cell, 2013. **155**(4): p. 765-77.

85. Lunin, V.V., et al., *The structure of the MAPK scaffold, MP1, bound to its partner, p14. A complex with a critical role in endosomal map kinase signaling.* J Biol Chem, 2004. **279**(22): p. 23422-30.

86. Schaeffer, H.J., et al., *MP1: a MEK binding partner that enhances enzymatic activation of the MAP kinase cascade.* Science, 1998. **281**(5383): p. 1668-71.

87. Wunderlich, W., et al., *A novel 14-kilodalton protein interacts with the mitogen-activated protein kinase scaffold mp1 on a late endosomal/lysosomal compartment.* J Cell Biol, 2001. **152**(4): p. 765-76.

88. Teis, D., W. Wunderlich, and L.A. Huber, *Localization of the MP1-MAPK scaffold complex to endosomes is mediated by p14 and required for signal transduction.* Dev Cell, 2002. **3**(6): p. 803-14.

89. Teis, D., et al., *p14-MP1-MEK1 signaling regulates endosomal traffic and cellular proliferation during tissue homeostasis.* J Cell Biol, 2006. **175**(6): p. 861-8.

90. Nada, S., et al., *The novel lipid raft adaptor p18 controls endosome dynamics by anchoring the MEK-ERK pathway to late endosomes.* EMBO J, 2009. **28**(5): p. 477-89.

91. Sancak, Y., et al., *Ragulator-Rag complex targets mTORC1 to the lysosomal surface and is necessary for its activation by amino acids.* Cell, 2010. **141**(2): p. 290-303.

92. Saucedo, L.J., et al., *Rheb promotes cell growth as a component of the insulin/TOR signalling network.* Nat Cell Biol, 2003. **5**(6): p. 566-71.

93. Inoki, K., et al., *Rheb GTPase is a direct target of TSC2 GAP activity and regulates mTOR signaling.* Genes Dev, 2003. **17**(15): p. 1829-34.

94. Palfy, M., A. Remenyi, and T. Korcsmaros, *Endosomal crosstalk: meeting points for signaling pathways.* Trends Cell Biol, 2012. **22**(9): p. 447-56.

95. Sorkin, A. and M. von Zastrow, *Endocytosis and signalling: intertwining molecular networks.* Nat Rev Mol Cell Biol, 2009. **10**(9): p. 609-22.

96. Weissbach, L., et al., *Identification of a human rasGAP-related protein containing calmodulin-binding motifs.* J Biol Chem, 1994. **269**(32): p. 20517-21.

97. White, C.D., H.H. Erdemir, and D.B. Sacks, *IQGAP1 and its binding proteins control diverse biological functions.* Cell Signal, 2012. **24**(4): p. 826-34.

98. Fukata, M., et al., *Regulation of cross-linking of actin filament by IQGAP1, a target for Cdc42.* J Biol Chem, 1997. **272**(47): p. 29579-83.

99. Mateer, S.C., et al., *The mechanism for regulation of the F-actin binding activity of IQGAP1 by calcium/calmodulin.* J Biol Chem, 2002. **277**(14): p. 12324-33.

100. Ho, Y.D., et al., *IQGAP1 integrates Ca2+/calmodulin and Cdc42 signaling.* J Biol Chem, 1999. **274**(1): p. 464-70.

101. Kuroda, S., et al., *Role of IQGAP1, a target of the small GTPases Cdc42 and Rac1, in regulation of E-cadherin- mediated cell-cell adhesion.* Science, 1998. **281**(5378): p. 832-5.

102. Briggs, M.W., Z. Li, and D.B. Sacks, *IQGAP1-mediated stimulation of transcriptional co-activation by beta-catenin is modulated by calmodulin.* J Biol Chem, 2002. **277**(9): p. 7453-65.

103. Mbele, G.O., et al., *The zinc- and calcium-binding S100B interacts and co-localizes with IQGAP1 during dynamic rearrangement of cell membranes.* J Biol Chem, 2002. **277**(51): p. 49998-50007.

104. Katata, T., et al., *Involvement of nectin in the localization of IQGAP1 at the cell-cell adhesion sites through the actin cytoskeleton in Madin-Darby canine kidney cells.* Oncogene, 2003. **22**(14): p. 2097-109.

105. Fukata, M., et al., *Rac1 and Cdc42 capture microtubules through IQGAP1 and CLIP-170.* Cell, 2002. **109**(7): p. 873-85.

106. Roy, M., Z. Li, and D.B. Sacks, *IQGAP1 binds ERK2 and modulates its activity.* J Biol Chem, 2004. **279**(17): p. 17329-37.

107. McNulty, D.E., et al., *MAPK scaffold IQGAP1 binds the EGF receptor and modulates its activation.* J Biol Chem, 2011. **286**(17): p. 15010-21.

108. Selfors, L.M., et al., *soc-2 encodes a leucine-rich repeat protein implicated in fibroblast growth factor receptor signaling.* Proc Natl Acad Sci U S A, 1998. **95**(12): p. 6903-8.

109. Matsunaga-Udagawa, R., et al., *The scaffold protein Shoc2/SUR-8 accelerates the interaction of Ras and Raf.* J Biol Chem, 2010. **285**(10): p. 7818-26.

110. Rodriguez-Viciana, P., et al., *A phosphatase holoenzyme comprised of Shoc2/Sur8 and the catalytic subunit of PP1 functions as an M-Ras effector to modulate Raf activity.* Mol Cell, 2006. **22**(2): p. 217-30.

111. Jeoung, M., et al., *Functional Integration of the Conserved Domains of Shoc2 Scaffold.* PLoS One, 2013. **8**(6): p. e66067.

112. Kaplan, F.M., et al., *SHOC2 and CRAF mediate ERK1/2 reactivation in mutant NRAS-mediated resistance to RAF inhibitor.* J Biol Chem, 2012. **287**(50): p. 41797-807.

113. Li, W., M. Han, and K.L. Guan, *The leucine-rich repeat protein SUR-8 enhances MAP kinase activation and forms a complex with Ras and Raf.* Genes Dev, 2000. **14**(8): p. 895-900.

114. Kaduwal, S., et al., *Sur8/Shoc2 promotes cell motility and metastasis through activation of Ras-PI3K signaling.* Oncotarget, 2015. **6**(32): p. 33091-105.

115. Moon, B.S., et al., *Sur8/Shoc2 involves both inhibition of differentiation and maintenance of self-renewal of neural progenitor cells via modulation of extracellular signal-regulated kinase signaling.* Stem Cells, 2011. **29**(2): p. 320-31.

116. Jang, E.R., et al., *Spatial control of Shoc2-scaffold-mediated ERK1/2 signaling requires remodeling activity of the ATPase PSMC5.* J Cell Sci, 2015. **128**(23): p. 4428-41.

117. Leon, G., et al., *Shoc2/Sur8 protein regulates neurite outgrowth.* PLoS One, 2014. **9**(12): p. e114837.

118. Jeoung, M., et al., *Shoc2-tranduced ERK1/2 motility signals--Novel insights from functional genomics.* Cell Signal, 2016. **28**(5): p. 448-459.

119. Young, L.C., et al., *An MRAS, SHOC2, and SCRIB complex coordinates ERK pathway activation with polarity and tumorigenic growth.* Mol Cell, 2013. **52**(5): p. 679-92.

120. Jang, E.R., et al., *HUWE1 is a molecular link controlling RAF-1 activity supported by the Shoc2 scaffold.* Mol Cell Biol, 2014. **34**(19): p. 3579-93.

121. Yi, J., et al., *Endothelial SUR-8 acts in an ERK-independent pathway during atrioventricular cushion development.* Dev Dyn, 2010. **239**(7): p. 2005-13.

122. Galperin, E., L. Abdelmoti, and A. Sorkin, *Shoc2 is targeted to late endosomes and required for Erk1/2 activation in EGF-stimulated cells.* PLoS One, 2012. **7**(5): p. e36469.

123. Takenouchi, T., et al., *Severe craniosynostosis with Noonan syndrome phenotype associated with SHOC2 mutation: clinical evidence of crosslink between FGFR and RAS signaling pathways.* Am J Med Genet A, 2014. **164A**(11): p. 2869-72.

124. Komatsuzaki, S., et al., *Mutation analysis of the SHOC2 gene in Noonan-like syndrome and in hematologic malignancies.* J Hum Genet, 2010. **55**(12): p. 801-9.

125. Wera, S. and B.A. Hemmings, *Serine/threonine protein phosphatases.* Biochem J, 1995. **311 (Pt 1)**: p. 17-29.

126. Barford, D., A.K. Das, and M.P. Egloff, *The structure and mechanism of protein phosphatases: insights into catalysis and regulation.* Annu Rev Biophys Biomol Struct, 1998. **27**: p. 133-64.

127. Santoni, M.J., et al., *The LAP family: a phylogenetic point of view.* Trends Genet, 2002. **18**(10): p. 494-7.

128. Yamben, I.F., et al., *Scrib is required for epithelial cell identity and prevents epithelial to mesenchymal transition in the mouse.* Dev Biol, 2013. **384**(1): p. 41-52.

129. Michaelis, U.R., et al., *The polarity protein Scrib is essential for directed endothelial cell migration.* Circ Res, 2013. **112**(6): p. 924-34.

130. Ono, Y., et al., *Muscle stem cell fate is controlled by the cell-polarity protein Scrib.* Cell Rep, 2015. **10**(7): p. 1135-48.

131. Bilder, D., M. Li, and N. Perrimon, *Cooperative regulation of cell polarity and growth by Drosophila tumor suppressors.* Science, 2000. **289**(5476): p. 113-6.

132. Kolch, W., *Erbin: sorting out ErbB2 receptors or giving Ras a break?* Sci STKE, 2003. **2003**(199): p. pe37.

133. Borg, J.P., et al., *ERBIN: a basolateral PDZ protein that interacts with the mammalian ERBB2/HER2 receptor.* Nat Cell Biol, 2000. **2**(7): p. 407-14.

134. Huang, Y.Z., et al., *Erbin is a protein concentrated at postsynaptic membranes that interacts with PSD-95.* J Biol Chem, 2001. **276**(22): p. 19318-26.

135. Huang, Y.Z., et al., *Erbin suppresses the MAP kinase pathway.* J Biol Chem, 2003. **278**(2): p. 1108-14.

136. Dai, P., W.C. Xiong, and L. Mei, *Erbin inhibits RAF activation by disrupting the sur-8-Ras-Raf complex.* J Biol Chem, 2006. **281**(2): p. 927-33.

137. Tao, Y., et al., *Erbin regulates NRG1 signaling and myelination.* Proc Natl Acad Sci U S A, 2009. **106**(23): p. 9477-82.

138. Shi, M., et al., *beta2-AR-induced Her2 transactivation mediated by Erbin confers protection from apoptosis in cardiomyocytes.* Int J Cardiol, 2013. **167**(4): p. 1570-7.

139. Harmon, R.M., et al., *Desmoglein-1/Erbin interaction suppresses ERK activation to support epidermal differentiation.* J Clin Invest, 2013. **123**(4): p. 1556-70.

140. Pervin, S., et al., *Reduced association of anti-apoptotic protein Mcl-1 with E3 ligase Mule increases the stability of Mcl-1 in breast cancer cells.* Br J Cancer, 2011. **105**(3): p. 428-37.

141. Shmueli, A. and M. Oren, *Life, death, and ubiquitin: taming the mule.* Cell, 2005. **121**(7): p. 963-5.

142. Zhong, Q., et al., *Mule/ARF-BP1, a BH3-only E3 ubiquitin ligase, catalyzes the polyubiquitination of Mcl-1 and regulates apoptosis.* Cell, 2005. **121**(7): p. 1085-95.

143. Bernassola, F., et al., *The HECT family of E3 ubiquitin ligases: multiple players in cancer development.* Cancer Cell, 2008. **14**(1): p. 10-21.

144. Chen, D., C.L. Brooks, and W. Gu, *ARF-BP1 as a potential therapeutic target.* Br J Cancer, 2006. **94**(11): p. 1555-8.

145. Confalonieri, S., et al., *Alterations of ubiquitin ligases in human cancer and their association with the natural history of the tumor.* Oncogene, 2009. **28**(33): p. 2959-68.

146. Adhikary, S., et al., *The ubiquitin ligase HectH9 regulates transcriptional activation by Myc and is essential for tumor cell proliferation.* Cell, 2005. **123**(3): p. 409-21.

147. Li, Z., et al., *USP4 inhibits p53 and NF-kappaB through deubiquitinating and stabilizing HDAC2.* Oncogene, 2016. **35**(22): p. 2902-12.

148. Zhao, X., et al., *The HECT-domain ubiquitin ligase Huwe1 controls neural differentiation and proliferation by destabilizing the N-Myc oncoprotein.* Nat Cell Biol, 2008. **10**(6): p. 643-53.

149. Ferry, C., et al., *SUG-1 plays proteolytic and non-proteolytic roles in the control of retinoic acid target genes via its interaction with SRC-3.* J Biol Chem, 2009. **284**(12): p. 8127-35.

150. Yim, J.H., et al., *Radiosensitizing effect of PSMC5, a 19S proteasome ATPase, in H460 lung cancer cells.* Biochem Biophys Res Commun, 2016. **469**(1): p. 94-100.

151. Su, K., et al., *Human Sug1/p45 is involved in the proteasome-dependent degradation of Sp1.* Biochem J, 2000. **348 Pt 2**: p. 281-9.

152. Cordeddu, V., et al., *Mutation of SHOC2 promotes aberrant protein N-myristoylation and causes Noonan-like syndrome with loose anagen hair.* Nat Genet, 2009. **41**(9): p. 1022-6.

153. Baldassarre, G., et al., *Phenotypic variability associated with the invariant SHOC2 c.4A>G (p.Ser2Gly) missense mutation.* Am J Med Genet A, 2014. **164A**(12): p. 3120-5.

154. Gargano, G., et al., *Hydrops fetalis in a preterm newborn heterozygous for the c.4A>G SHOC2 mutation.* Am J Med Genet A, 2014. **164A**(4): p. 1015-20.

155. Gripp, K.W., et al., *Expanding the SHOC2 mutation associated phenotype of Noonan syndrome with loose anagen hair: structural brain anomalies and myelofibrosis.* Am J Med Genet A, 2013. **161A**(10): p. 2420-30.

156. Hoban, R., et al., *Noonan syndrome due to a SHOC2 mutation presenting with fetal distress and fatal hypertrophic cardiomyopathy in a premature infant.* Am J Med Genet A, 2012. **158A**(6): p. 1411-3.

157. Choi, J.H., et al., *Moyamoya syndrome in a patient with Noonan-like syndrome with loose anagen hair.* Pediatr Neurol, 2015. **52**(3): p. 352-5.

158. Hannig, V., et al., *A Novel SHOC2 Variant in Rasopathy.* Hum Mutat, 2014. **35**(11): p. 1290-4.

159. Gripp, K.W., et al., *A novel rasopathy caused by recurrent de novo missense mutations in PPP1CB closely resembles Noonan syndrome with loose anagen hair.* Am J Med Genet A, 2016. **170**(9): p. 2237-47.

160. Akimenko, M.A., et al., *Differential induction of four msx homeobox genes during fin development and regeneration in zebrafish.* Development, 1995. **121**(2): p. 347-57.

161. Kimmel, C.B., et al., *Stages of embryonic development of the zebrafish.* Dev Dyn, 1995. **203**(3): p. 253-310.

162. Jao, L.E., S.R. Wente, and W. Chen, *Efficient multiplex biallelic zebrafish genome editing using a CRISPR nuclease system.* Proc Natl Acad Sci U S A, 2013. **110**(34): p. 13904-9.

163. Detrich, H.W., 3rd, et al., *Intraembryonic hematopoietic cell migration during vertebrate development.* Proc Natl Acad Sci U S A, 1995. **92**(23): p. 10713-7.

164. Kimmel, C.B., et al., *The shaping of pharyngeal cartilages during early development of the zebrafish.* Dev Biol, 1998. **203**(2): p. 245-63.

165. de Araujo, M.E., L.A. Huber, and T. Stasyk, *Isolation of endocitic organelles by density gradient centrifugation.* Methods Mol Biol, 2008. **424**: p. 317-31.

166. Gargano, G., et al., *Hydrops fetalis in a preterm newborn heterozygous for the c.4A>G SHOC2 mutation.* Am J Med Genet A, 2014.

167. Capalbo, D., et al., *Clinical Heterogeneity in two patients with Noonanlike Syndrome associated with the same SHOC2 mutation.* Ital J Pediatr, 2012. **38**(1): p. 48.

168. Dooley, K. and L.I. Zon, *Zebrafish: a model system for the study of human disease.* Curr Opin Genet Dev, 2000. **10**(3): p. 252-6.

169. Penberthy, W.T., E. Shafizadeh, and S. Lin, *The zebrafish as a model for human disease.* Front Biosci, 2002. **7**: p. d1439-53.

170. Ward, A.C. and G.J. Lieschke, *The zebrafish as a model system for human disease.* Front Biosci, 2002. **7**: p. d827-33.

171. Kulkeaw, K. and D. Sugiyama, *Zebrafish erythropoiesis and the utility of fish as models of anemia.* Stem Cell Res Ther, 2012. **3**(6): p. 55.
172. Howe, K., et al., *The zebrafish reference genome sequence and its relationship to the human genome.* Nature, 2013. **496**(7446): p. 498-503.
173. Mork, L. and G. Crump, *Zebrafish Craniofacial Development: A Window into Early Patterning.* Curr Top Dev Biol, 2015. **115**: p. 235-69.
174. Gore, A.V., et al., *The zebrafish: A fintastic model for hematopoietic development and disease.* Wiley Interdiscip Rev Dev Biol, 2018. **7**(3): p. e312.
175. Rosen, J.N., M.F. Sweeney, and J.D. Mably, *Microinjection of zebrafish embryos to analyze gene function.* J Vis Exp, 2009(25).
176. Krens, S.F., et al., *Characterization and expression patterns of the MAPK family in zebrafish.* Gene Expr Patterns, 2006. **6**(8): p. 1019-26.
177. Krens, S.F., et al., *ERK1 and ERK2 MAPK are key regulators of distinct gene sets in zebrafish embryogenesis.* BMC Genomics, 2008. **9**: p. 196.
178. Boisset, J.C. and C. Robin, *On the origin of hematopoietic stem cells: progress and controversy.* Stem Cell Res, 2012. **8**(1): p. 1-13.
179. Lawson, N.D. and B.M. Weinstein, *In vivo imaging of embryonic vascular development using transgenic zebrafish.* Dev Biol, 2002. **248**(2): p. 307-18.
180. Ransom, D.G., et al., *Characterization of zebrafish mutants with defects in embryonic hematopoiesis.* Development, 1996. **123**: p. 311-9.
181. Stachura, D.L. and D. Traver, *Cellular dissection of zebrafish hematopoiesis.* Methods Cell Biol, 2016. **133**: p. 11-53.
182. Traver, D., *Cellular dissection of zebrafish hematopoiesis.* Methods Cell Biol, 2004. **76**: p. 127-49.
183. Paik, E.J. and L.I. Zon, *Hematopoietic development in the zebrafish.* Int J Dev Biol, 2010. **54**(6-7): p. 1127-37.
184. Hsu, K., et al., *The pu.1 promoter drives myeloid gene expression in zebrafish.* Blood, 2004. **104**(5): p. 1291-7.
185. Lieschke, G.J., et al., *Zebrafish SPI-1 (PU.1) marks a site of myeloid development independent of primitive erythropoiesis: implications for axial patterning.* Dev Biol, 2002. **246**(2): p. 274-95.
186. Amatruda, J.F. and L.I. Zon, *Dissecting hematopoiesis and disease using the zebrafish.* Dev Biol, 1999. **216**(1): p. 1-15.
187. Willett, C.E., et al., *Expression of zebrafish rag genes during early development identifies the thymus.* Dev Biol, 1997. **182**(2): p. 331-41.
188. Iuchi, I. and M. Yamamoto, *Erythropoiesis in the developing rainbow trout, Salmo gairdneri irideus: histochemical and immunochemical detection of erythropoietic organs.* J Exp Zool, 1983. **226**(3): p. 409-17.
189. Le Guyader, D., et al., *Origins and unconventional behavior of neutrophils in developing zebrafish.* Blood, 2008. **111**(1): p. 132-41.
190. de Jong, J.L. and L.I. Zon, *Use of the zebrafish system to study primitive and definitive hematopoiesis.* Annu Rev Genet, 2005. **39**: p. 481-501.
191. Walker, M.B. and C.B. Kimmel, *A two-color acid-free cartilage and bone stain for zebrafish larvae.* Biotech Histochem, 2007. **82**(1): p. 23-8.
192. Kell, M.J., et al., *Targeted deletion of the zebrafish actin-bundling protein L-plastin (lcp1).* PLoS One, 2018. **13**(1): p. e0190353.

193. Willett, C.E., et al., *Expression of ZebrafishragGenes during Early Development Identifies the Thymus.* Developmental Biology, 1997. **182**(2): p. 331-341.

194. Langenau, D.M., et al., *In vivo tracking of T cell development, ablation, and engraftment in transgenic zebrafish.* Proc Natl Acad Sci U S A, 2004. **101**(19): p. 7369-74.

195. Chang, T.Y., et al., *Fully automated cellular-resolution vertebrate screening platform with parallel animal processing.* Lab Chip, 2012. **12**(4): p. 711-6.

196. Meyer, H. and C.C. Weihl, *The VCP/p97 system at a glance: connecting cellular function to disease pathogenesis.* J Cell Sci, 2014. **127**(Pt 18): p. 3877-83.

197. Meyer, H., M. Bug, and S. Bremer, *Emerging functions of the VCP/p97 AAA-ATPase in the ubiquitin system.* Nat Cell Biol, 2012. **14**(2): p. 117-23.

198. DeLaBarre, B., et al., *Central pore residues mediate the p97/VCP activity required for ERAD.* Mol Cell, 2006. **22**(4): p. 451-62.

199. Nowis, D., E. McConnell, and C. Wojcik, *Destabilization of the VCP-Ufd1-Npl4 complex is associated with decreased levels of ERAD substrates.* Exp Cell Res, 2006. **312**(15): p. 2921-32.

200. Lim, P.J., et al., *Ubiquilin and p97/VCP bind erasin, forming a complex involved in ERAD.* J Cell Biol, 2009. **187**(2): p. 201-17.

201. van den Boom, J. and H. Meyer, *VCP/p97-Mediated Unfolding as a Principle in Protein Homeostasis and Signaling.* Mol Cell, 2018. **69**(2): p. 182-194.

202. Schuberth, C. and A. Buchberger, *UBX domain proteins: major regulators of the AAA ATPase Cdc48/p97.* Cell Mol Life Sci, 2008. **65**(15): p. 2360-71.

203. Marchese, A. and J. Trejo, *Ubiquitin-dependent regulation of G protein-coupled receptor trafficking and signaling.* Cell Signal, 2013. **25**(3): p. 707-16.

204. Grabbe, C., K. Husnjak, and I. Dikic, *The spatial and temporal organization of ubiquitin networks.* Nat Rev Mol Cell Biol, 2011. **12**(5): p. 295-307.

205. Yi, L. and S.G. Kaler, *Interaction between the AAA ATPase p97/VCP and a concealed UBX domain in the copper transporter ATP7A is associated with motor neuron degeneration.* J Biol Chem, 2018. **293**(20): p. 7606-7617.

206. Buchberger, A., H. Schindelin, and P. Hanzelmann, *Control of p97 function by cofactor binding.* FEBS Lett, 2015. **589**(19 Pt A): p. 2578-89.

207. Kirchner, P., M. Bug, and H. Meyer, *Ubiquitination of the N-terminal region of caveolin-1 regulates endosomal sorting by the VCP/p97 AAA-ATPase.* J Biol Chem, 2013. **288**(10): p. 7363-72.

208. Hanzelmann, P. and H. Schindelin, *The structural and functional basis of the p97/valosin-containing protein (VCP)-interacting motif (VIM): mutually exclusive binding of cofactors to the N-terminal domain of p97.* J Biol Chem, 2011. **286**(44): p. 38679-90.

209. Bruderer, R.M., C. Brasseur, and H.H. Meyer, *The AAA ATPase p97/VCP interacts with its alternative co-factors, Ufd1-Npl4 and p47, through a common bipartite binding mechanism.* J Biol Chem, 2004. **279**(48): p. 49609-16.

210. Tang, W.K. and D. Xia, *Role of the D1-D2 Linker of Human VCP/p97 in the Asymmetry and ATPase Activity of the D1-domain.* Sci Rep, 2016. **6**: p. 20037.

211. Song, C., Q. Wang, and C.C. Li, *ATPase activity of p97-valosin-containing protein (VCP). D2 mediates the major enzyme activity, and D1 contributes to the heat-induced activity.* J Biol Chem, 2003. **278**(6): p. 3648-55.

212. Schweitzer, K., A. Pralow, and M. Naumann, *p97/VCP promotes Cullin-RING-ubiquitin-ligase/proteasome-dependent degradation of IkappaBalpha and the preceding liberation of RelA from ubiquitinated IkappaBalpha.* J Cell Mol Med, 2016. **20**(1): p. 58-70.

213. Besche, H.C., et al., *Isolation of mammalian 26S proteasomes and p97/VCP complexes using the ubiquitin-like domain from HHR23B reveals novel proteasome-associated proteins.* Biochemistry, 2009. **48**(11): p. 2538-49.

214. Tang, W.K. and D. Xia, *Mutations in the Human AAA(+) Chaperone p97 and Related Diseases.* Front Mol Biosci, 2016. **3**: p. 79.

215. Zhang, X., et al., *Altered cofactor regulation with disease-associated p97/VCP mutations.* Proc Natl Acad Sci U S A, 2015. **112**(14): p. E1705-14.

216. Halawani, D., et al., *Hereditary inclusion body myopathy-linked p97/VCP mutations in the NH2 domain and the D1 ring modulate p97/VCP ATPase activity and D2 ring conformation.* Mol Cell Biol, 2009. **29**(16): p. 4484-94.

217. Magnaghi, P., et al., *Covalent and allosteric inhibitors of the ATPase VCP/p97 induce cancer cell death.* Nat Chem Biol, 2013. **9**(9): p. 548-56.

218. Lan, B., et al., *VCP/p97/Cdc48, A Linking of Protein Homeostasis and Cancer Therapy.* Curr Mol Med, 2017. **17**(9): p. 608-618.

219. Zhou, H.J., et al., *Discovery of a First-in-Class, Potent, Selective, and Orally Bioavailable Inhibitor of the p97 AAA ATPase (CB-5083).* J Med Chem, 2015. **58**(24): p. 9480-97.

220. Gareau, A., et al., *In vitro efficacy of a first-generation valosin-containing protein inhibitor (CB-5083) against canine lymphoma.* Vet Comp Oncol, 2018. **16**(3): p. 311-317.

221. Le Moigne, R., et al., *The p97 Inhibitor CB-5083 Is a Unique Disrupter of Protein Homeostasis in Models of Multiple Myeloma.* Mol Cancer Ther, 2017. **16**(11): p. 2375-2386.

222. Bastola, P., et al., *Specific mutations in the D1-D2 linker region of VCP/p97 enhance ATPase activity and confer resistance to VCP inhibitors.* Cell Death Discov, 2017. **3**: p. 17065.

223. Bastola, P., et al., *VCP inhibitors induce endoplasmic reticulum stress, cause cell cycle arrest, trigger caspase-mediated cell death and synergistically kill ovarian cancer cells in combination with Salubrinal.* Mol Oncol, 2016. **10**(10): p. 1559-1574.

224. Hanzelmann, P. and H. Schindelin, *The Interplay of Cofactor Interactions and Post-translational Modifications in the Regulation of the AAA+ ATPase p97.* Front Mol Biosci, 2017. **4**: p. 21.

225. Fernandez-Saiz, V. and A. Buchberger, *Imbalances in p97 co-factor interactions in human proteinopathy.* EMBO Rep, 2010. **11**(6): p. 479-85.

226. Mali, P., et al., *RNA-guided human genome engineering via Cas9.* Science, 2013. **339**(6121): p. 823-6.

227. Yi, J., et al., *Endothelial SUR-8 acts in an ERK-independent pathway during atrioventricular cushion development.* Developmental dynamics : an official publication of the American Association of Anatomists, 2010. **239**(7): p. 2005-13.

228.	Hoban, R., et al., *Noonan syndrome due to a SHOC2 mutation presenting with fetal distress and fatal hypertrophic cardiomyopathy in a premature infant.* American journal of medical genetics. Part A, 2012. **158A**(6): p. 1411-3.

229.	Rauen, K.A., *The RASopathies.* Annu Rev Genomics Hum Genet, 2013.

230.	Huang, X. and J.P. Saint-Jeannet, *Induction of the neural crest and the opportunities of life on the edge.* Dev Biol, 2004. **275**(1): p. 1-11.

231.	Mayor, R. and E. Theveneau, *The neural crest.* Development, 2013. **140**(11): p. 2247-51.

232.	Newbern, J., et al., *Mouse and human phenotypes indicate a critical conserved role for ERK2 signaling in neural crest development.* Proc Natl Acad Sci U S A, 2008. **105**(44): p. 17115-20.

233.	Teng, L., et al., *Requirement for Foxd3 in the maintenance of neural crest progenitors.* Development, 2008. **135**(9): p. 1615-24.

234.	Mundell, N.A. and P.A. Labosky, *Neural crest stem cell multipotency requires Foxd3 to maintain neural potential and repress mesenchymal fates.* Development, 2011. **138**(4): p. 641-52.

235.	Kim, J., et al., *SOX10 maintains multipotency and inhibits neuronal differentiation of neural crest stem cells.* Neuron, 2003. **38**(1): p. 17-31.

236.	Simoes-Costa, M. and M.E. Bronner, *Establishing neural crest identity: a gene regulatory recipe.* Development, 2015. **142**(2): p. 242-57.

237.	Niemeyer, C.M., *RAS diseases in children.* Haematologica, 2014. **99**(11): p. 1653-62.

238.	Flotho, C., et al., *Mutational analysis of SHOC2, a novel gene for Noonan-like syndrome, in JMML.* Blood, 2010. **115**(4): p. 913.

239.	Monteiro, R., C. Pouget, and R. Patient, *The gata1/pu.1 lineage fate paradigm varies between blood populations and is modulated by tif1gamma.* EMBO J, 2011. **30**(6): p. 1093-103.

240.	Jeoung, M., et al., *Shoc2-tranduced ERK1/2 motility signals - Novel insights from functional genomics.* Cell Signal, 2016. **28**(5): p. 448-59.

241.	Liu, L., et al., *K-ras/PI3K-Akt signaling is essential for zebrafish hematopoiesis and angiogenesis.* PLoS One, 2008. **3**(8): p. e2850.

242.	Razzaque, M.A., et al., *Germline gain-of-function mutations in RAF1 cause Noonan syndrome.* Nat Genet, 2007. **39**(8): p. 1013-7.

243.	Hartmann-Petersen, R., et al., *The Ubx2 and Ubx3 cofactors direct Cdc48 activity to proteolytic and nonproteolytic ubiquitin-dependent processes.* Curr Biol, 2004. **14**(9): p. 824-8.

244.	Niwa, H., et al., *The role of the N-domain in the ATPase activity of the mammalian AAA ATPase p97/VCP.* J Biol Chem, 2012. **287**(11): p. 8561-70.

245.	Ballar, P., et al., *The role of a novel p97/valosin-containing protein-interacting motif of gp78 in endoplasmic reticulum-associated degradation.* J Biol Chem, 2006. **281**(46): p. 35359-68.

246.	Li, J.M., et al., *The p97-UFD1L-NPL4 protein complex mediates cytokine-induced IkappaBalpha proteolysis.* Mol Cell Biol, 2014. **34**(3): p. 335-47.

247.	Ritz, D., et al., *Endolysosomal sorting of ubiquitylated caveolin-1 is regulated by VCP and UBXD1 and impaired by VCP disease mutations.* Nat Cell Biol, 2011. **13**(9): p. 1116-23.

248. Nguyen, L.K., W. Kolch, and B.N. Kholodenko, *When ubiquitination meets phosphorylation: a systems biology perspective of EGFR/MAPK signalling.* Cell Commun Signal, 2013. **11**: p. 52.

249. Sasaki, A.T., et al., *Ubiquitination of K-Ras enhances activation and facilitates binding to select downstream effectors.* Sci Signal, 2011. **4**(163): p. ra13.

250. Jura, N., et al., *Differential modification of Ras proteins by ubiquitination.* Mol Cell, 2006. **21**(5): p. 679-87.

251. Nada, S., et al., *p18/LAMTOR1: a late endosome/lysosome-specific anchor protein for the mTORC1/MAPK signaling pathway.* Methods Enzymol, 2014. **535**: p. 249-63.

252. Locke, M., J.I. Toth, and M.D. Petroski, *Lys11- and Lys48-linked ubiquitin chains interact with p97 during endoplasmic-reticulum-associated degradation.* Biochem J, 2014. **459**(1): p. 205-16.

253. Ju, J.S. and C.C. Weihl, *Inclusion body myopathy, Paget's disease of the bone and fronto-temporal dementia: a disorder of autophagy.* Hum Mol Genet, 2010. **19**(R1): p. R38-45.

254. Blythe, E.E., et al., *Ubiquitin- and ATP-dependent unfoldase activity of P97/VCP*NPLOC4*UFD1L is enhanced by a mutation that causes multisystem proteinopathy.* Proc Natl Acad Sci U S A, 2017. **114**(22): p. E4380-E4388.

<div align="center">**Vita**</div>

<div align="center">**HyeIn Jang**</div>

EDUCATION:

2012-2018	Graduate student in Department of Molecular & Cellular Biochemistry
	University of Kentucky
2011-2012	Integrated Biomedical Sciences (IBS) program
	University of Kentucky
2008	B.S. Biotechnology, Yeungnam University
	South Korea

RESEARCH EXPERIENCE:

2011-2018	Graduate Student
	University of Kentucky
	Mentor: Emilia Galperin, Ph.D.
2010-2011	Research Assistant
	University of Kentucky
2008	Research Assistant
	Korean Institute of Science and Technology (KIST)
	South Korea

GRANT FUNDING:

2015-2017	Pre-doctoral Fellowship
	American Heart Association (15PRE25090207)

ACADEMIC AWARDS AND HONORS:

2018	Poster Presentation Award
	The Molecular and Cellular Biochemistry Departmental Spring
	Research Conference
2018	Max Steckler Award

Molecular and Cellular Biochemistry Department

University of Kentucky

2017   Graduate Travel Award

American Society for Biochemistry and Molecular Biology

Meeting (ASBMB)

2015   Alumni Fellowship

Yeungnam University Alumni

2013   Graduate Travel Award

American Society for Biochemistry and Molecular Biology

Meeting (ASBMB)

2012-2013   Graduate School Travel Award

University of Kentucky Graduate School

2011-2012   GSAY1 Fellowship

Integrated Biomedical Sciences (IBS) program

University of Kentucky

PROFESSIONAL MEMBERSHIP:

2018   American Society for Cell Biology

2015-2017   American Heart Association

2017   American Society for Biochemistry and Molecular Biology

UNIVERSITY SERVICE:

2015, 2018   Judge for annual College of Medicine Postdoctoral Poster Session

University of Kentucky

PRESENTATIONS:

2018   The Molecular and Cellular Biochemistry Departmental Spring

Research Conference

"Shoc2 mediates hematopoietic signals of the ERK1/2 pathway"

Lexington, KY

2017   The Molecular and Cellular Biochemistry Departmental Spring

Research Conference

"Shoc2 mediates hematopoietic signals of the ERK1/2 pathway"

2017	American Society for Biochemistry and Molecular Biology Meeting (ASBMB)
	"Shoc2 mediates hematopoietic signals of the ERK1/2 pathway"
	Chicago, IL
2017	University of Kentucky Zebrafish Group Meeting
	"Shoc2 mediates hematopoietic signals of the ERK1/2 pathway"
2016	NIH, NIGMS Sixth Biennial National IDeA Symposium of Biomedical Research excellence (NISBRE)
	"Shoc2 mediates hematopoietic signals of the ERK1/2 pathway"
	Washington, DC
2016	The Molecular and Cellular Biochemistry Departmental Spring Research Conference
	"Shoc2 mediates hematopoietic signals of the ERK1/2 pathway"
	Lexington, KY
2015	Southeast Regional IDeA Meeting
	"Spatial control of Shoc2-mediated ERK1/2 signaling requires remodeling activity of the ATPase PSMC5"
	Biloxi, MS
2015	Midwest Membrane Trafficking and Signaling Symposium
	"Shoc2 mediates hematopoietic and vasculogenic ERK1/2 signals in zebrafish"
	Louisville, KY
2015	The Molecular and Cellular Biochemistry Departmental Spring Research Conference
	"Shoc2 mediates hematopoietic and vasculogenic ERK1/2 signals in zebrafish"
	Lexington, KY
2014	Midwest Membrane Trafficking and Signaling Symposium
	"Shoc2 in hematopoiesis and vasculature development in zebrafish"

Louisville, KY

2013	The Molecular and Cellular Biochemistry Departmental Spring Research Conference "The Role of Shoc2 in Regulating Cell Motility" General Butler State Resort Park, KY
2013	American Society for Biochemistry and Molecular Biology Meeting (ASBMB) "The Role of Shoc2 in Regulating Cell Motility" Boston, MA

PUBLICATIONS:

1. **<u>Jang, H.</u>**; Jang, ER.; Wilson P.; Anderson, D.; and Galperin, E. (in preparation). "Valosin containing protein (VCP) controls signals of the ERK1/2 pathway transmitted via the Shoc2 scaffolding complex."

2. **<u>Jang, H.</u>**; Oakley, E.; Forbes-Osborne, M.; Kesler, M.; Norcross, R.; Morris, A.; and Galperin, E. "Hematopoietic and neural crest defects in zebrafish *shoc2* mutants: a novel vertebrate model for Noonan-like syndrome." Human Molecular Genetics, 2018.

3. Song, E.S.; **<u>Jang, H.</u>**; Guo, H.; Juliano, M.A.; Juliano, L.; Morris, A.J.; Galperin, E.; Rodgers, D.W.; Hersh, L.B. "Inositol phosphates and phosphoinositides activate insulin degrading enzyme while phosphoinositides mediate its binding to endosomes." Proceedings of the National Academy of Sciences, 2017.

4. Jang, E.R.; **<u>Jang, H.</u>**; Shi, P; Popa, G; Jeoung, M; Galperin, E. "Spatial control of Shoc2 scaffold-mediated ERK1/2 signaling requires remodeling activity of the ATPase PSMC5". Journal of Cell Science, 2015.

5. Jang, E.R.; Shi, P.; Bryant, J.; Chen, J.; Dukhante, V.; Gentry, M.S.; **<u>Jang, H.</u>**; Jeoung, M.; Galperin, E. "HUWE1 Is a Molecular Link Controlling RAF-1 Activity Supported by the Shoc2 Scaffold." Molecular Cell Biology, 2014.

6. Park, J.Y.; **Jang, H.**; Curry, T. E.; Sakamoto, A.; Jo, M. "Prostate androgen-regulated mucin-like protein 1: a novel regulator of progesterone metabolism." Molecular Endocrinology, 2013.

7. Li, F.; **Jang, H.**; Puttabyatappa, M.; Jo, M.; Curry, T. E., Jr. "Ovarian FAM110C (family with sequence similarity 110C): induction during the periovulatory period and regulation of granulosa cell cycle kinetics in rats." Biology of Reproduction, 2012.